VAPOR PHASE BECKMANN REARRANGEMENT ON INDUSTRIAL NANOCATALYSTS: STRUCTURE AND REACTION MECHANISMS

INTRODUCTION

The Beckmann rearrangement, the conversion of an oxime into an amide, was discovered in 1886 by Ernst Beckmann, is one of the important methods in organic synthesis. The conversion of cyclohexanone oxime into ε-caprolactam by this reaction is also utilized in the chemical manufacture of Nylon-6 polymer in industry (Scheme 1) where the annual market consumption is a million tons at the present time.

SCHEME 1

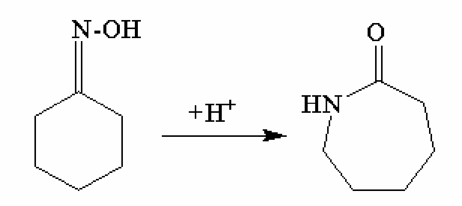

Cyclohexanone oxime ε-Caprolactam

Conventionally, this reaction is carried out in the sulfuric acid or another strong acid yielding a relatively large amount of undesired byproducts such as ammonium sulfate which occurs from neutralization process approximately 1-5 times per unit of ε-caprolactam. Moreover, the use of a corrosive sulfuric acid poses not only an environmental problem but also the wear of equipments. The environmentally acceptable alternative to the conventional process is a vapor-phase Beckmann rearrangement catalyzed by solid acids as zeolites. Zeolites as MFI, FAU, MOR, Beta, etc. were all tested for the vapor-phase rearrangement of cyclohexanone oxime for investigating the acid strength and the framework effect for this reaction. Zeolite proves to be an excellent candidate for taking over the catalytic function, thus their use has the benefit not only from an economical point of view, but from an ecological viewpoint also.

Zeolites are crystalline silicates and aluminosilicates which are linked through oxygen atoms producing a three dimensional structure which contains channels and cavities of molecular sizes. Nowadays, over 130 different zeolite frameworks are known and about one tenth of these are found in catalysts of commercial interest such as MFI, FAU and MOR etc. as shown in the Table 1. It is due mainly to the characteristic properties of zeolite: high surface area, molecular dimensions of pores, high adsorption capacity, acid-base property, therefore, zeolites play a vital role as catalysts and molecular sieves in a large number of major industrial processes. Thus, there are many studies to investigate the catalytic activity of zeolites corresponding to the demand in each reaction. It is found that when reaction demanding low acidities are to be catalyzed, zeolites with low Si:Al ratios will be preferred. In contrast, when strong acidities are required, zeolites with high Si:Al ratios will be chosen. Therefore, the fine tuning the acid strength is a very interesting property of a zeolite in catalysis and importance for controlling reaction selectivity. Furthermore, it is found that the acidity not only depends on the Si:Al ratios but it also relies on the zeolite structure which has an important impact on adsorption and stabilization of the activated complex penetrating in the pores of the zeolite. Is not only studied by using experimental techniques, but theoretical calculations and modeling studies have been also carried out by using the ab initio calculation that attempts to predict quantitative results of experimental zeolite properties. These use the bare cluster models, embedded cluster models and periodic systems to mimic zeolite structures with increasing the range of interaction from short to medium and long range as illustrated in the Figure 1.

Table 1 Zeolite structures and dimensional parameters.

Type	Structure	Details
MFI	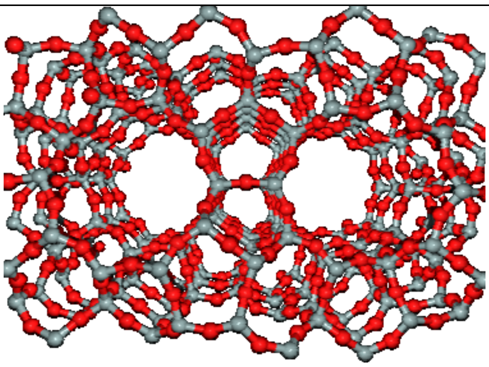	• Channels: **[100]** 10T (5.1 x 5.5) **[010]** 10T (5.3 x 5.6)
FAU	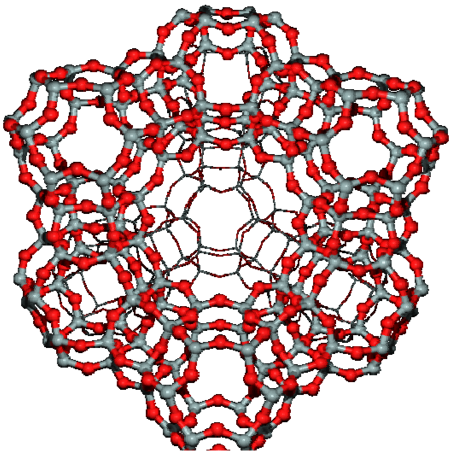	• Channels: **[111]** 12T (7.4 x 7.4)
MOR	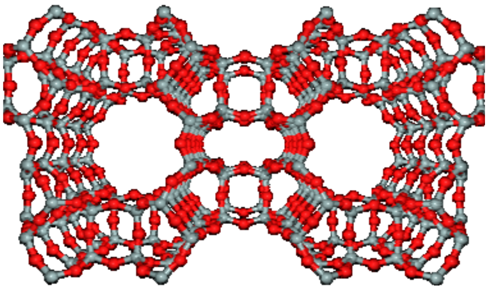	• Channels: **[001]** 12T (6.5 x 7.0) **[001]** 8T (2.6 x 5.7)

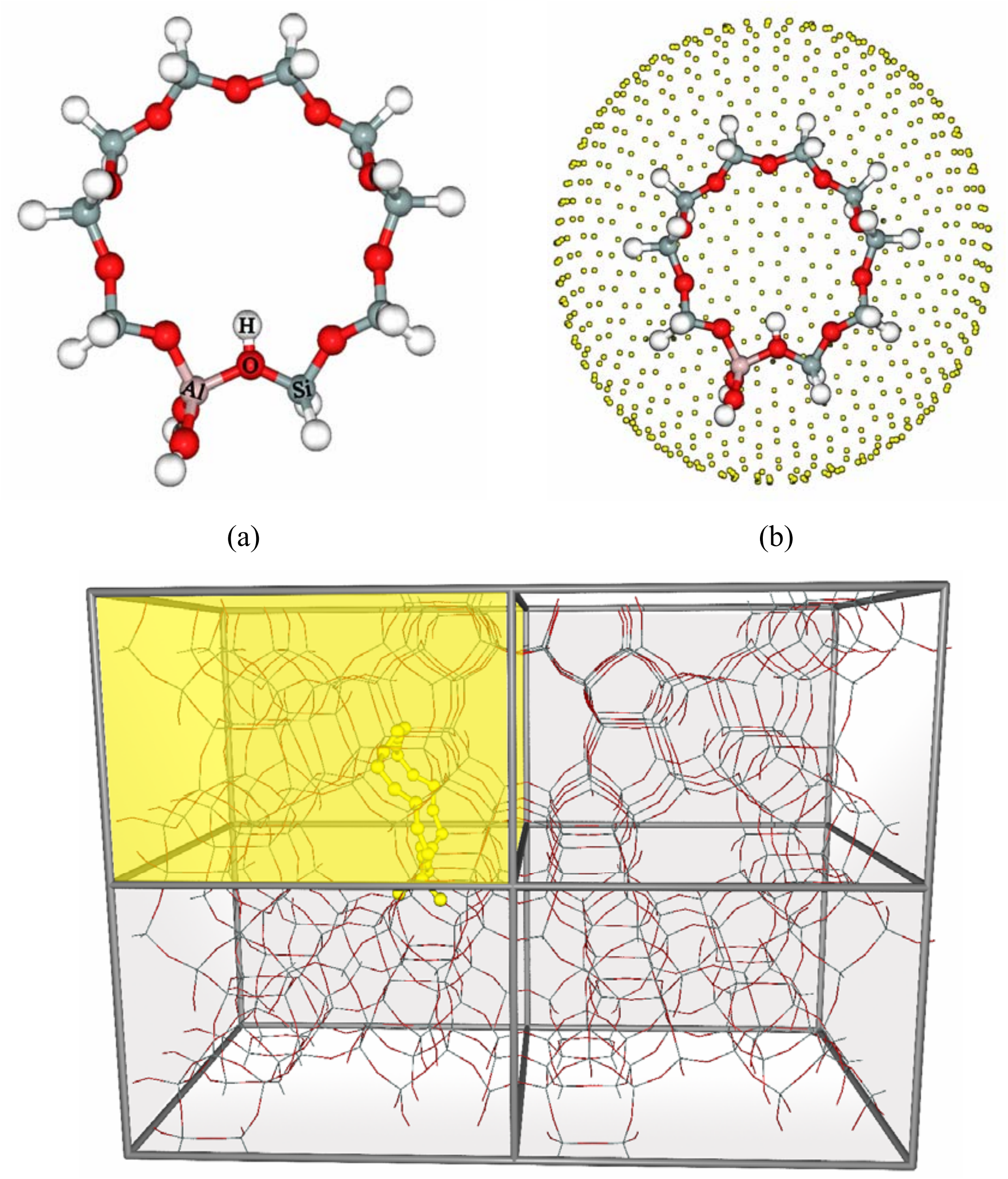

(a) (b)

(c)

Figure 1 The illustrative models used in ab initio calculation: (a) the bare cluster model representing the active region of H-ZSM-5 zeolite, (b) the embedded cluster model which is imitation of the electrostatic potential from zeolite framework by point charges which surround on the bare cluster model and (c) the periodic model of H-ZSM-5, where the highlighted box is a supercell in the periodic calculation.

For the reaction mechanism of Beckmann rearrangement was noted in organic textbooks, it generally starts from converting the OH group to a better leaving group by using the strong acid reagent (e.g., proton acids convert it to OH_2^+). After that, the trans-R group (may be alkyl, aryl or hydrogen) at carbon center transfers to the nitrogen center and concurrently releases the water molecule. Subsequently, the displaced water molecule binds to the carbon atom, simultaneously, transferring a proton to the acid catalyst. The last transforming step is the tautomerization from the enol-formed amide complex to the keto-formed amide as shown in the Scheme 2.

SCHEME 2

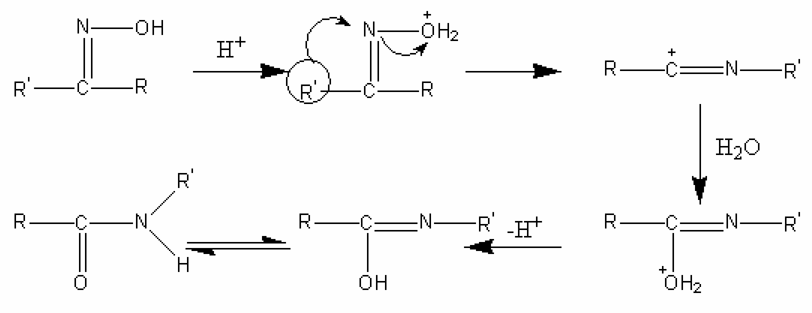

Although the reaction mechanism of Beckmann rearrangement was reported in organic textbooks, the mechanistic aspects of this reaction taking into account the environmental effects which is crucial to control the reaction path remain poorly understood and the rate determining step of reaction has not been identified experimentally. Therefore, there have been various experimental and computational studies of the Beckmann rearrangement for understanding the nature of this reaction.

For understanding better in this reaction, I performed a systematic theoretical investigation on the mechanism of the vapor-phase Beckman rearrangement in H-ZSM-5 and H-FAU zeolites. The objectives of this thesis are: 1) to understand the nature of the Beckmann rearrangement in the zeolite system; 2) to investigate the effects of the zeolite framework, particularly the effect of the Madelung potential, on the mechanism of the BR process; 3) to study the effect of the sizes of reactant on the mechanism and energetic profile of the Beckmann rearrangement.

LITERATURE REVIEWS

A large number of heterogeneous catalysts have been applied to catalyze the Beckmann rearrangement reaction of oxime compound. Experimental techniques such as XRD, FT-IR, HPLC, MAS-NMR and GC have been employed to study mechanism of this reaction on heterogeneous catalysts and to develop procedure of Nylon-6 precursor. Recently, many computational methodologies such as Hartree Fock (HF), density functional theory (DFT), have been employed to investigate mechanism of reaction as an alternative.

As for experimental results, the vapor phase Beckmann rearrangement in various types of zeolite has been intensively investigated in nowadays because the use of zeolite as a catalyst is proved to be an excellent candidate to take over the catalytic job not only from an economical point of view but also from an ecological viewpoint. Therefore, many researchers have reported the relationship between the vapor phase Beckmann rearrangement catalysis and the effects of the acid strength and the pore size in various types of zeolite such as **MFI** (Röseler *et al.*, 1996; Singh *et al.*, 1996; Yashima *et al*, 1997; Parker Jr, 1999; Misono *et al.*, 1999; Heitmann *et al.*, 2000; Komatsu *et al.*, 2000; O'Sullivan *et al.*, 2001; Fois *et al.*, 2001; Takahashi *et al.*, 2001; Kath *et al.*, 2001; Ichihashi *et al.*, 2002; Flego *et al.*, 2003; Takahashi *et al.*, 2004; Forni *et al.*, 2004; Li *et al.*, 2005), **FAU** (Dai *et al.*, 1999; O'Sullivan *et al.*, 2001; Fois *et al.*, 2001; Takahashi *et al.*, 2001; Ngamcharussrivichai *et al.*, 2004; Ngamcharussrivichai *et al.*, 2005), **Beta** (Camblor *et al.*, 1998; Heitmann *et al.*, 1999; Chung *et al.*, 2000; Chung *et al.*, 2001; O'Sullivan *et al.*, 2001; Zhang *et al.*, 2005), **MOR**(Yashima *et al*, 1997; O'Sullivan et al., 2001; Takahashi *et al.*, 2001), **SAPO-11** (Singh *et al.*, 1996), **FER** (Yashima *et al.*, 1997; Anand *et al.*, 2002), **FSM-16** (Dai *et al.*, 1998; Shouro *et al.*, 2000; Shouro *et al.*, 2001) **MCM-41** (Dai *et al.*, 1998; Chaudhari *et al.*, 2002; Savidha *et al.*, 2003; Maheswari *et al.*, 2003; Forni *et al.*, 2004; Ngamcharussrivichai *et al.*, 2004). It has been reported (Acajou *et al.*, 1986; Corma *et al.*, 1991) that the activity and selectivity for the formation of ε-caprolactam in the vapor phase Beckmann rearrangement are very much dependent upon the acidic character of zeolite. They found that the strong Brønsted acid site of the Y zeolite is responsible for the formation of ε-caprolactam. Moreover, Sato *et al.* (2001) suggested that the strong acid site of ZSM-5 play a significant role on increasing of the catalytic activity and selectivity to ε-caprolactam. They also found that the activity and selectivity were almost inversely proportional to the acid amount on the external surface of ZSM-5 crystals. Furthermore, Camblor *et al.* (1998) focused on the strength of the acid sites in the Beta zeolite responsible for this reaction. They found that the Brønsted acid sites of Beta zeolite are very active and selective for the formation of the amide. In addition, they also found that the external silanol groups preferentially catalyze the hydrolysis of the oxime, while, internal silanol groups can catalyze the Beckmann rearrangement. The different catalytic behavior of the two types of silanols may relate with the acid strength of silanol. They assumed that the internal silanols are more acidic than the external site owing to the strong electric fields on the electronic confinement occurring inside the zeolite pores to increase the interaction between the internal silanols and the reactant which penetrates in the pores of the zeolite. However, there are other groups which are in contrast with the previous investigators. They have suggested that the very weak as [B]-ZSM-5 (Röseler *et al.*, 1996; Alber *et al.,* 1998; Heitmann *et al.*, 2000), [B]-Beta (Heitmann *et al.*, 1999) or medium-strength acid sites as [Al]-SAPO-11 (Singh *et al.*, 1996) or even almost neutral silanol groups of the zelites as Silicalite-1 (Komatsu *et al.*, 2000; Kath *et al.*, 2001; Flego *et al.*, 2003) are favorable for this reaction.

Although the vapor phase rearrangement can eliminate problems which occur during the using of the homogenous catalysts, it introduces other problems, i.e. the rapid catalyst deactivation and the low ε-caprolactam which is due to the coke formation on the catalyst surface. Therefore, there are many works which focus on the role of diluent solvent for improvement of the catalyst performances. Dai *et al.* (1999) studied the catalytic performance of USY zeolites for the vapor phase Beckmann rearrangement of cyclohexnone oxime was greatly improved by adjusting the Si:Al ratio and by using an appropriate diluent. They found that the USY zeolite with Si:Al ratios of 27 and 62 exhibited excellent catalytic activity and selectivity when 1-hexanol was used as diluent. Chung *et al.* (2001) elucidated the solvent effect on the conversion of cyclohexanone oxime on the H-Beta zeolite. They suggested that a solvent having the appropriate balancing between the dielectric constant and polar nature as MEK (methyl ethyl ketone) is preferred to accelerate by stabilizing the transition structure and also by promoting the migration of OH_2^+ group. While, the non-polar solvents as toluene which have low dielectric constant can not stabilize the ionic species in the 1,2 H-shift of the N-protonated oxime. Furthermore, these non-polar solvents are also less efficient in assisting the migration of OH_2^+ group from nitrogen to carbon atom. In the case of polar protic solvent such as methanol, ethanol, etc., it is clear that the ability of protonation of oxime through the adsorption of substrate on the active site depends on the competitive adsorption between substrate and solvent. Therefore, the conversion of oxime solvating with the protic solvent can not occur. It is due mainly to the inaccessibility of oxime causing the predominant adsorption of polar protic solvent at the active center.

Despite the fact that there are some reports attempting to measure the rate constant and the associated activation energies of the Beckmann rearrangement, the rate determining step has not been identified experimentally yet, and the mechanistic aspect of the reaction has not be understood. Therefore, many techniques both from experimental and computational studies have been used to investigate the reaction mechanism of Beckmann rearrangement. One of the acceptable mechanisms was proposed by Nguyen *et al.* (1997), which used the MP2 level of theory to investigate the mechanism of the Beckmann rearrangement in the liquid phase. The proposed reaction path was divided in two key steps. The first step is called 1,2 H-shift which connects the N-protonated oxime and the O-protonated oxime. The second step, called the Beckmann rearrangement, is a migration of the alkyl group to the nitrogen atom and an elimination of water molecule, giving a nitrilium cation. The activation energy of gas phase model by using the MP4/6-311++G(d,p)//MP2/6-31G(d,p) level of theory is 53.8 and 10.5 kcal/mol for 1,2 H-shift and rearrangement steps, respectively. While the reaction mechanism on solid acid, it has been experimentally observed by Fois *et al.* (2001) and Chung *et al.* (2001). The FT-IR study confirms that the initial step of the rearrangement is not the O-protonation but the N-protonation of oxime which have characteristic peak for ν ($C=N^+$) around 1685 cm^{-1}, while the characteristic peak for ν (C=N) around 1664 cm^{-1} was not observed at all. It indicates that cyclohexanone oxime is already adsorbed and exists as a protonated form. For O-protonation complex, they found the small shoulder around 1720 cm^{-1} for δ (O^+-H_2)$_{asym}$ vibration. The appearance of this shoulder may be an evidence for the existence of the O-protonated oxime. And they also suggested that the 1,2 H-shift is possible the rate determining step of reaction because the formation of O-protonated oxime is considered to be short-lived as compared with the N-protonated oxime. Once the O-protonated oxime is formed, it can be converted rapidly to the corresponding amide. Recently, Bucko *et al.* (2004) employed a periodic DFT ab initio technique to investigate the reaction mechanism of the Beckmann rearrangement of cyclohexanone oxime to ε-caprolactam which was catalyzed by varying the active sites in MOR zeolite. They found that the most favorable active site for the Beckmann rearrangement in MOR is the Brønsted acid site, where the rate determining step of reaction is the 1,2 H-shift step which has an energy barrier of about 20 kcal/mol which corresponds to the experimental suggestions of Chung *et al.* (2001). On the other hand, the activation energy of the last two steps is 15.3 and 9.6 kcal/mol for the rearrangement and tautomerization steps, respectively. Furthermore, they also investigated the Beckmann rearrangement on the silanol groups both in the internal and in the external sites. The rate determining step of reaction on both sites is the rearrangement step which has the energy barrier about 36 and 53 kcal/mol for the internal and external silanol groups, respectively. Their results suggest that the activity of acid sites in MOR zeolite decreases in the order Brønsted acid site > internal silanols > external silanols which agrees well with the experimental results (Camblor *et al.*, 1998; Heitmann *et al.*, 1999; Forni *et al.*, 2004)

METHODS OF CALCULATIONS

Density functional theory (DFT)

Density functional theory (DFT) is one of the most widely used techniques for computational chemistry at the present time. It is due to its advantages including less computational demand, less computational time and better agreement with the experimental results than that of Hartree-Fock procedures.

In 1965, Kohn and Sham proposed a key breakthrough which was utilized for solving the electron-electron interaction term in the Hamiltonian. In a key breakthrough, Kohn and Sham realized that things would be considerably simpler if only Hamiltonian operator were treated as non-interacting system of electrons. Therefore, the Hamiltonian can be expressed as sum of one-electron operators, has eigenfunctions that are Slater determinants of the individual one-electron eigenfunctions and has eigenvalues that are simply the sum of the one-electron eigenvalues as shown in Eq. 1-3.

$$H^0 = \sum_{i=1}^{n} h_i \tag{1}$$

where H^0 is the sum of the one-electron operators. Because the Hamiltonian operator defined by Eq. (1) is separable, its may-electrons can be constructed as products of one-electron eigenfunctions. That is

$$\Psi^0 = \psi_1\psi_2 \ldots \psi_N \tag{2}$$

The energy of many-electrons in non-interacting system is a sum of the one-electron energy as found from proving in Hartree-product in the relevant text books as shown in Eq. (3).

$$H^0\Psi = \left(\sum_{i=i}^{N} \varepsilon_i\right)\Psi \tag{3}$$

where ε_i is the one-electron energy which is a product of one-electron eigenfunction. While, the densities corresponding to each electron can be calculated by using Eq. (4):

$$\rho_i(r) = \left|\phi_i(r)\right|^2 \tag{4}$$

And the total density of electrons is a sum of individual electron densities:

$$\rho_{tott}(r)=\sum_{i=1}^{N}\rho_i(r)=\sum_{i=1}^{N}\left|\phi_i(r)\right|^2 \tag{5}$$

From non-interacting system, the ground state energy is written as

$$E_0=\overline{T}[\rho]+\overline{V}_{Ne}[\rho]+\overline{V_{ee}}[\rho] \tag{6}$$

where $\overline{T}[\rho]$ term is electronic kinetic energy and $\overline{V}_{Ne}[\rho]$, $\overline{V_{ee}}[\rho]$ are electron-nuclear attraction and electron-electron repulsions, respectively. Kohn and Sham considered a fictitious reference system. The electrons in this system do not interact with one another, so the Hamiltonian of the reference system is

$$h_i=\sum_{i=1}^{n}\left[-\frac{1}{2}\nabla_i^2+v_s(r_i)\right] \tag{7}$$

where $v_s(r_i)$ is the external potential function to make the ground-state electron probability density of reference system equal to the exact ground-state electron density of the molecule we are interested.

The basis idea in the Kohn and Sham (KS) formalism is to split the kinetic energy functional into two parts, one of which can be calculated exactly from non-interacting system, and a small correction term for solving the main problem in Thomas-Fermi models is that the kinetic energy is represented poorly. For a closed shell ground state, the electrons are paired in the Kohn-Sham orbital, with two electrons of opposite spin having the same spatial Kohn-Sham orbital. Kohn and Sham rewrote the equation (6) as follows. Let $\Delta\overline{T}[\rho]$ be defined by

$$\Delta\overline{T}[\rho]\equiv\overline{T}[\rho]-\overline{T_s}[\rho] \tag{8}$$

The $\Delta\overline{T}[\rho]$ is the difference in the average ground-state electronic kinetic energy between the molecule and the reference system of non-interacting electrons with electron density equal to that in the molecule. Let

$$\Delta\overline{V_{ee}}[\rho]\equiv\overline{V_{ee}}[\rho]-\frac{1}{2}\int\int\frac{\rho(r')\rho(r)}{|r'-r|}drdr' \tag{9}$$

The $\frac{1}{2}\iint \frac{\rho(r')\rho(r)}{|r'-r|}drdr'$ is the classical expression for the electrostatic inter-electronic repulsion energy. With the equations (6), (8) and (9) becomes

$$E_0[\rho] = \overline{V}_{Ne}[\rho] + \overline{T_s}[\rho] + \frac{1}{2}\iint \frac{\rho(r_1)\rho(r_2)}{r_{12}}dr_1 dr_2 + E_{xc}[\rho] \qquad (10)$$

where $E_{xc}[\rho]$ is the exchange-correlation energy which equals to $\Delta\overline{T}[\rho] + \Delta\overline{V_{ee}}[\rho]$. The $E_{xc}[\rho]$ part is remaining part after subtraction of the non-interacting kinetic energy, and the $\overline{V}_{Ne}[\rho]$ and the electrostatic inter-electronic repulsion energy terms. If the exact $E_{xc}[\rho]$ was known, DFT would provide the exact total energy, including electron correlation. Thus, many types of functionals are available; the simplest approximation is the ***local-density approximation (LDA)***, which is dependent only on the electron density. The ***Generalized Gradient Approximation (GGA)*** functionals are included the gradient of the electron density as well as the electron density. The ***Hybrid functional*** using the incorporation between HF and DFT exchange for calculating the $E_{xc}[\rho]$ term has also been proposed. Of all modern functionals, B3LYP has proven the most popular to date. The B3LYP model is defined by:

$$\begin{aligned} E_{xc}^{B3LYP} &= (1-a_0-a_x)E_x^{LSDA} + a_0 E_x^{exact} \\ &\quad + a_x E_x^{B88} + (1-a_c)E_c^{VWN} + a_c E_c^{LYP} \end{aligned} \qquad (11)$$

where E_x^{LSDA}, E_x^{exact} and E_x^{B88} are the LSDA (Local Spin Density Approximation) exchange energy, the Hartree-Fock exchange energy and the B88 (Beck's 1988) exchange energy, respectively. The terms E_c^{VWN} and E_c^{LYP} are the VWN (Vosko-Wilk-Nusiar) correlation energy and the LYP (Lee-Yang-Parr) correlation energy.

SCREEP method
(The Surface Charge Representation of the Electrostatic Embedding Potential)

In the quantum calculation of crystalline solids, one usually treats quantum only a small part of the crystal lattice quantum mechanically neglecting the effects from the rest of the crystal. There are many ways by which these effects may be used in quantum calculations such as the embedded cluster (Hiller *et al.*, 1994; Allavena *et al.* 1990; Barbosa *et al.*, 1986; Stefanovich *et al.*, 1998), ONIOM (Svensson *et al.*, 1996), QM-POT (Brändle and Sauer, 1997), and also periodic techniques (Kresse *et al.*, 1993; Segall *et al.*, 2002). Periodic quantum calculations can model the entire infinite crystal but it is not practical for the system which has the large unit cell as ZSM-5 zeolite and sometimes introduces unrealistic periodicities. To overcome the computational limitations of periodic method, while accounting for the effects of zeolite, two general embedding schemes have been developed: “electronic” and “mechanical”. The mechanical embedding procedures represent the crystal environment as a force field and the defect site is treated by using a quantum calculation. Here, the potential of the crystal environment is not included in the Fock matrix of the cluster, thus it does not polarize the cluster’s wave function directly. Nowadays, there are various types of mechanical embedding schemes which have been used for including the environmental effects, for example, the IMOMM (the integrated molecular orbitals/molecular mechanics), which was introduced by Maseras and Morokuma (1995); the QM-POT (Brändle and Sauer, 1997). Recently, Morokuma and co-workers introduced one of the most useful of the mechanical embedding procedures, the ONIOM formalism (Svensson *et al.*, 1996). In the ONIOM method, a small cluster is extended with an outer layer that is large enough for representing the effects of the neighbor atoms around the cluster. The atoms in the outer layer can be treated with a less expensive level than that for the atoms in the cluster. However, the long-range electrostatic contribution of the infinite crystal lattice of the framework is not included in this model. Also, the accuracy of the ONIOM method also depends on the method/model combinations. Alternatively, the electronic embedding schemes focus only on including the electronic environmental effect in the Fock matrix of a quantum mechanical cluster, effectively embedding the cluster in the external electrostatic field. Several methods have been developed for representing this electrostatic potential including: embedding the cluster in a finite set of lattice point charges where formal charges, half formal charges or charges derived from population analyses of cluster calculation are used (Allavena *et al.*, 1990); embedding the cluster in a finite set of point charges derived to represent the Madelung potential (Stephen *et al.*, 1994). The SCREEP method which is used in this study is one type of the electronic embedding scheme. In the SCREEP method, a finite set of point charges is derived from a mathematical device to represent the Madelung potential obtained from the Ewald summation.

In embedded cluster calculations, the model is divided into two parts: the inner part, the small part of crystal lattice which is treated with quantum mechanical, and the outer part, the action of the environment on electrons in the cluster which is represented by an embedding potential, Vembd(r). For many crystals, the electrostatic, or Madelung, potential Vel(r) makes a dominant contribution to the total embedding potential. Hence, many accurate methods have been developed for calculating the Madelung Potential, Vel(r) at any given point in the bulk and near crystal surfaces. The Ewald summation method is the best method for calculating the electrostatic potential at these points. But, the matrix elements of the Madelung potential of the Ewald summation, $\langle \mu | V_{el}(r) | \nu \rangle$ is not a trivial task. In the SCREEP method (Stefanovich and Troung, 1998), the idea is to replace the electrostatic potential from the extended charge distribution of the infinite crystal lattice by the potential from a finite set of point charges which make it appropriate for using in quantum chemistry programs. Also in the SCREEP model, there is an external Madelung potential which is divided by two sets of point charges. The potential from the unit cells that are nearest to the quantum cluster is represented by point charges located at the lattice sites (explicit point charges), where half formal charges are used. While the remaining component which is equal to the difference between potentials obtained from Ewald summation and explicit point charges is represented by a set of surface charges determined from the SCREEP method (surface point charges) as shown in Figure 2.

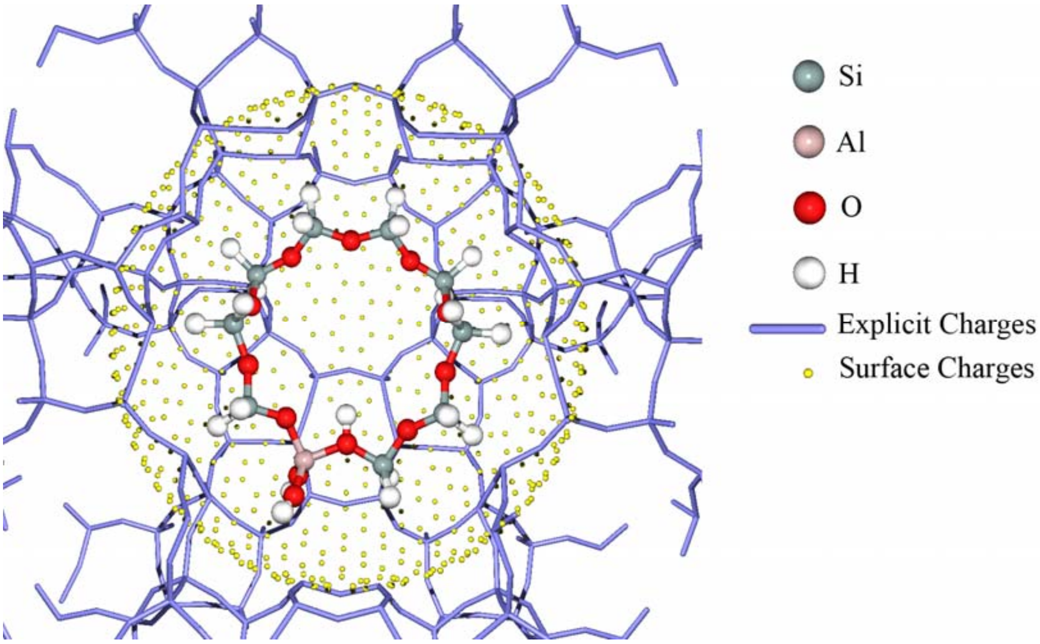

Figure 2 The embedded cluster models created from SCREEP approach**.**

Models and methodologies

1. ZSM-5 system

ZSM-5 has 12 unique tetrahedral (T) sites where an aluminum atom can substitute for the Si atom in the framework to form a Brønsted acid site. In this study, the active site is assumed to be the T12 site since it was predicted to be among the most stable Al-substitution sites and has been used to model the active site of ZSM-5 in many theoretical studies. In addition, it locates at the intersection of the main and sinusoidal channels and thus it is accessible adsorbates. The 10T cluster model, which is taken from the framework of ZSM-5 and is terminated by H atom and Si-H bonds are aligned with the corresponding Si-O bonds of the structure of ZSM-5 zeolite, was used to represent a complete 10-membered-ring of the main channel of ZSM-5 as illustrated in Figure 3.

2. FAU system

The bare cluster and embedded cluster models were used to determine the adsorbed structure of oxime molecules on zeolite (active site). The FAU zeolite is represented by the 12T cluster model (Figure 4) which is surrounded by two supercages taken from the crystal structure of the FAU to model the FAU system. A proton is added to one of the oxygen atoms bonded directly to the aluminum atom. There are four distinct bridging configurations. In this work, the proton is added to the O1 site which is usual convention for the oxygen atom in faujasite zeolite.

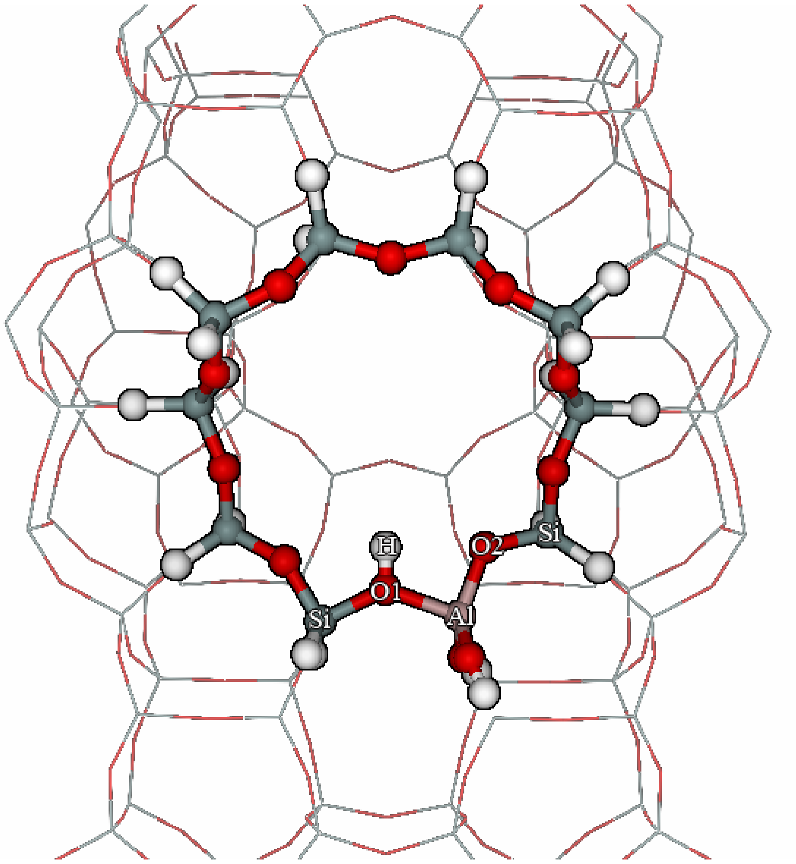

Figure 3 Presentation of the 10T bare cluster model of H-ZSM-5 zeolite**.**

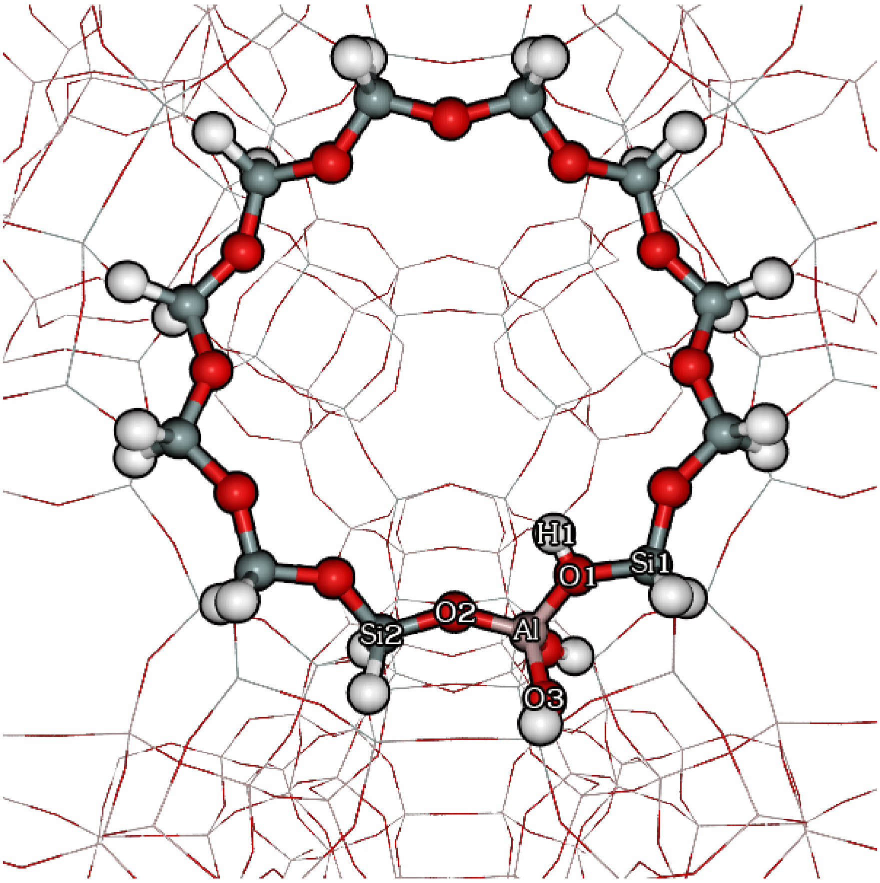

Figure 4 Presentation of the 12T bare cluster model of H-FAU zeolite**.**

For quantum calculation in two systems, the hybrid density functional theory, B3LYP level was used. Due to the size of the cluster, we used a mixed basis set to represent the whole system. In particular, the 6-31G(d,p) basis set was used for the active site region ($H_2Si1OAl(OH)_2O(H)Si2H_2$) and the adsorbate while a smaller 3-21G basis set was used for the remaining part of the cluster. In an attempt to improve the energetic properties, single-point energy calculations were done at the MP2 level of theory using the 6-311G(d,p) for the whole system.

In all geometrical optimizations of both systems, only the capping hydrogen atoms are fixed to be along the lattice Si-O bonds. Normal mode analyses were performed to verify that the optimized transition state does connect the intended reactant and product. All calculations were performed using the Gaussian98 program (Frisch *et al.*, 1998).

RESULTS AND DISCUSSION

Mechanism of Beckmann rearrangement in zeolite catalyst

1. Brønsted acidic site of ZSM-5 zeolite

Selected optimized bond lengths in the active site region are displayed in Figure 5. Values in parentheses are from the bare cluster calculations. Comparing the results between the cluster and the embedded cluster models, the Madelung potential has the effect of lengthening the O1-H1 bond distance (Brønsted acid site) from 97.0 to 97.7 pm. and shortening the adjacent Al-O bond, which is in accordance with Gutmann's rules. In addition, the Mulliken population on the H1 atom is slightly increased from 0.38 to 0.41, indicating that the Brønsted proton is more acidic due to the Madelung potential effect. From our previous calculations on smaller clusters, we found that the structure of the Brønsted site is not very sensitive to the cluster size. However, in this study, the 10T cluster is needed to accurately describe short-range electrostatic, repulsion-dispersion, and polarization interactions between the local regions surrounding the active site with the adsorbate.

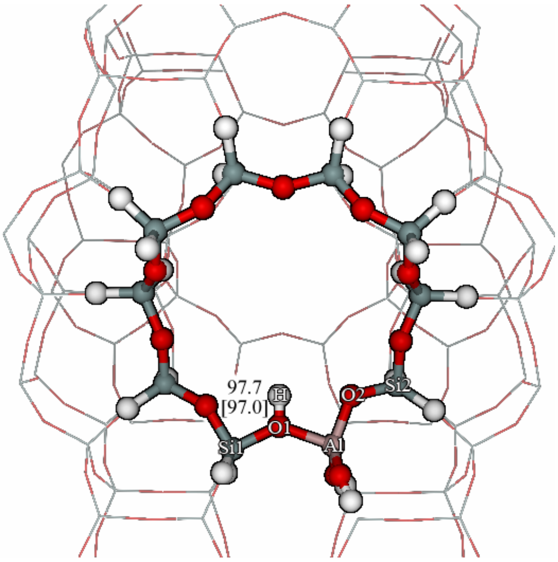

Figure 5 Optimized structures of 10T cluster and embedded cluster of H-ZSM-5 zeolite at B3LYP/6-31G(d,p) level of theory. (The values in parentheses are taken from the bare cluster.)

2. Adsorption complexes of formaldehyde oxime

There are two possible configurations for the adsorbed formaldehyde oxime (CH_2NOH) to interact with the Brønsted proton (H1) of ZSM-5 zeolite. One is where H1 forms a hydrogen bond with the Nitrogen atom of the oxime in what is referred to as the N-bound configuration, and the other is where H1 forms a hydrogen bond with the OH group to form the O-bound configuration. The key issue is whether the Brønsted site is able to protonate the adsorbed formaldehyde oxime.

Selected optimized geometrical parameters and adsorption energies for the N-bound complex calculated using both the bare and embedded cluster models are listed in Table 2. For simplicity in the discussion below, all energetic information is determined at the MP2/6-311G(d,p)//B3LYP level of theory, unless otherwise specified. Selected bond lengths are also shown in Figure 6(a) to facilitate the discussion. Both models predict that the N-bound complex is protonated. The adsorbed protonated complex forms two hydrogen bonds $O1^{\cdots}H1$ and $O2^{\cdots}H2$ in a seven-membered ring configuration where the oximes are nearly in the same plane with the 10T ring (the dihedral angle O1O2O5N is 166 degrees, see also Figure 6(a). The adsorption energy is predicted to be -42.2 kcal/mol from the embedded cluster model. Note that it is much larger than the value of -27.2 kcal/mol from the bare cluster model. This indicates that the effects of the Madelung potential are significant. In fact, the N-protonated oxime appears to be more ionic, as indicated by the total Mulliken population on the protonated $[CH_2N\mathbf{H}OH]^+$ subunit of 0.76 from the embedded cluster model as compared to that of 0.67 from the bare cluster model. It is interesting to note that the Madelung potential further separates the protonated oxime moiety from the zeolite framework as the O1-H1 and O2-H2 bond distances elongated by about 20 pm. This effect is similar to the solvation of an ion-pair complex. Similarly, the results for the O-bound complex are also shown in Table 2 and Figure 6(b). Here we observed even larger effects of the Madelung potential from the zeolite framework. In fact, it promotes protonation of the O-bound complex. This is evident by the fact that only a molecular adsorbed state was found using the bare cluster model, whereas only the protonated complex was found using the embedded cluster model. The adsorbed protonated O-bound complex also forms two hydrogen bonds with the two bridging oxygen atoms O1 and O2 of the zeolite framework, but in a six-membered ring configuration, where the oxime fragment is almost perpendicular to the plane of the 10T ring, (the dihedral angle O1O2O5N is 98 degrees, see also Figure 6(b). The adsorption energy of the protonated O-bound complex is -27.1 kcal/mol. Despite the Madelung potential inducing changes in the adsorption mode of the O-bound complex, it has a smaller increase on the adsorption energy (6.8 kcal/mol) as compared to 15.0 kcal/mol observed for the N-bound complex.

The protonated N-bound complex is much more stable than the protonated O-bound species by 15.1 kcal/mol from the embedded model, which can be compared to that of 18.4 kcal/mol in the isolated protonated formaldehyde oxime system (Nguyen *et al.*, 1997). This result suggests that the initial structure of the Beckman rearrangement is the protonated N-bound oxime. This finding is consistent with experimental observations by Fois *et al.* (2001) and Chung *et al.* (1999, 2001). The bare cluster model also predicts the N-protonated complex is more stable than the O-bound complex but only by 6.9 kcal/mol. This indicates that the Madelung potential has a larger degree of stabilization for the N-bound complex. However, as pointed out in previous theoretical studies, the N-bound complex does not lead directly to the Beckmann rearrangement. It must first transform to the O-bound complex. The mechanism for such a process is discussed below.

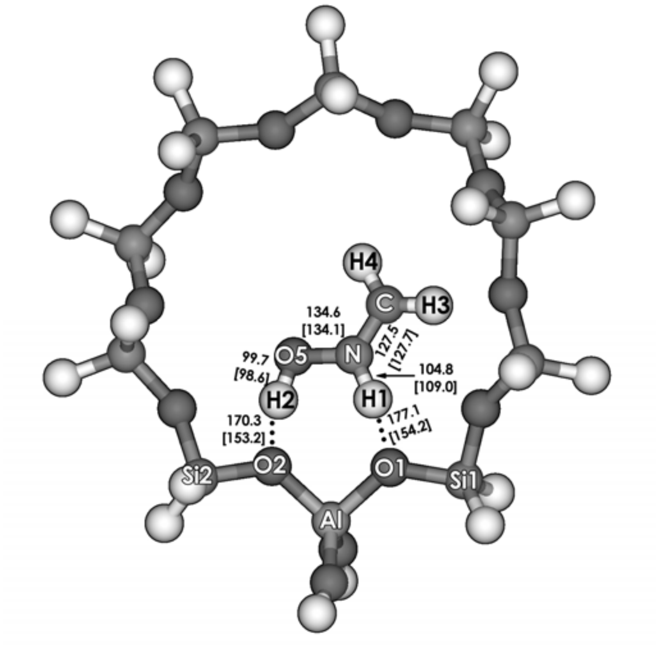

(a)

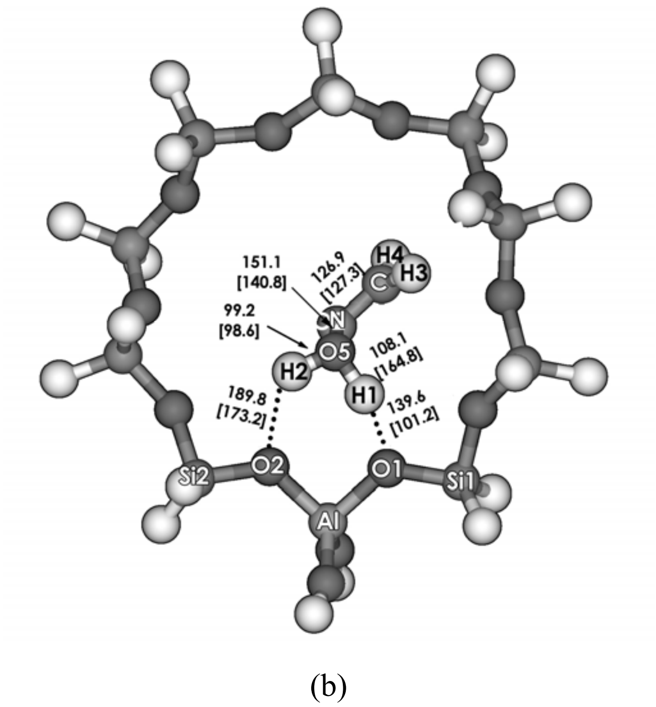

(b)

Figure 6 Optimized adsorption complexes on the 10T cluster and embedded cluster of H-ZSM-5 zeolite at B3LYP/6-31G(d,p) level of theory. (a) N-bound complexes. (b) O-bound complexes (The values in parentheses are taken from the bare cluster.)

Table 2 Optimized geometries and adsorption energy, ΔE_{ads} (in kcal/mol) for N-complexes and O-complexes in the bare clusters and embedded cluster at B3LYP/6-31G(d,p) level of theory. (Distances are in pm. and angles in degrees.)

Parameters	Models			
	N-complexes		O-complexes	
	10T cluster	10T embedded	10T cluster	10T embedded
O1-H1	154.2	177.1	101.2	139.6
N-H1	109.0	104.8	-	-
N-O1	262.0	279.2	-	-
O5-H1	-	-	164.8	108.1
O5-O1	-	-	261.5	245.7
O2-H2	153.2	170.3	173.2	189.8
H2-O5	98.6	99.7	98.6	99.2
O2-O5	254.0	268.1	257.4	266.4
N-O5	134.1	134.6	140.8	151.1
N-C	127.7	127.5	127.3	126.9
∠O1-H1-N	168.9	163.7	-	-
∠O2-H2-O5	165.7	165.7	-	-
∠O1-H1-O5	-	-	158.0	165.3
∠O2-H2-O5	-	-	141.0	131.8
∠O1-O2-O5-N	165.8	165.8	133.0	98.2
ΔE_{ads}	-32.2	-46.6	-20.5	-27.7
	-33.0^{a}	-48.2^{a}	-24.6^{a}	-30.0^{a}
	-27.2^{b}	-42.2^{b}	-20.3^{b}	-27.1^{b}

[a] The values are obtained at MP2//B3LYP level of theory.

[b] The values are obtained at MP2/6-311G(d,p)//B3LYP level of theory.

3. Mechanism of the Beckmann rearrangement

The mechanism of the Beckmann rearrangement of formaldehyde oxime on H-ZSM-5 zeolite consists of three steps. The first step is the 1,2 H-shift, which is the transformation from the N-bound configuration structure to the O-bound configuration structure. The second step is the rearrangement of the O-bound oxime complex to the amide complex, in which a hydrogen atom transfers from the CH_2 group to the nitrogen atom and a water molecule is displaced. The next step is the water binding to the carbon atom, then transferring a hydrogen atom to the NH group to form the intermediate product. The last step is tautomerization from the intermediate product to the amide product. The general feature of the potential energy surface for the first two steps is similar to the results obtained by Nguyen *et al.* for the protonated formaldehyde oxime system; however there are distinct differences as discussed below. The schematic energy profile reported by Fois *et al.* also consists of three steps. Unfortunately, no structural information along the reaction path was reported, thus making more detailed comparisons difficult.

For the first step, the 1,2 hydrogen shift, the optimized structure of the transition state is illustrated in Figure 7(a), and selected geometrical parameters and relative energies with the reference point being the infinitely separated oxime and zeolite are given in Table 3. The nature of the 1,2 H-shift for isomerization between the N-protonated oxime and the O-protonated oxime in ZSM-5 is very different when compared to that in the isolated protonated oxime system. In the isolated protonated oxime system, as studied by Nguyen *et al.* (1997), the transition state for the 1,2 H-shift has a rather tight structure where the active N-H and O-H bonds are less than 125 pm., whereas the transition state in the ZSM-5 zeolite has a rather loose structure where these active bonds are longer than 193.4 pm. In fact, at the transition state, the formaldehyde oxime is not protonated by ZSM-5 since the O1-H1 bond is only about 100.3 pm. Thus, the zeolite framework assists the 1,2 H-shift step by forming a neutral hydrogen bond complex rather than the ion-pair complex thus relieving most of the structural constraints seen in the tight transition state of the isolated protonated case. Consequently, the barrier for this step in ZSM-5 is only 23.8 kcal/mol from the embedded model as compared to 53.8 kcal/mol in the isolated protonated system reported by Nguyen *et al.,* 1997. The bare cluster model predicts the barrier for this step to be only 9.5 kcal/mol. This indicates that the Madelung potential from the zeolite framework has a much larger degree of stabilization of the N-bound protonate oxime than at the transition state.

Table 3 Optimized geometries and adsorption energy, ΔE_{ads} (in kcal/mol) for 1,2 H-shift transition state in the 10T bare cluster and embedded cluster at B3LYP/6-31G(d,p) level of theory. (Distances are in pm. and angles in degrees.)

Parameters	Models	
	10T cluster	10T embedded
O1-H1	98.2	100.3
N-H1	220.6	193.4
O5-H1	216.0	202.6
O5-O1	308.4	298.8
N-O1	306.8	283.7
H2-O5	98.5	97.6
H2-O2	180.0	202.7
O2-O5	272.6	288.3
N-O5	140.9	143.0
∠O1-H1-N	145.7	148.4
∠O1-H1-O5	156.1	160.0
∠O2-H2-O5	155.2	145.3
∠O1-O2-O5-N	58.9	60.2
ΔE_{ads}	-15.6	-16.0
	-20.0[a]	-19.6[a]
	-17.7[b]	-18.4[b]

[a] The values are obtained at MP2//B3LYP level of theory.

[b] The values are obtained at MP2/6-311G(d,p)//B3LYP level of theory.

Table 4 Optimized geometries and adsorption energy, ΔE_{ads} (in kcal/mol) for rearrangement step in the 10T bare cluster and embedded cluster at B3LYP/6-31G(d,p) level of theory. (Distances are in pm. and angles in degrees.)

Parameters	Rearrangement transition state		Enol-amide complex	
	10T cluster	10T embedded	10T cluster	10T embedded
O1-H1	193.6	232.4	101.3	113.6
O5-H1	98.5	97.4	157.5	129.7
O2-H2	176.4	205.4	196.6	209.3
O5-H2	99.3	97.6	98.5	98.0
O5-O1	275.6	309.9	256.6	242.2
O5-O2	270.2	293.0	265.1	269.1
N-O5	217.9	228.3	-	-
N-O2	400.0	475.4	428.1	427.4
N-H4	117.9	129.2	102.0	102.0
N-C	120.0	119.3	126.0	125.0
C-H3	111.4	110.5	109.3	108.9
C-H4	136.5	128.3	-	-
C-O5	-	-	136.4	139.7
∠C-N-O5	108.3	100.8	-	-
∠N-C-O5	-	-	120.6	117.9
∠O1-H1-O5	139.0	136.0	164.6	168.9
∠O2-H2-O5	156.1	148.4	124.4	117.6
ΔE_{ads}	44.8	6.2	-59.5	-63.2
	40.2[a]	0.1[a]	-66.0[a]	-69.0[a]
	44.3[b]	3.0[b]	-62.2[b]	-66.0[b]

[a] The values are obtained at MP2//B3LYP level of theory.

[b] The values are obtained at MP2/6-311G(d,p)//B3LYP level of theory.

Table 5 Optimized geometries and adsorption energy, ΔE_{ads} (in kcal/mol) for tautomerization step in the 10T bare cluster and embedded cluster at B3LYP/6-31G(d,p) level of theory. (Distances are in pm. and angles in degrees.)

Parameters	Tautomerization transition state		Keto-amide complex	
	10T cluster	10T embedded	10T cluster	10T embedded
O1-H1	102.2	137.6	107.5	163.8
O5-H1	154.0	109.0	140.0	101.4
O2-H2	-	-	196.0	185.4
O5-H2	130.0	123.0	-	-
O5-O1	256.7	245.3	247.0	264.6
O5-O2	287.2	288.2	343.4	368.7
N-O2	428.3	403.1	294.9	286.7
N-H4	101.0	101.0	100.0	101.2
N-H2	136.0	141.0	102.0	103.1
N-C	129.0	126.0	132.4	130.3
C-H3	108.0	108.0	109.0	108.9
C-O5	130.0	136.0	124.0	128.3
∠N-C-O5	106.8	103.7	125.5	124.7
∠O1-H1-O5	174.2	167.4	168.6	171.5
∠O5-H2-N	103.0	102.8	62.2	61.8
ΔE_{ads}	-25.8	-40.5	-78.3	-93.9
	-31.2[a]	-41.6[a]	-82.7[a]	-97.6[a]
	-26.1[b]	-36.3[b]	-78.5[b]	-94.5[b]

[a] The values are obtained at MP2//B3LYP level of theory.

[b] The values are obtained at MP2/6-311G(d,p)//B3LYP level of theory.

Table 6 Comparison of the adsorption energy, ΔE_{ads} (in kcal/mol) along the Beckmann rearrangement of formaldehyde oxime on 10T H-ZSM-5 zeolite in bare cluster and embedded cluster models by different methods. The values in square parentheses are obtained by the bare cluster model.

Geometry/method	ΔE_{ads}		
	B3LYP	MP2//B3LYP	MP2/6-311G(d,p)//B3LYP
N-bound complex	-46.6	-48.2	-42.2
	[-32.2]	[-33.0]	[-27.2]
1,2 H-shift TS	-16.0	-19.6	-18.4
complex	[-15.6]	[-20.0]	[-17.7]
O-bound complex	-27.7	-30.0	-27.1
	[-20.5]	[-24.6]	[-20.3]
Rearrangement TS	6.2	0.1	3.0
	[44.8]	[40.2]	[44.3]
Enol-amide complex	-63.2	-69.0	-66.0
	[-59.5]	[-66.0]	[-62.2]
Tautomerization TS	-40.5	-41.6	-36.3
	[-25.8]	[-31.2]	[-26.1]
Keto-amide complex	-93.9	-97.6	-94.5
	[-78.3]	[-82.7]	[-78.5]

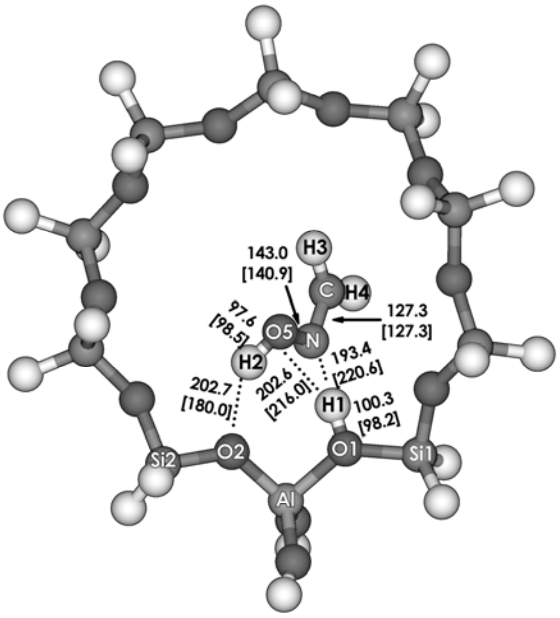

(a)

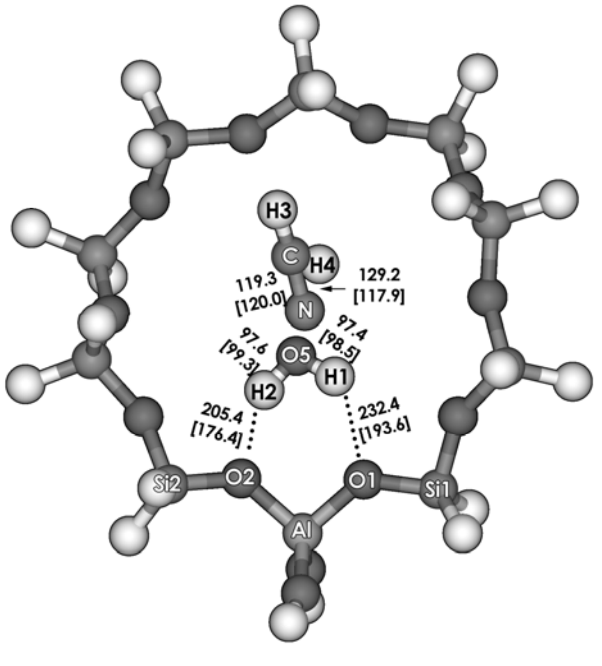

(b)

Figure 7 Optimized complexes on 10T H-ZSM-5 zeolite at B3LYP/ 6-31G(d,p) level of theory. (a) 1,2 H-shift transition state complexes. (b) Beckmann rearrangement transition state complexes. (The values in parentheses are taken from the bare cluster.)

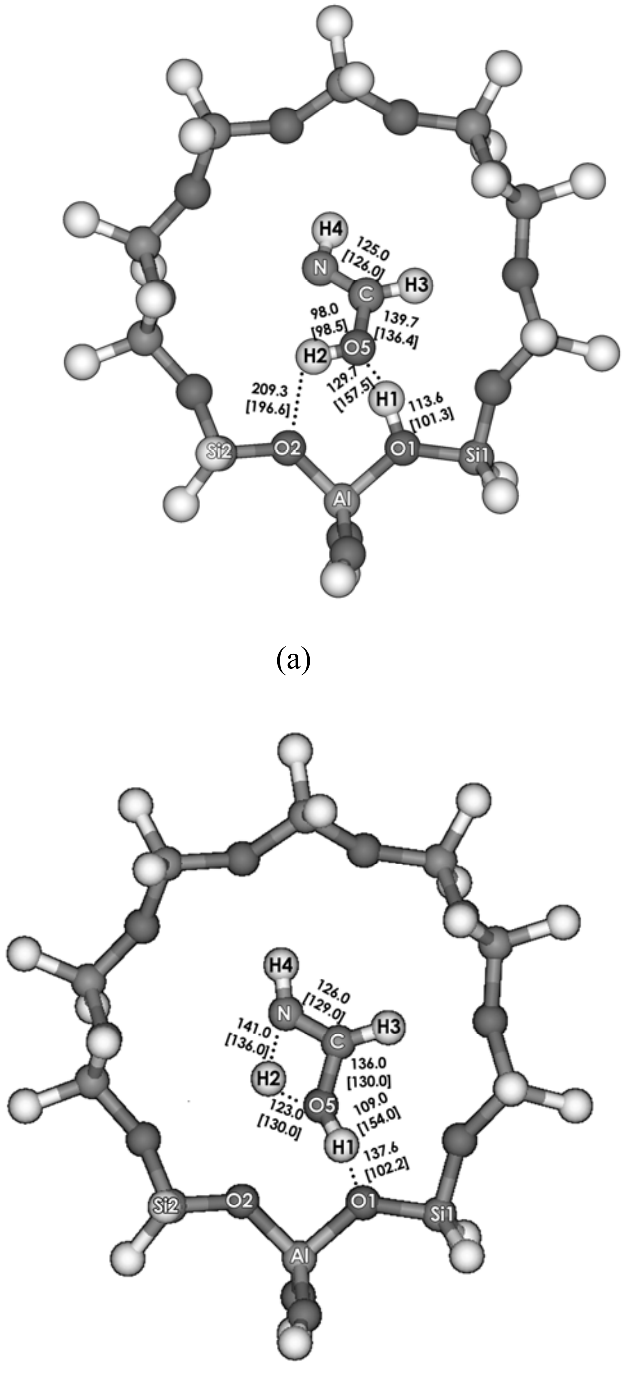

(a)

(b)

Figure 8 Optimized complexes on 10T H-ZSM-5 zeolite at B3LYP/ 6-31G(d,p) level of theory. (a) enol-amide acid complexes. (b) tautomerization transition state complexes. (The values in parentheses are taken from the bare cluster.)

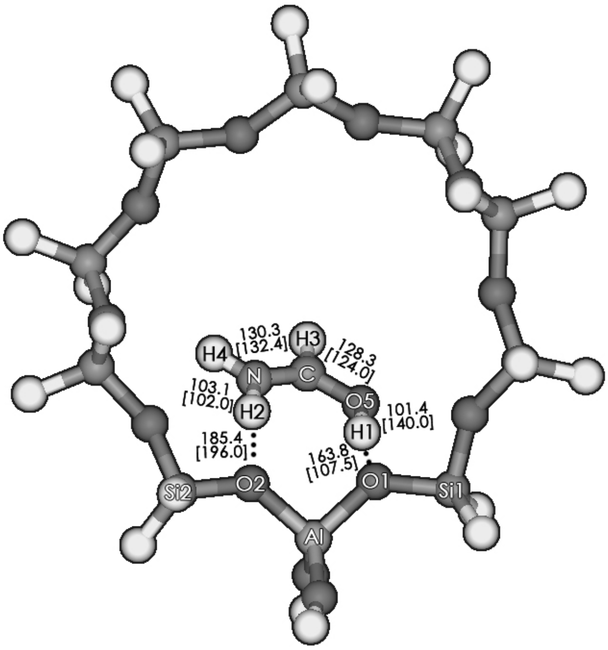

Figure 9 Optimized the keto-amide complex on 10T H-ZSM-5 zeolite at B3LYP/6-31G(d,p) level of theory. (The values in parentheses are taken from the bare cluster.)

Optimized geometry of the transition state for the rearrangement step is shown in Figure 7(b), with selected geometrical parameters and relative energies given in Table 4, along with the information for the intermediate, HNCHOH···HZ complex. Optimized geometry of the adsorbed enol-amide complex (formimidic acid) is also given in Figure 8(a). The rearrangement step consists of a concerted 1,2 H-shift from the CH_2 group to the nitrogen atom while releasing a water molecule by breaking the N-O bond. The transition state geometry qualitatively resembles that from the previous study on the protonated formaldehyde oxime. However, quantitatively there are differences, namely the transition state for reaction in zeolite is closer to the product side than that in the isolated system. Particularly, for reaction in zeolite the migrating hydrogen atom H4 is at the mid-way point between the C and N atoms (C-H4 and N-H4 bond distances are 128.3 and 129.2 pm., respectively) whereas it is still much closer to the reactant side for the isolated protonated oxime system (C-H and N-H active bond distances are 119.2 and 142.4 pm., respectively). The breaking N-O bond is also longer for reaction in zeolite (228.3 versus 205.6 pm.). The calculated barrier for this step is 30.1 kcal/mol from the embedded model that is almost 20 kcal/mol higher than the previously reported value of 10.5 kcal/mol for the isolated protonated oxime system. Comparing results between the embedded and bare cluster models we found that the Madelung potential noticeably shifts the transition state toward the primary product. The effect of the Madelung potential on the barrier height of this step, however, is much larger. Particularly, it lowers the activation energy by 34.5 kcal/mol.

However, the final product of the Beckmann rearrangement reaction of formaldehyde oxime is not formimidic acid (HNCHOH) which is the primary product obtained from the rearrangement step, but formamide, keto-amide complex (H_2NCHO). The final step is the tautomerization of the primary product, enol-amide complex (HNCHOH$\cdots$HZ complex) to the more stable product, keto-amide complex ($H_2NCHO\cdots HZ$ complex) by migrating the hydrogen atom (H2) from the oxygen atom (O5) to the nitrogen atom (N). Optimization geometry of the transition state for the tautomerization step is shown in Figure 8(b) and selected geometrical parameters are given in Table 5. The transferring proton (H2) is at the mid-way point between the O5 and N atoms (N-H2 and O2-H2 bond distance are 141.0 and 123.0 pm., respectively), which happens simultaneously with the slight shortening of the C-O5 bond and the elongating of the N-C bond for shifting to amide compound. However, comparing the tautomerized transition state structure between both models, we found that the protonation occurred concurrently during tautomerization in the embedded cluster model. The O1-H1 bond elongated by about 35 pm. to form an O-H single bond. The energy barrier for this step is predicted to be 29.7 kcal/mol by using the embedded cluster model. The effect of the Madelung potential from the zeolite framework has a slight effect in lowering the activation energy as compared to that obtained from the bare cluster model. The results obtained agree well with previous studies which have been investigated in the same reaction for other different molecules such as N-nitrobenzene-sulfonamides (Cox, 1997), isocyanates (Raspoet *et al.*, 1998), β-lactams (Pitarch *et al.*, 1998), carbodiimine (Lewis *et al.*, 1998) and acetamide (Barbosa *et al.*, 2000). The activation energy for the tautomerization step of these molecules is about 25-30 kcal/mol. Comparing to the activation energy for the previous arrangement step, it is slightly lower and thus both of these rearrangement steps could be the rate limiting step for the whole mechanism.

Finally, the final product of the reaction is formamide. The optimized geometry of the adsorbed keto-amide complex (formamide complex) is given in Figure 9. From the embedded cluster model, the adsorbed protonated formamide, $[H_2NC(O\mathbf{H})H]^+$ forms two strong hydrogen bonds of both -C=O$^+$-H and -NH$_2$ groups which interact with the two bridging oxygen atoms O1 and O2 of the zeolite framework in the eight-membered ring configuration whereas only the neutral formed complex was found from using the bare cluster model. Both adsorption complexes obtained correspond with their transition state structure in the tautomerization step. The adsorption energy of protonated formamide is calculated to be -94.5 kcal/mol by using the embedded cluster model. Comparison of the optimized structure which was obtained from both models with the isolated formamide, the structure of adsorbed formamide provides the lengthening of the C-O bond distance (by 2.4 and 6.7 pm. for the bare and embedded clusters, respectively) and shortening the C-N bond distance (by 4.1and 5.8 pm. for the bare and embedded clusters, respectively). The C-O bond length presents rather a single bond character while the C-N bond length shows rather a double bond character, similar to that observed by Cho *et al.* (1997). Changing of the C-O and C-N bond lengths is due mainly to the mesomeric effects resulting from the donation of the lone pair of electrons from the nitrogen atom that pass through the π-bond of the C=O bond to give a different resonance of formamide. In this study, it seems that the framework effect which is represented by the Madelung potential plays an important role the stabilization of the protonated N, O-formaldehyde oxime and formamide configurations, which is the crucial step for the Beckmann rearrangement reaction to occur.

The effects of the Madelung potential of the extended zeolite framework on the energetic and mechanism of this reaction can also be seen from Figure 10. In particular, the Madelung potential tends to stabilize the stable intermediates by 4-16 kcal/mol. It also lower the activation energies for all steps involved in this mechanism. The largest effect is at the rearrangement step from the O-bound oxime to the formimidic acid (Figure 6(b) → Figure 8(a)) where the Madelung potential lowers the activation energy by 34.5 kcal/mol. Consequently, it makes this rearrangement step having comparable activation energy with that of the tautomization from formimidic to formamide (Figure 8(a) → Figure 9) step, thus either could be the rate limiting step.

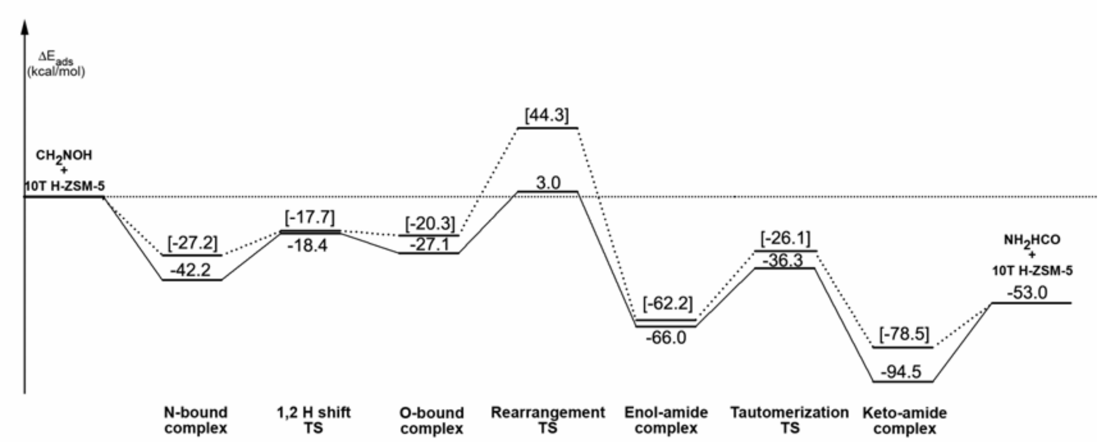

Figure 10 Energetic profile along the pathway Beckmann rearrangement of formaldehyde oxime adsorbed on 10T H-ZSM-5 zeolite at MP2/6-311G(d,p)//B3LYP level of theory. The energetic changes for the embedded cluster (solid line) and the bare cluster (dash line) complexes are in kcal/mol.

4. Discussion

From this study, we can conclude that the Beckmann rearrangement of the oxime molecule on the Brønsted acid site of zeolite consists of five steps as shown in the Scheme 3.

SCHEME 3

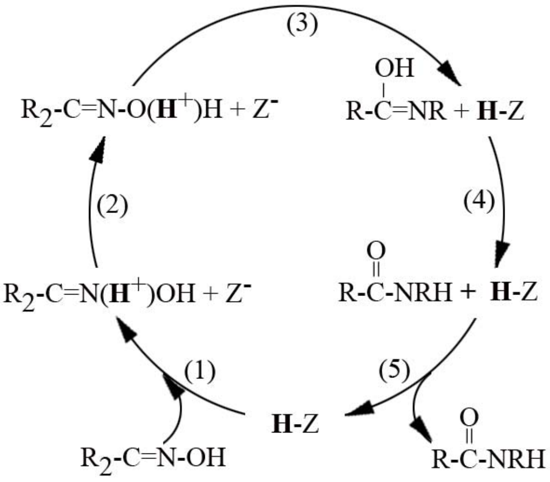

Step (1) is the adsorption of the oxime molecule, which is the interaction between the nitrogen atom of the oxime molecule and the Brønsted acid site of zeolite, to produce the protonation at the nitrogen atom of the oxime molecule (designated by N-bound). Then in Step (2), called the 1,2 H-shift step, the hydrogen is transferred from the nitrogen-end to the oxygen atom of the oxime molecule (designated as O-Bound). The rearrangement step, Step (3), involves the rearrangement of the O-Bound complex to the enol-amide complex (designated by enol-amide) in which an -R group (R = alkyl, aryl or hydrogen) at the trans-position transfers to the nitrogen atom and a water molecule is displaced. Subsequently, the displaced water molecule binds to the carbon atom, simultaneously, transferring a proton to the acid catalyst. The last transforming step, Step (4), is the tautomerization from the enol-amide complex to the amide complex (designated by keto-amide) and desorption of the amide molecule in the final step, Step (5).

From these results, it is indicated that the bare cluster model can not be used to describe the catalytic ability of the active site of the ZSM-5 zeolite and will also provide inaccurate results. Using the embedded cluster model (10T), the N-bound complex is more stable than that the O-bound complex by about 15 kcal/mol. The energy barrier for the 1,2 H-shift connecting N, O protonated species is 23.8 kcal/mol. Decreasing of the activation energy of this step, as compared with the gas phase model (≈ 60 kcal/mol), is due mainly to the zeolite framework assisting this step by catching the migrating hydrogen between one end and putting it on the other end. For the rearrangement step, it has the activation energy of 30.1 kcal/mol. The electrostatic field from the zeolite framework plays a significant role in stabilizing the ionic species in the rearrangement step. Therefore, the activation energy of the embedded cluster model in this step is significantly lower than that of the bare cluster model by about 30 kcal/mol. Furthermore, we found that the extended framework significantly affects results in the protonation of the formaldehyde oxime at both ends. In the last step, the activation energy of tautomerization step is slightly decreased when taking into account the extended framework. From the embedded cluster model calculations, one can conclude that the rate-determining step of reaction is either the rearrangement or tautomerization step which has an energy barrier of about 30 kcal/mol. From these results, the embedded technique is one of the possibly computational techniques to investigate the chemistry of very large systems with high precision. For understanding the behavior of the zeolite framework effect clearly, different types of zeolite such as FAU was used in the next step of this thesis work.

The influence of the framework to structures and energetic profiles of the vapor phase of the Beckmann rearrangement on different types of zeolite

In this part, the Beckmann rearrangement of formaldehyde oxime under a different zeolite framework, FAU zeolite, is investigated and the effects of different frameworks on the geometrical adsorption and energetic profile are compared. The selected optimized geometrical parameters and the adsorption energies for all species relating to the formaldehyde oxime system, which is calculated by using both the bare and embedded cluster models of FAU zeolite, are listed in the Tables 7-10 and illustrated in Figures 11-14. Comparing the results between the cluster and the embedded cluster models, it can be seen that the Madelung potential has the effect of lengthening the O1-H1 bond distance (Brønsted acid site) from 97.0 to 97.6 pm. and slightly shortening the adjacent Al-O bond indicating that the Brønsted proton is more acidic as a result of the Madelung potential effect as similar to that found in the ZSM-5 system described in part 1.

1. 1,2 H shift step

Optimized geometries of all complexes relating to this step are shown in the Figures 11 (a, b) and 12 (a), with selected geometrical parameters and relative energies given in Table 7. Comparing the adsorbed structures of formaldehyde oxime on the FAU system, the N-bound complex is in the form of a protonated complex and consists of the two strong hydrogen bond interactions between O5-H2-O2 and N-H1-O1 which can be observed from both the bare cluster and embedded cluster models. The O-bound complex forms a protonated complex only in the embedded cluster model which consists of two weak hydrogen bond interactions between O5-H1-O1 and O5-H2-O2. The adsorption energy of both modes is calculated to be -47.7 and -29.4 kcal/mol for N-bound and O-bound complexes, respectively. The transition state for connecting both adsorption complexes is the 1,2 H-shift. The structure of the transition state is shown in Figure 11 (b). The activation energy of this step is calculated to be 26.8 kcal/mol. The transition state structure obtained from bare cluster and embedded cluster calculations are quite similar. The O1-H1 bond distance of the embedded cluster model is slightly changed by about 3 pm. in comparison with that of bare cluster model. The higher energy barrier as compared with that of the bare cluster model can be explained by the fact that the N-protonated complex is effectively stabilized by the long-range electrostatic potential from the zeolite framework as similarly as observed in the ZSM-5 system. However, the activation energy obtained from the embedded cluster model of FAU zeolite is slightly higher by 3 kcal/mol as compared with that of ZSM-5 zeolite. It corresponds to the proton affinity (PA) of the H-ZSM-5 and H-FAU zeolites which were calculated by Eichler *et al.* (1997) (288.3 kcal/mol for H-ZSM-5 and 279.6 kcal/mol for H-FAU by using the QM-POT model). The larger the PA, the stronger the tendency of the zeolite framework to catch a proton. It can be observed from increasing the bond length between the oxime and the migrating hydrogen as shown in the Figures 7(a) and 11 (b) for H-ZSM-5 and H-FAU systems, respectively. The distance between the transferring proton (H1) and both N and O of the oxime are 186.0 and 188.0 pm., respectively, while in the case of H-ZSM-5 system, these bond lengths are lengthened (202.6 and 193.4 pm., respectively). This indicates that a zeolite having the larger proton affinity (PA) induces a more positive catalytic effect. This is in line with the solvent effects in the liquid phase in the study of Nguyen *et al.* (1997).

2. Rearrangement step

Optimized geometries of the transition state structure in this step are shown in Figure 12 (b), with selected geometrical parameters and relative energies given in Table 8. In this step, which consists of a concerted 1,2 H-shift from the -CH_2 group to the nitrogen atom while releasing a water molecule by breaking the N-O bond, the transition state geometry, qualitatively, resembles that from the previous studies both in the H-ZSM-5 system in the previous part. However, quantitatively there are differences, namely the transition state for this step in FAU zeolite is almost in the same plane with the 12T ring. While, in the ZSM-5 zeolite, the transition state structure is almost perpendicular to the plane of the 10T ring. The geometrical differences in transition state structure in both zeolites is due to the differences in pore dimensions. Indeed, ZSM-5 zeolite has a pore size of 0.55 nm, while FAU has a pore size of 7.4 nm. Thus, the transition state of formaldehyde oxime in this step is barely able to locate in the same plane of 10T of ZSM-5 zeolite. In the FAU system, the migrating hydrogen atom (H4) is nearly at the mid-way point between the C and N atoms (C-H4 and N-H4 bond distances are 137.0 and 119.0 pm., respectively), whereas it is still much closer to the reactant side for the isolated protonated oxime system (C-H and N-H active bond distances are 119.2 and 142.4 pm., respectively). But the calculated barrier for this step is 50.4 kcal/mol, which is almost double the previously evaluated value, 33.9 kcal/mol in the H-ZSM-5 system. This significant change may be due to the different topology of both zeolites which affect the stabilization of the transition state complex. From the previous studies (Corma *et al.*, 2003), they concluded that when the size of a guest molecule approaches the size of the pores and cavities of the zeolite, the electronic confinement can strongly influence the energetic situation of the reactant, changing its reactivity. In this case, the ZSM-5 zeolite has the size of pores and cavities smaller than that of FAU zeolite. Comparing the sizes between the reactant and the pore dimension of zeolites, we found that the ZSM-5 zeolite has the pore size and cavity which is more appropriate than that of FAU zeolite. Therefore, when the effect from the Madelung potential is taken into account, its effect in the ZSM-5 system is to significantly stabilize the TS structure more than that found in the FAU zeolite.

As a reaction intermediate, the enol-amide complex forms one hydrogen bond with the Brønsted acid site of FAU zeolite in both models, as illustrated in Figure 13(a). The adsorption energy of the enol-amide complex is -66.0 kcal/mol which coincidentally equals the evaluated value obtained from the embedded cluster model of H-ZSM-5 zeolite. The Madelung potential from the zeolite framework has an effect in increasing the adsorption energy by 10 kcal/mol as compared to that obtained from the bare cluster model. In comparison to the configuration O-bound complex, it is more stable by 36.6 kcal/mol. This is slightly less than the energy difference between the O-bound complex and the enol-amide complex in the ZSM-5 system (ΔE = 38.9 kcal/mol).

3. Tautomerization step

The optimized geometry of the transition state for the tautomerization step is shown in Figure 13(b) and selected geometrical parameters are given in Table 9. The transferring proton (H2) is at the mid-way point between the O5 and N atoms (N-H2 and O2-H2 bond distance are 141.2 and 123.2 pm., respectively), which happens simultaneously with the slight shortening of the C-O5 bond and the elongation of the N-C bond for shifting to the amide compound. Comparing the tautomerized transition state structure between both zeolites, it was found that the protonation occurred concurrently during tautomerization in the embedded cluster model, similar to that found in the H-ZSM-5 system in part 1. The O1-H1 bond was elongated by about 40 pm. to form an O-H single bond. Using the embedded cluster model, the energy barrier for this step is predicted to be 25.1 kcal/mol. The effect of the Madelung potential from the zeolite framework has a slight effect in lowering the activation energy as compared with that obtained from the bare cluster model by about 8 kcal/mol. The activation energy for this part of the reaction is slightly lower by 4 kcal/mol compared to that for the H-ZSM-5 system.

The final product of the embedded cluster model is the protonated keto-amide complex $[H_2NC(O\mathbf{H})H]^+$ which shows significant changing of the C-N and C-O5 bond distances. The C-N bond distance is shortened from 132.3 to 130.1 pm. and the C-O5 bond distance is lengthened from 125.0 to 128.4 pm. The desorption energy of the keto-amide complex in faujasite is 50.6 kcal/mol, which is higher than that of the N-bound complex in FAU zeolite (-47.7 kcal/mol). The high value indicates that the desorption of the product from zeolite might contribute significantly to the overall reaction rate which agrees well with the experimental observations mentioned in the Literature Review section, namely the strongly adsorbed product on the Brønsted acid site tends to increase the coke formation which causes of the catalyst deactivation.

The effects of the Madelung potential of the extended zeolite framework on the energetic and mechanism of this reaction can also be seen from Figures 15-16. In particular, the Madelung potential tends to stabilize the stable intermediates by 6-20 kcal/mol. But in this case, it slightly lowers the activation energies for all steps involved in this mechanism. The largest effect is at the rearrangement step from the O-bound oxime to the enol-amide complex (Figure 13(a) → Figure 14) where the Madelung potential decreases the activation energy by 10 kcal/mol. The calculated activation energy of the rearrangement step on the embedded cluster model of H-FAU is 50.4 kcal/mol, over 20 kcal/mol higher than that of H-ZSM-5 zeolite. It is the rate limiting step of the reaction which is actually too high to be real as opposed to the investigation in the H-ZSM-5 system in part 1. From these results, it is indicated that the embedded cluster model provides different results to those obtained from the bare cluster model, which predicted similar activation energy for all steps involved in this mechanism as shown in Figures 15-16. This shows that the influences from the zeolite lattice have an important effect on both the reaction mechanism and the energetic profile.

Table 7 Optimized geometries and adsorption energy, ΔE_{ads} (in kcal/mol) N-bound, 1,2 H-shift and O-bound complexes of formaldehyde oxime on the 12T bare cluster and embedded cluster at the B3LYP level of theory. The values in square parentheses are taken from the bare cluster model. (Distances are in pm. and angles in degrees.)

Parameters	Models					
	N-bound complex		1,2 H-shift TS		O-bound complex	
O1-H1	[142.4]	165.6	[104.0]	100.6	[102.8]	135.3
N-H1	[111.0]	105.0	[159.0]	188.0	-	
N-O1	[252.0]	268.0	[255.0]	284.0	-	
N-O5	[133.0]	134.0	[142.0]	144.0	[142.0]	152.0
O5-H1		-	[155.0]	186.0	[151.0]	109.0
O5-H2	[102.0]	100.0	[99.0]	97.0	[98.0]	98.0
O5-O1		-	[249.0]	278.0	[251.0]	243.0
O5-O2	[260.0]	273.0	[259.0]	294.0	[272.0]	283.0
O2-H2	[159.0]	174.0	[174.0]	218.0	[192.0]	215.0
O1-H1-N	[170.4]	165.4	[153.1]	161.9	-	
O1-H1-O5			[147.4]	151.0	[161.6]	170.5
O2-H2-O5	[170.8]	171.1	[142.8]	134.5	[136.4]	125.8
C1-N-O5	[120.9]	121.4	[113.4]	110.7	[111.0]	107.5
O1-O2-O5-N	[7.53]	6.36	[71.8]	62.1	[115.4]	96.6
ΔE_{ads}	-51.9		-20.8		-31.7	
	[-32.6]		[-3.3]		[-21.3]	

Table 8 Optimized geometries and adsorption energy, ΔE_{ads} (in kcal/mol) rearrangement transition state and enol-amide complexes of formaldehyde oxime on the 12T bare cluster and embedded cluster at the B3LYP level of theory. T he values in square parentheses are taken from the bare cluster model. (Distances are in pm. and angles in degrees.)

Parameters	Models			
	Rearrangement TS		Enol-Amide complex	
O1-H1	[172.1]	165.0	[100.7]	110.6
N-C1	[119.0]	120.0	[125.0]	124.0
N-H3	[120.0]	119.0	[102.0]	102.0
O5-H1	[98.0]	98.0	[159.8]	133.1
O5-O1	[269.8]	253.2	[260.4]	243.4
O2-H2	[219.0]	171.0	[302.0]	281.0
C1-O5	-	-	[137.0]	140.0
C1-H3	[133.0]	137.0	-	-
C1-H4	[112.0]	109.0	[108.0]	108.0
O1-H1-O5	[168.8]	147.0	[175.7]	174.7
O2-H2-O5	[125.7]	134.5	[98.9]	102.2
C1-N-O5	[112.9]	108.7	-	-
N-C1-O5	-	-	[120.5]	117.8
ΔE_{ads}	26.3 [38.7]		-64.1 [-55.1]	

Table 9 Optimized geometries and adsorption energy, ΔE_{ads} (in kcal/mol) tautomerization transition state and keto-amide complexes of formaldehyde oxime on the 12T bare cluster and embedded cluster at the B3LYP level of theory. The values in square parentheses are taken from the bare cluster model. (Distances are in pm. and angles in degrees.)

Parameters	Models			
	Tautomerization TS		Keto-Amide complex	
O1-H1	[102.3]	137.9	[109.9]	162.8
N-C1	[129.0]	126.7	[132.3]	130.1
N-O2	-	-	[286.8]	287.9
N-H2	[136.1]	141.2	[102.6]	103.0
N-H3	[101.5]	101.8	[101.0]	101.5
O5-H1	[153.6]	108.9	[134.8]	101.4
O5-H2	[129.2]	123.2	-	-
O5-O1	[256.0]	246.6	[244.4]	263.3
O2-H2	-	-	[186.2]	185.8
C1-O5	[131.2]	137.5	[125.0]	128.4
C1-H4	[108.9]	109.1	[109.7]	108.9
O1-H1-O5	[179.4]	174.7	[173.9]	169.9
O2-H2-N	-	-	[166.0]	170.2
N-C1-O5	[106.4]	103.2	[125.8]	125.8
O5-H2-N	[103.4]	102.9	-	-
ΔE_{ads}	-41.6 [-24.5]		-103.9 [-82.3]	

Table 10 Comparison of the adsorption energy, ΔE_{ads} (in kcal/mol) along the Beckmann rearrangement of formaldehyde oxime on the 12T H-FAU zeolite in the bare cluster and embedded cluster models by different methods. The values in square parentheses are taken from the bare cluster model.

Geometry/method	ΔE_{ads}		
	B3LYP	MP2//B3LYP	MP2/6-311G(d,p)//B3LYP
N-bound complex	-51.9	-52.3	-47.7
	[-32.6]	[-33.4]	[-29.6]
1,2 H-shift TS complex	-20.8	-23.3	-20.9
	[-3.3]	[-6.6]	[-5.1]
O-bound complex	-31.7	-32.8	-29.4
	[-21.3]	[-23.6]	[-21.2]
Rearrangement TS	26.3	21.4	21.0
	[38.7]	[34.0]	[39.1]
Enol-Amide complex	-64.1	-68.3	-66.0
	[-55.1]	[-59.7]	[-57.7]
Tautomerization TS	-41.6	-45.1	-40.9
	[-24.5]	[-28.0]	[-24.5]
Keto-Amide complex	-103.9	-107.4	-103.6
	[-82.3]	[-85.7]	[-82.5]

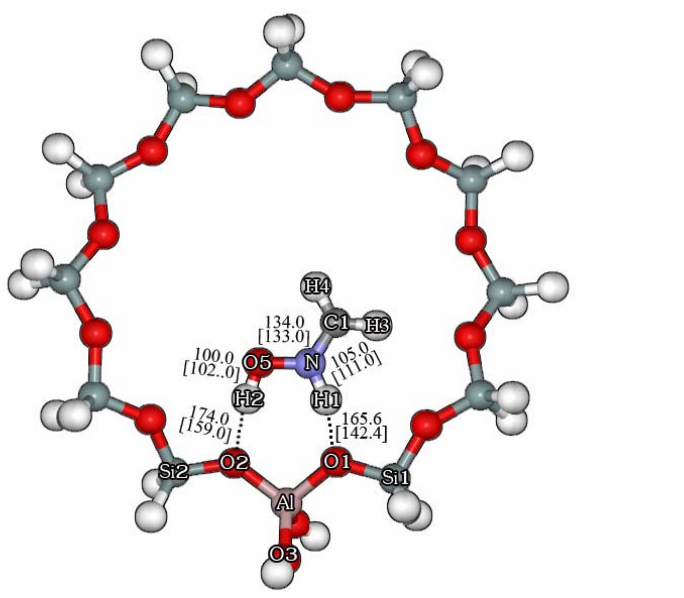

(a)

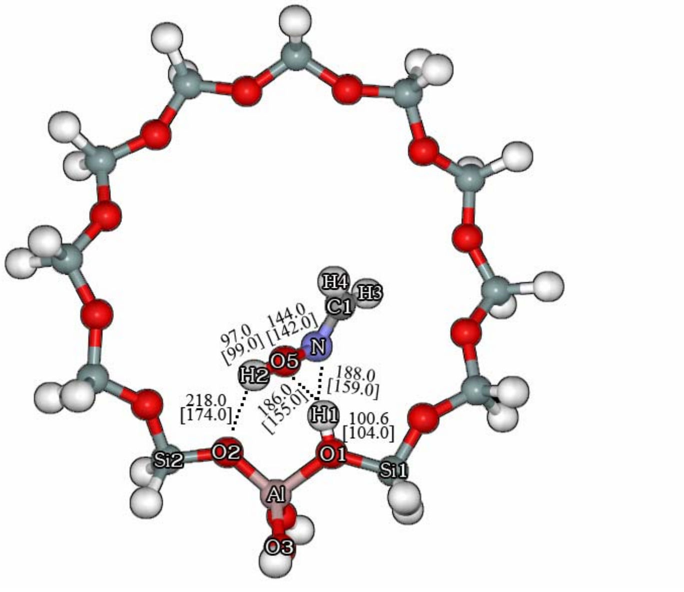

(b)

Figure 11 Optimized complexes on the 12T FAU zeolite at B3LYP/ 6-31G(d,p) level of theory. (a) N-bound complex. (b) 1,2 H-shift transition state complexes. (The values in parentheses are taken from the bare cluster.)

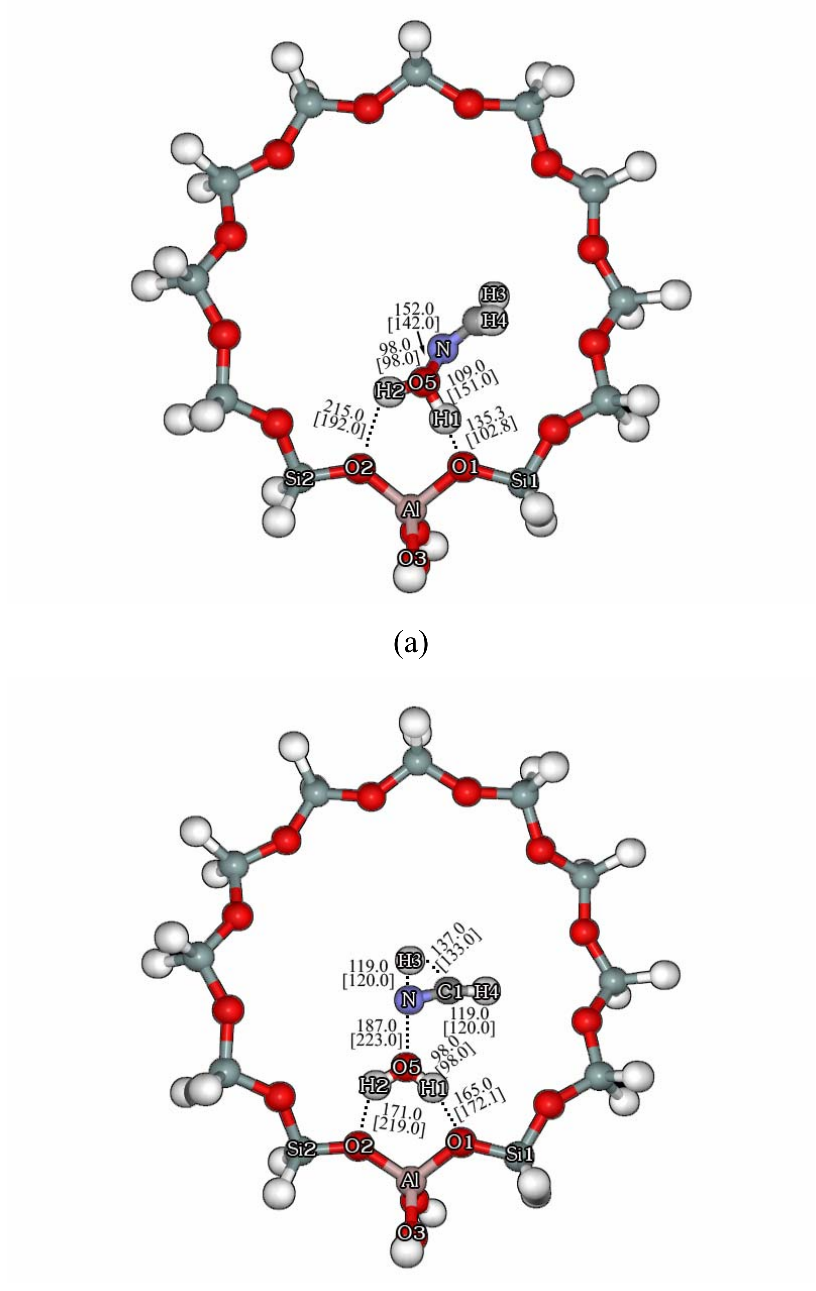

(a)

(b)

Figure 12 Optimized complexes on the 12T FAU zeolite at B3LYP/6-31G(d,p) level of theory. (a) O-bound complex. (b) Beckmann rearrangement transition state complex. (The values in parentheses are taken from the bare cluster.)

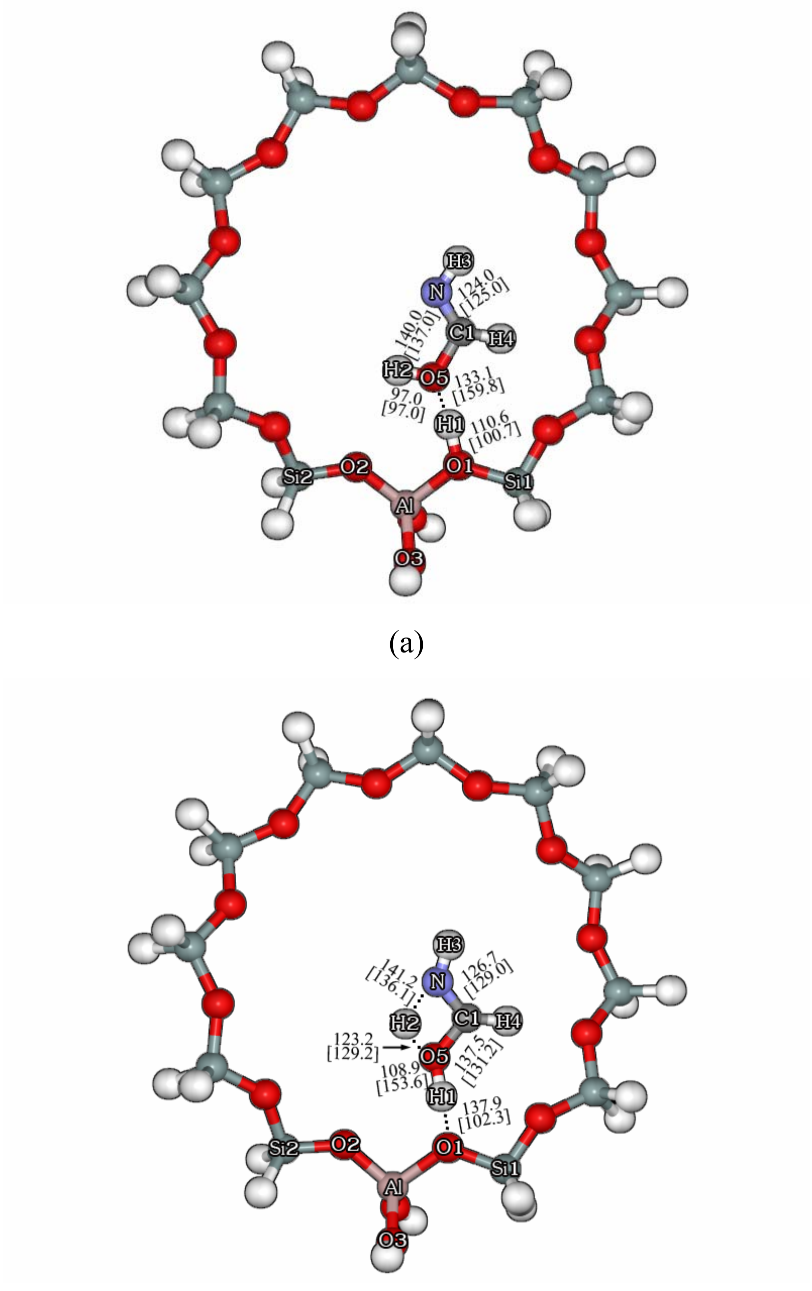

(a)

(b)

Figure 13 Optimized complexes on the 12T FAU zeolite at B3LYP/ 6-31G(d,p) level of theory. (a) enol-Amide complex. (b) tautomerization transition state complex. (The values in parentheses are taken from the bare cluster.)

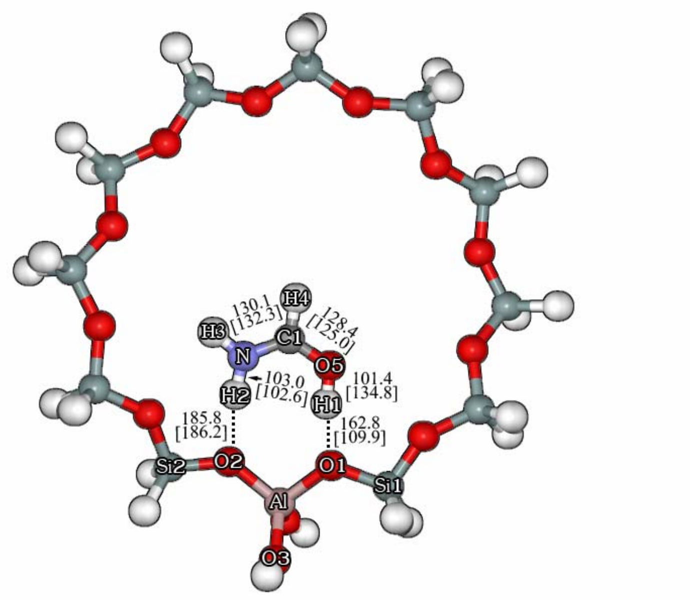

Figure 14 Optimized enol-amide complex on the 12T H-FAU zeolite at B3LYP/ 6-31G(d,p) level of theory. (The values in parentheses are taken from the bare cluster.)

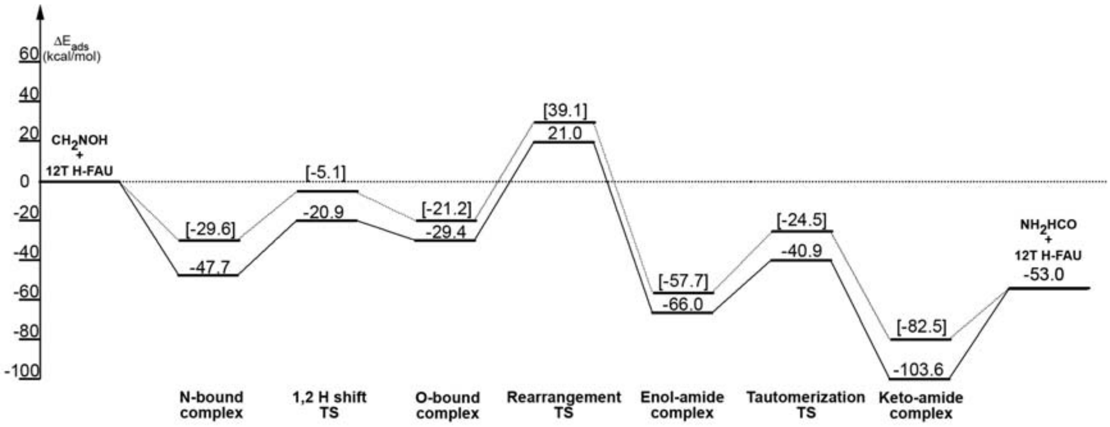

Figure 15 Energetic profile along the pathway Beckmann rearrangement of formaldehyde oxime adsorbed on the 12T H-FAU zeolite at MP2/6-311G(d,p)//B3LYP level of theory. The energetic changes for the embedded cluster (solid line) and the bare cluster (dash line) complexes are in kcal/mol.

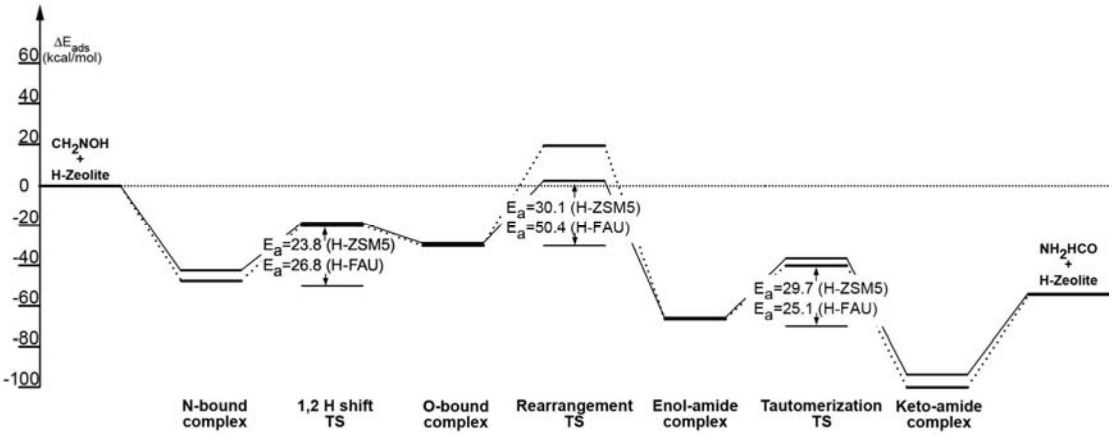

Figure 16 Energetic profile along the pathway Beckmann rearrangement of formaldehyde oxime adsorbed on zeolites at MP2/6-311G(d,p)//B3LYP level of theory. The energetic changes for the embedded cluster model of 10T of H-ZSM-5 zeolite (solid line) and the embedded cluster model of 12T of H-FAU zeolite (dot line) complexes are in kcal/mol.

4. **Discussion**

The mechanism of Beckmann rearrangement reaction on H-FAU starts with protonation of the formaldehyde oxime at the nitrogen-ended to form the O-bound complex via the 1,2 H-shift step. Comparing the energetic profile obtained from both zeoltes as shown in the Figure 16, the activation of the first step of FAU system is 26.8 kcal/mol, slightly higher than that of ZSM-5 system (23.8 kcal/mol). The height of energy barrier in this step corresponds to the proton affinity value of the zeolite framework which indicates the tendency of the zeolite framework to catch a proton. Therefore, the zeolite having the larger proton affinity (PA) induces a more positive catalytic activity in this step. The rearrangement step which is expected to be the rate-determining step of reaction which has a barrier equal to 50.6 kcal/mol which is significantly higher than the energy barrier of this step in H-ZSM-5 zeolite (30.1 kcal/mol). It is due principally to the size of formaldehyde oxime which is quite fit with the sizes of pores and cavities in H-ZSM-5 more than the sizes of pores and cavities in H-FAU zeolite. Therefore, when taking into account the extended framework, its effect in ZSM-5 system significantly stabilizes the TS structure better than that found in the FAU zeolite. In the last step, the tautomerization step on the H-FAU zeolite (25.1 kcal/mol) has the energy barrier slightly less than that of ZSM-5 system (29.7 kcal/mol). From a quantitative point of view, the ZSM-5 has catalytic activity better than the FAU zeolite in rearranging the formaldehyde oxime to the formamide which is the final product of the Beckmann rearrangement reaction. For answering the unsuitable relationship between the size of formaldehyde oxime molecule as compared with the sizes of pores and cavities of FAU zeolite, therefore in the next step of investigation, the formaldehyde oxime was increased its size by substituting the methyl group at the carbon atom of formaldehyde oxime.

Influence of the framework and substituted group effects to structures and energetic profiles

In order to investigate the reactivity of oximes having different molecular sizes, we chose the formaldehyde oxime as the smallest oxime model and increased its size by substituting the methyl group at the carbon-end of formaldehyde oxime. It is divided into two ways. First, one methyl group is replaced in the formaldehyde oxime at the cis-, and trans- positions, respectively. In the next model, both H atoms at the carbon-end are substituted with two methyl groups, actone oxime. The purpose of investigating both Z-, E-$(CH_3)CHN$-OH and $(CH_3)_2CN$-OH systems have two aims: (1) investigating the effect of the mono-substituted methyl group as an electron donating group and migrating group to the energetic profile; (2) In the case of $(CH_3)_2CN$-OH system, it imitates the effect of the larger oximes such as cyclohexanone oxime. For facilitating the presentation of data hereafter, we designated the notations H_2C=NOH, Z-MeHC=NOH, E-MeHC=NOH and Me_2C=NOH standing for the formaldehyde oxime, Z-acetaldehyde oxime, E-acetaldehyde oxime and acetone oxime systems, respectively. The calculated results are summarized in the Figures 17-23.

1. 1,2 H-shift step

Selected geometrical parameters of the N-bound and O-bound complexes calculated using both the bare and embedded cluster models are illustrated in Figure 17-18. The adsorption energy of the N-bound complex is -47.7, -54.9, -51.0 and -58.2 kcal/mol for the H_2C=NOH, Z-MeHC=NOH, E-MeHC=NOH and Me_2C=NOH systems, respectively. This N-bound complex is in the form of a protonated complex consisting of the two strong hydrogen bond interactions between O5-H2-O2 and N-H1-O1, which can be observed from both the bare cluster and embedded cluster models, and correspond to the previous calculated results in the ZSM-5 zeolite. The O-bound complex also forms a protonated complex, but only in the embedded cluster model which consists of two weak hydrogen bond interactions between O5-H1-O1 and O5-H2-O2. The adsorption energy of this complex is -29.4, -35.3, -36.4 and -38.3 kcal/mol for the $H_2C=NOH$, Z-MeHC=NOH, E-MeHC=NOH and $Me_2C=NOH$ systems, respectively. The increase of the adsorption energy of the N-bound and O-bound complexes in the system with the methyl group substitution at the carbon center agrees well with enhancement of the basicity of both N and O centers. These results from the inductive effect of the substituted methyl groups which attach at the C atom that acts as the electron donating group. From previous calculations (Nguyen *et al.*, 1997) using the MP4/6-311G(d,p)//MP2/6-31G(d) + ZPE, it is found that the order of PA (proton affinity) at the N center of all oximes is $H_2C=NOH$ < Z-MeHC=NOH ≈ E-MeHC=NOH < $Me_2C=NOH$, respectively, while the order of the PA at the O center is $H_2C=NOH$ < Z-MeHC=NOH < E-MeHC=NOH < $Me_2C=NOH$. In the transition state connecting between both complexes (see Figure 19), the active H atom locates in the midway point between the N and O atoms with the N-H and O-H active distance being about 185 pm., which corresponds to the previous study in zeolite systems: MOR (Bucko *et al.*, 2004) (≈190 pm.), ZSM-5 (≈195 pm.). It is, therefore, indicated that the nature of the 1,2 H-shift in zeolite systems is less tight than in the gas phase model where the active N-H and O-H bonds are less than 125 pm. in length. In this step, it can be concluded that the zeolite framework plays an important role in assisting the shuttling-proton (H1). For the embedded cluster model, the activation energy of this step is 26.8, 30.5, 26.2, and 31.2 kcal/mol for the $H_2C=NOH$, Z-MeHC=NOH, E-MeHC=NOH and $Me_2C=NOH$ systems, respectively and is quantitatively similar to the previous calculations: in ZSM-5 (23.7 kcal/mol) and MOR (21.0 kcal/mol) zeolites. It is clearly that the barrier height of this step corresponds to the difference of PA between at the N center and at the O center [ΔPA=PA(N)-PA(O)]. The order of ΔPA is $H_2C=NOH$ < E-MeHC=NOH < Z-MeHC=NOH < $Me_2C=NOH$, respectively.

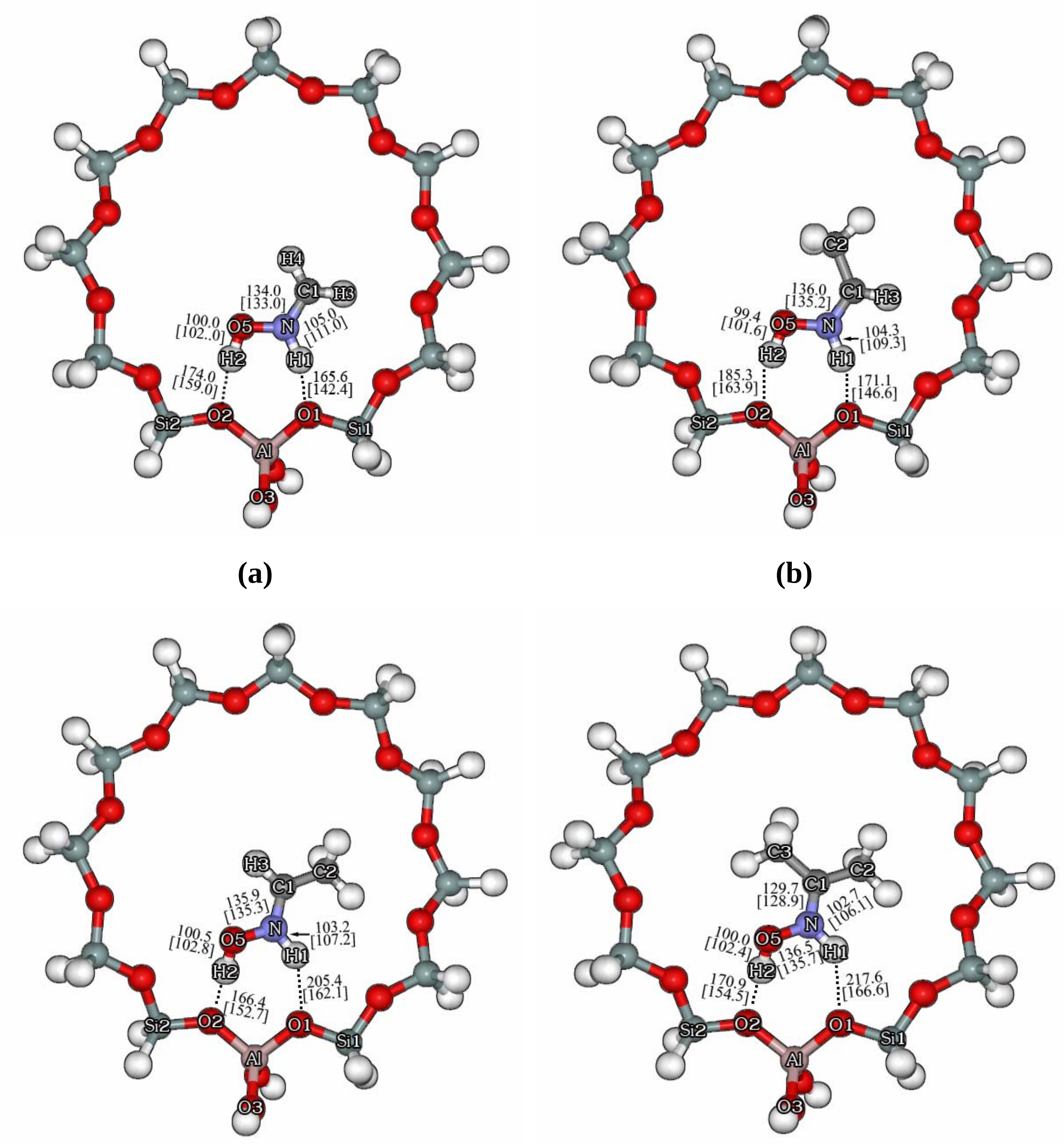

(a) **(b)**

(c) **(d)**

Figure 17 Optimized geometrical parameters of the corresponding N-bound complexes of (a) $H_2C=NOH$, (b) Z-MeHC=NOH, (c) E-MeHC=NOH, and (d) $Me_2C=NOH$ molecules on the 12T cluster and embedded cluster of H-FAU zeolite at the B3LYP/6-31G(d,p) level of theory.

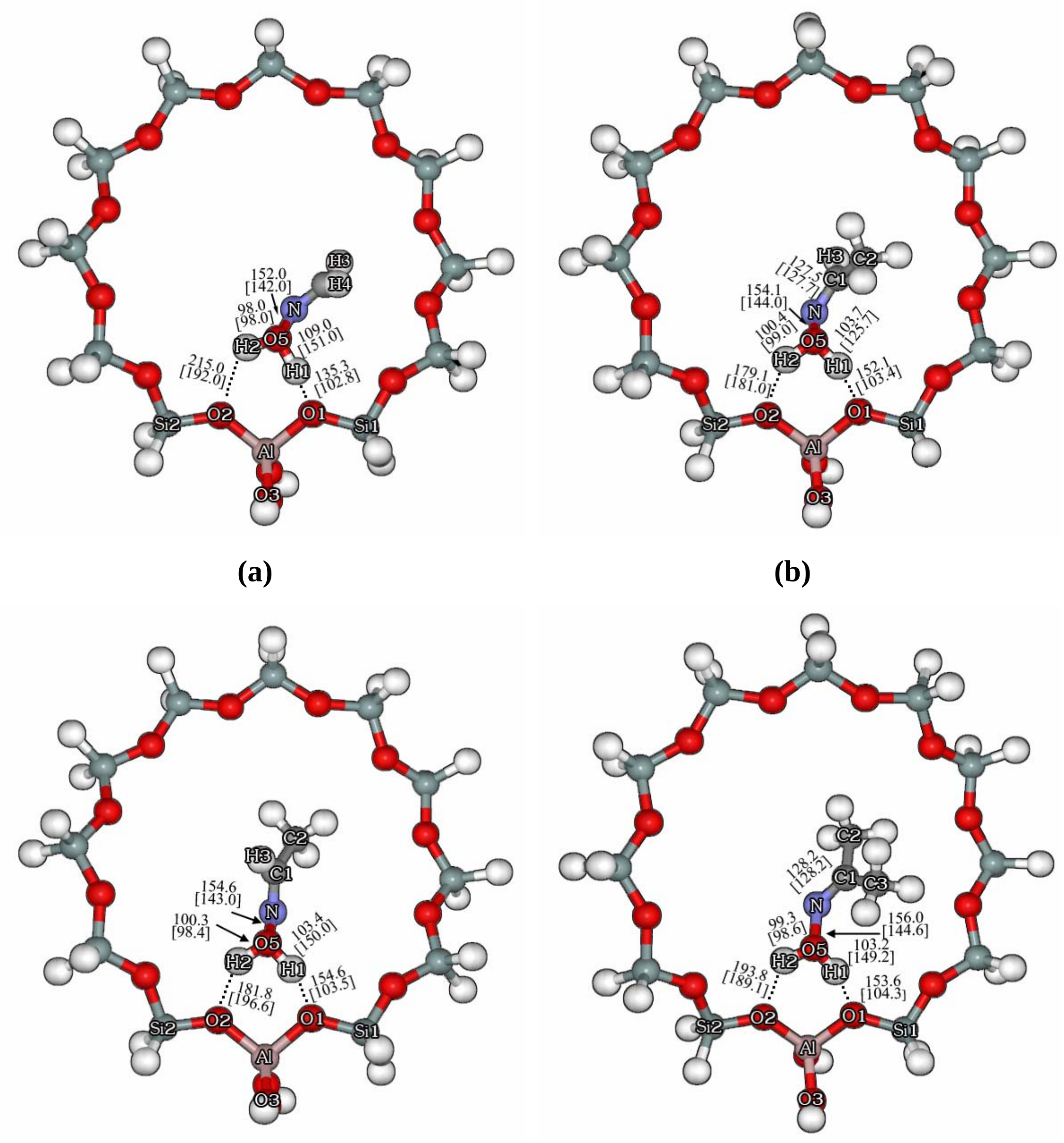

(a) **(b)**

(c) **(d)**

Figure 18 Optimized geometrical parameters of the corresponding O-bound complexes of (a) H_2C=NOH, (b) Z-MeHC=NOH, (c) E-MeHC=NOH, and (d) Me_2C=NOH molecules on the 12T cluster and embedded cluster of H-FAU zeolite at the B3LYP/6-31G(d,p) level of theory.

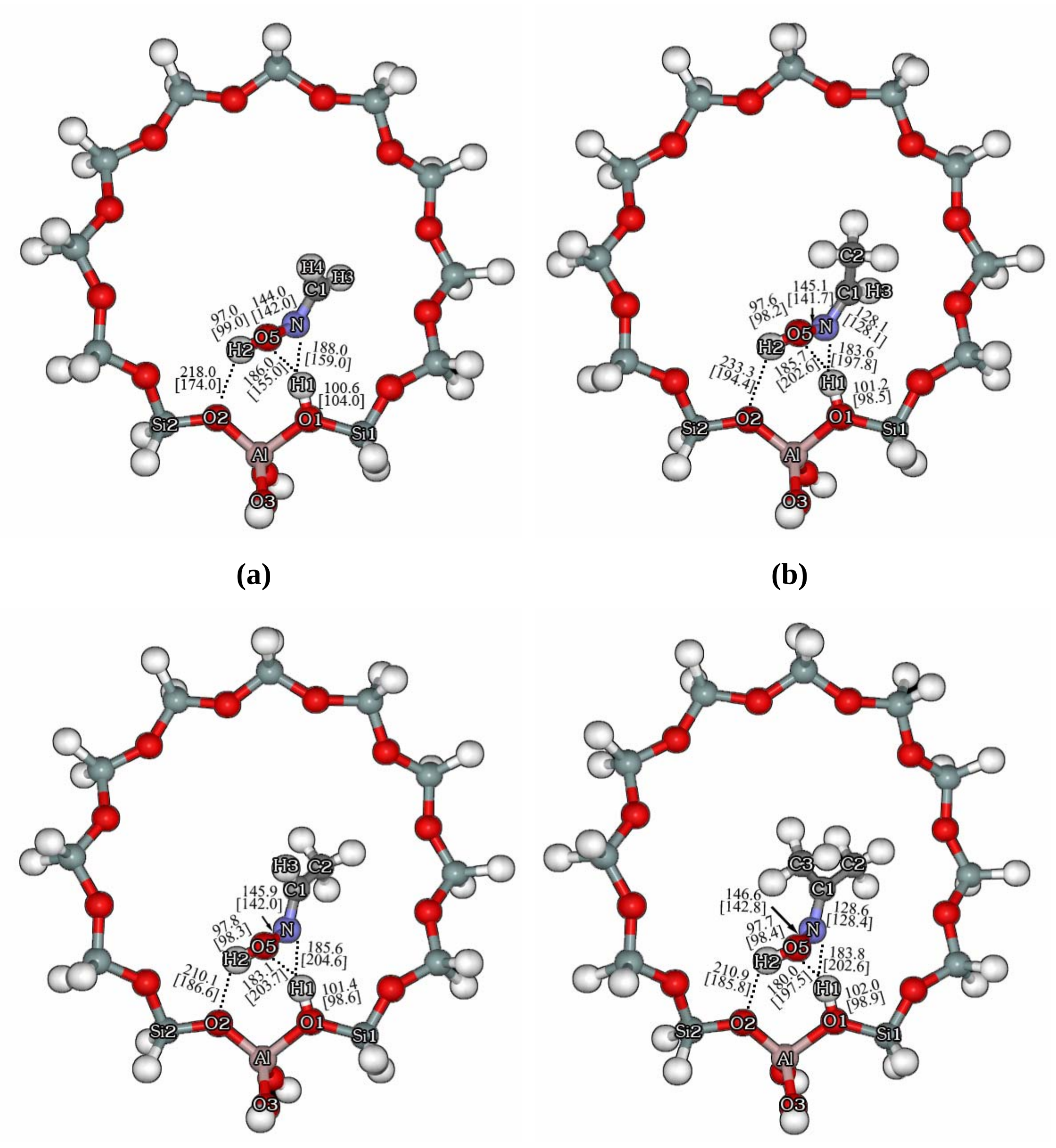

(a) **(b)**

(c) **(d)**

Figure 19 Optimized geometrical parameters of the corresponding 1,2 H-shift transition state structure of (a) $H_2C=NOH$, (b) Z-MeHC=NOH, (c) E-MeHC=NOH, and (d) $Me_2C=NOH$ molecules on the 12T cluster and embedded cluster of H-FAU zeolite at the B3LYP/6-31G(d,p) level of theory.

2. Rearrangement step

The optimized geometry of the transition state for the rearrangement step is shown in Figure 20. This rearrangement step consists of a concerted 1,2-H-shift from the CH_2 group in the case of the H_2C=NOH and Z-MeHC=NOH systems or the methyl migration in the case of the E-MeHC=NOH and Me_2C=NOH systems to the nitrogen atom accompanied by the release of a water molecule from the cleavage of the N-O bond. The transition state geometry qualitatively resembles that from the previous study of formaldehyde oxime on the H-ZSM-5 zeolite. Only in the H_2C=NOH system, the migrating H3 is closer to the N atom than the C1 atom, whereas in the remaining systems, the migrating group is still closer to the C1 atom of the oxime molecules. The breaking N-O bond distance is elongated to about 200-240 pm. for each system, which is similar to the previous theoretical studies in other zeolites such as ZSM-5 (217 pm.), MOR (260.2 pm.). In this rearrangement step, the effect of the substituted-CH_3 group is divided into two ways. First, in the case where the substituted methyl acts as a migrating group (H_2C=NOH vs. E-MeHC=NOH), the C1-H3 and N-H3 bond distances of the H-migration are shorter than the bond distances of the CH_3-migration (C1-C2 and N-C2) which corresponds to the nature of the strength of the C-C and C-H bonds. The result of this is that the activation energy of the CH_3 migration (26.6 kcal/mol for E-MeHC=NOH) is lower than that of the H migration (50.4 kcal/mol for H_2C=NOH). Where the substituted methyl acts as an electron donating group (H_2C=NOH vs. Z-MeHC=NOH), the calculated barrier for this step of Z-MeHC=NOH is 21.4 kcal/mol from the embedded model, which is lower than that of the H_2C=NOH system. Decreasing of the energy barrier is due mainly to the CH_3 group playing an important role in stabilizing the positive charge at the carbon center to be better than the hydrogen atom in the case of the H_2C=NOH system. For the rearrangement step in Me_2C=NOH, a geminal effect of two methyl groups plays a significant role in decreasing the activation energy from 50.4 to 14.4 kcal/mol for the H_2C=NOH and Me_2C=NOH systems, respectively. The transferring CH_3 group locates near the carbon center atom (C1) (the C1-C2 and N-C2 bond distances are 177.5 and 192.6 pm., respectively). However, the calculated result for this step of all oxime molecules is almost higher than the previously reported value for the isolated protonated oxime systems. Particularly, the barrier energy in the protonated complex of $Me_2C=NOH$ in the gas phase model is calculated to be about 2 kcal/mol. This is actually too small to be real. Comparing results between the embedded and bare cluster models, we found that the Madelung potential noticeably shifts the transition state toward the primary product, the enol-amide complex (see Figure 21), whilst the barrier height of this step is much stronger. In particular, it lowers the activation energy by about 30 kcal/mol, except in the $H_2C=NOH$ system, which slightly decreases the activation energy only 10 kcal/mol. It appears reasonable to assume that in $H_2C=NOH$, the size of the formaldehyde oxime is too small in comparison with the pore size of FAU zeolite. Therefore, the long-range electrostatic potential from the framework of FAU has slightly effected the activation energy as compared with that in the substituted systems of Z-MeHC=NOH, E-MeHC=NOH and $Me_2C=NOH$, respectively.

The adsorption energy for the enol-amide complex is calculated to be -66.0, -72.6, -59.3 and -65.6 kcal/mol for the $H_2C=NOH$, Z-MeHC=NOH, E-MeHC=NOH and $Me_2C=NOH$ systems, respectively. The optimized geometry of the adsorbed enol-amide complex of all systems is given in Figure 21. From the calculated results, we found that only the adsorbed enol-amide complex in the $H_2C=NOH$ system is a neutrally formed complex in both the bare cluster and embedded cluster models, while in the CH_3-substituted system, the embedded model predicts that the enol-amide complex is protonated, whereas only the neutral formed complex was found by using the bare cluster model. The geometrical adsorption of enol-amide complex can be separated into two adsorbed structures. The first is the adsorbed enol-amide complex in the $H_2C=NOH$ and E-MeHC=NOH systems formimg the one strong hydrogen bond between the O5 and the Brønsted acid site of FAU zeolite (H1-O1), while in the Z-MeHC=NOH and $Me_2C=NOH$ systems, the adsorbed enol-amide complex forms two slightly stronger hydrogen bonds to the OH_2 group which interacts with the two bridging oxygen atoms, O1 and O2, of the zeolite framework in the six-membered ring configuration. The difference of geometrical adsorption is due mainly to the skeleton of the adsorbent molecule and the zeolite framework as shown in Figure 21.

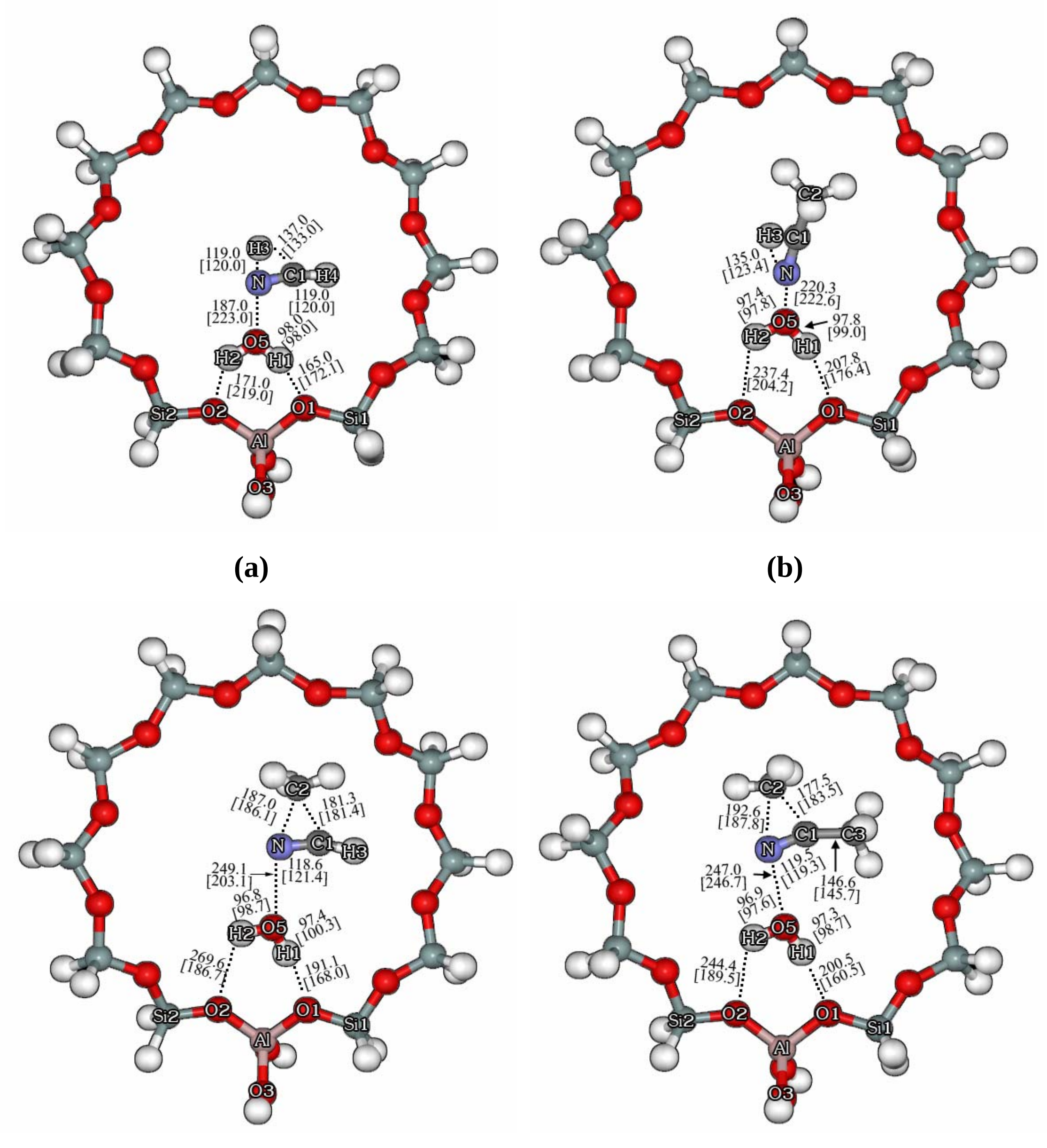

(a) **(b)**

(c) **(d)**

Figure 20 Optimized geometrical parameters of the corresponding rearrangement transition state structure of (a) $H_2C{=}NOH$, (b) Z-MeHC=NOH, (c) E-MeHC=NOH, and (d) $Me_2C{=}NOH$ molecules on the 12T cluster and embedded cluster of H-FAU zeolite at the B3LYP/6-31G(d,p) level of theory.

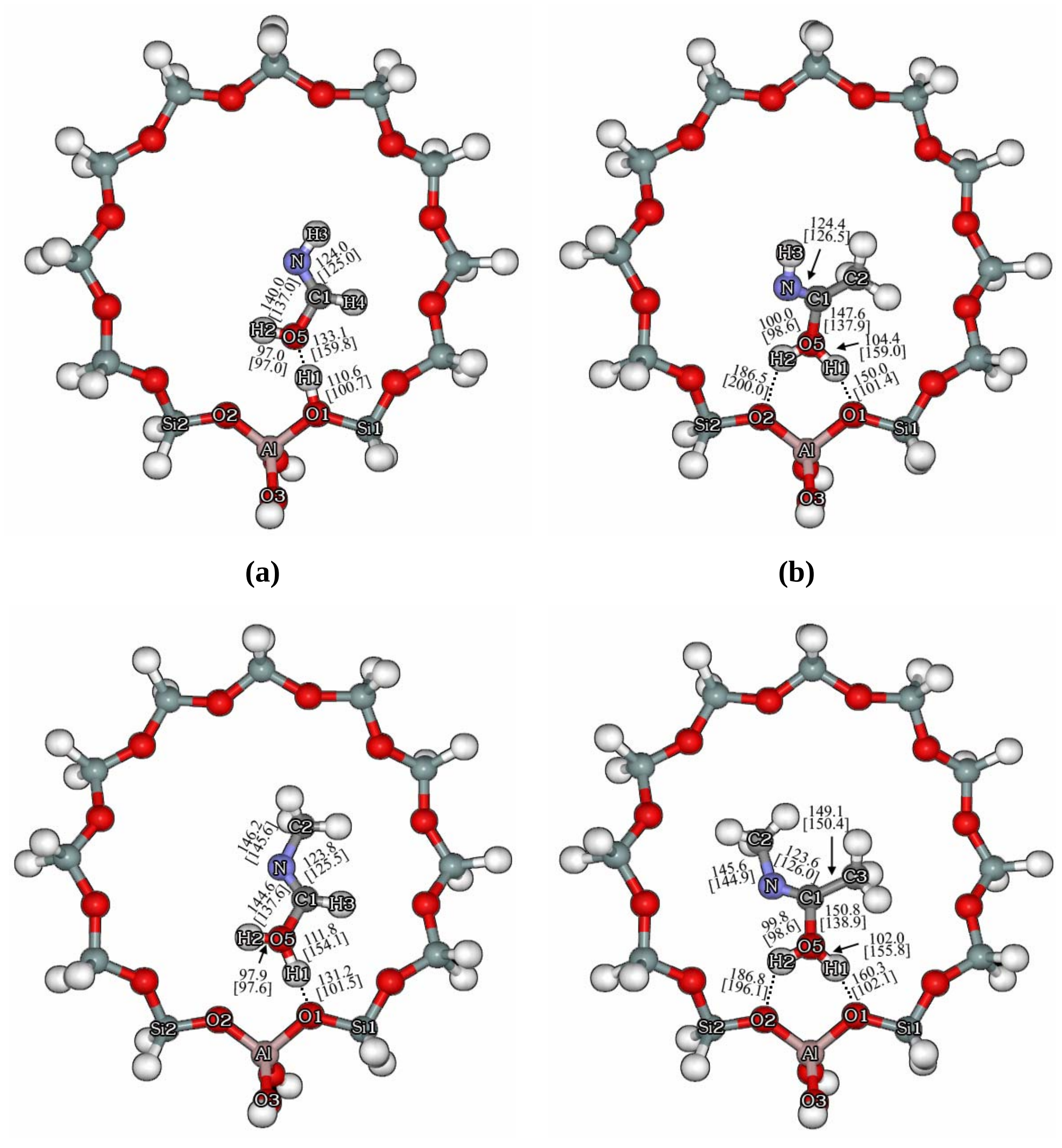

(a) **(b)**

(c) **(d)**

Figure 21 Optimized geometrical parameters of the corresponding enol-amide complex of (a) H_2C=NOH, (b) Z-MeHC=NOH, (c) E-MeHC=NOH, and (d) Me_2C=NOH molecules on the 12T cluster and embedded cluster of H-FAU zeolite at the B3LYP/6-31G(d,p) level of theory.

3. Tautomerization step

The optimized geometry of the transition state for the tautomerization step is shown in Figure 22. In this final step of this reaction, the enol-form amide is transformed to the most stable form of the amide molecule, the keto-amide form. The transferring proton (H2) is at the midway point between the O5 and N atoms (the N-H2 and O2-H2 bond distances of all oximes is in average about 140 and 122 pm., respectively), which happens simultaneously with the shortening of the C-O5 bond and the elongation of the N-C bond for shifting to the amide compound, keto-amide complex. Using the embedded cluster model, the activation energy for this step is calculated to be 25.1, 23.0, 20.8 and 17.9 kcal/mol for the $H_2C=NOH$, Z-MeHC=NOH, E-MeHC=NOH and $Me_2C=NOH$ systems, respectively. The energy barrier in this step of substituted systems: Z-MeHC=NOH, E-MeHC=NOH and $Me_2C=NOH$ decreased, due mainly to the enhancement of the basicity of the N atom in the substituted systems, which is a result of the electron donating methyl group. In addition, we found that the effect of the Madelung potential of the zeolite framework plays a significant role in stabilizing the ionic species in the TS structure. Therefore, the activation energy of the embedded cluster model is lower than that of the bare cluster model by about 10 kcal/mol. The enol-amide complex is converted into the final product of this reaction, an amide molecule (keto-amide complex as illustrated in Figure 23) via the tautomerization step. Using the embedded cluster model, the interaction between the keto-amide complex of all systems and the Brønsted acid is in the form of a protonated complex and consists of the two strong hydrogen bond interactions between O5-H1-O1 and N-H2-O2. The adsorbed structure of the keto-amide complex provides the lengthening of the C-O5 bond distance by about 7 pm. and the shortening of the C-N bond distance by about 6 pm., respectively. The desorption energy of these products is calculated to be -50.6, -69.2, 43.4 and -60.1 kcal/mol, for the $H_2C=NOH$, Z-MeHC=NOH, E-MeHC=NOH and $Me_2C=NOH$ systems, respectively. The strong interaction of the keto-amide complex as compared with the adsorption energy of the N-bound complex indicated that the amide molecule might obstruct the adsorption of the oxime molecule in the first step of the reaction. This agrees well with the previous experimental data which concluded that the reaction on the Brønsted acid of FAU is very active in the conversion of the cyclohexanone oxime into ε-caprolactam, but must encounter the problem from a difficulty in the desorption step.

Table 11 Calculated proton affinities, PA (in kcal/mol) of corresponding amides of methylated derivaties at MP4/6-311G(d,p)//MP2/6-31G(d,p) level of theory.

Oxime	PA(N)	PA(O)	ΔPA[a]
$H_2C=NOH$	210	165	45
Z-MeHC=NOH	218	170	48
E-MeHC=NOH	217	198	19
$Me_2C=NOH$	242	225	17

[a] ΔPA = PA(N) – PA(O)

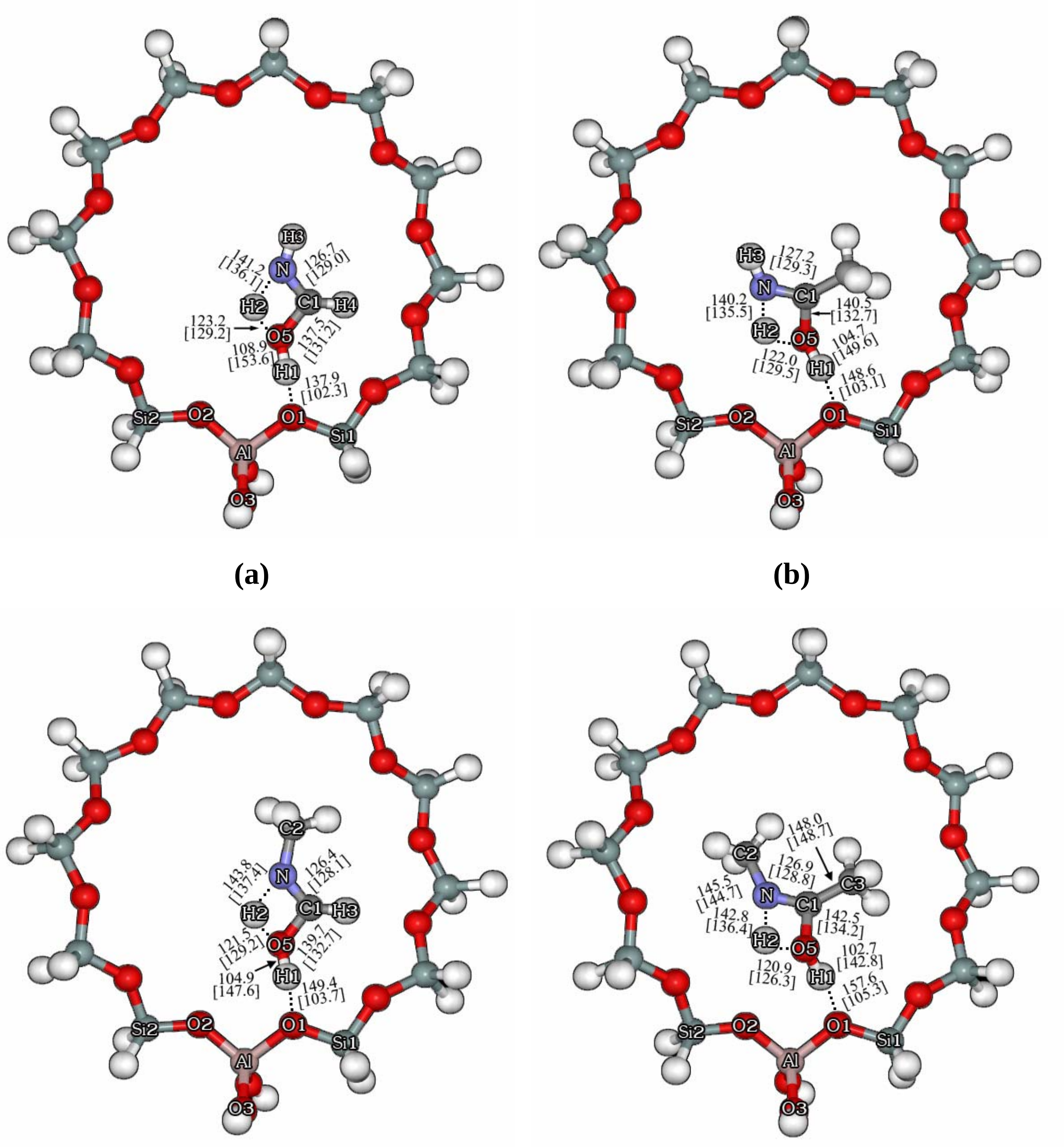

(a) **(b)**

(c) **(d)**

Figure 22 Optimized geometrical parameters of the corresponding tautomerization transition state structure complex of (a) $H_2C=NOH$, (b) Z-$MeHC=NOH$, (c) E-$MeHC=NOH$, and (d) $Me_2C=NOH$ molecules on the 12T cluster and embedded cluster of H-FAU zeolite at the B3LYP/6-31G(d,p) level of theory.

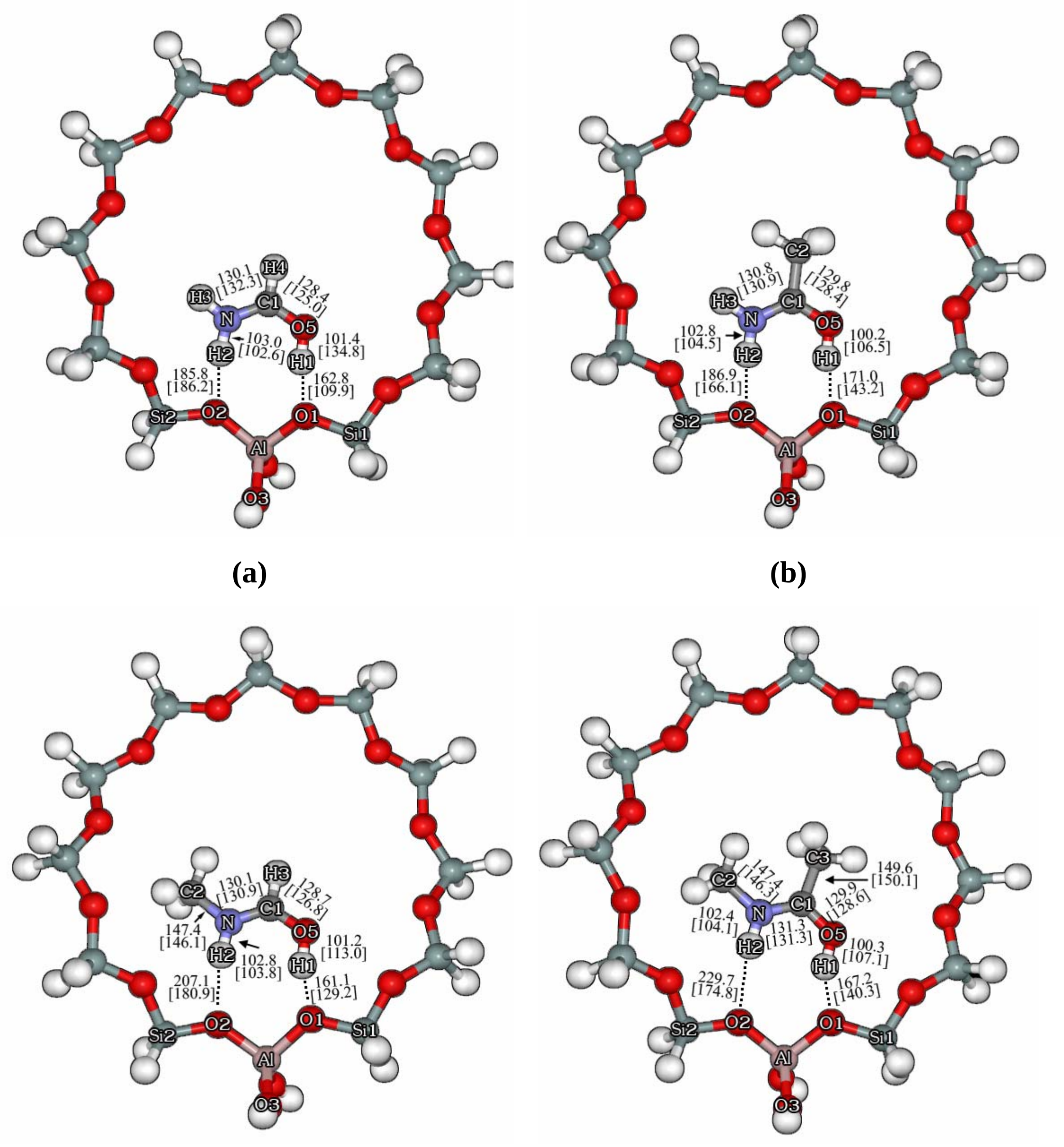

(a) **(b)**

(c) **(d)**

Figure 23 Optimized geometrical parameters of the corresponding keto-amide complex of (a) $H_2C=NOH$, (b) Z-MeHC=NOH, (c) E-MeHC=NOH, and (d) $Me_2C=NOH$ molecules on the 12T cluster and embedded cluster of H-FAU zeolite at the B3LYP/6-31G(d,p) level of theory.

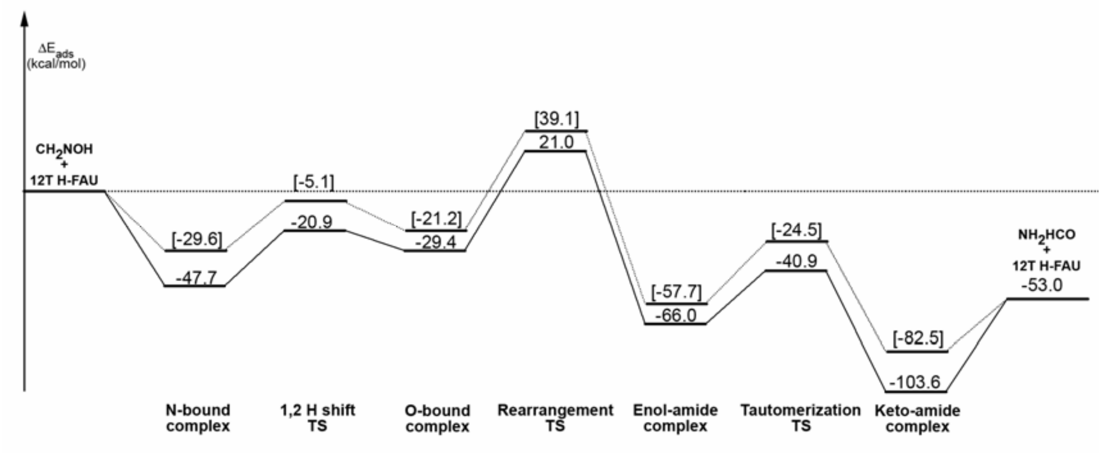

(a)

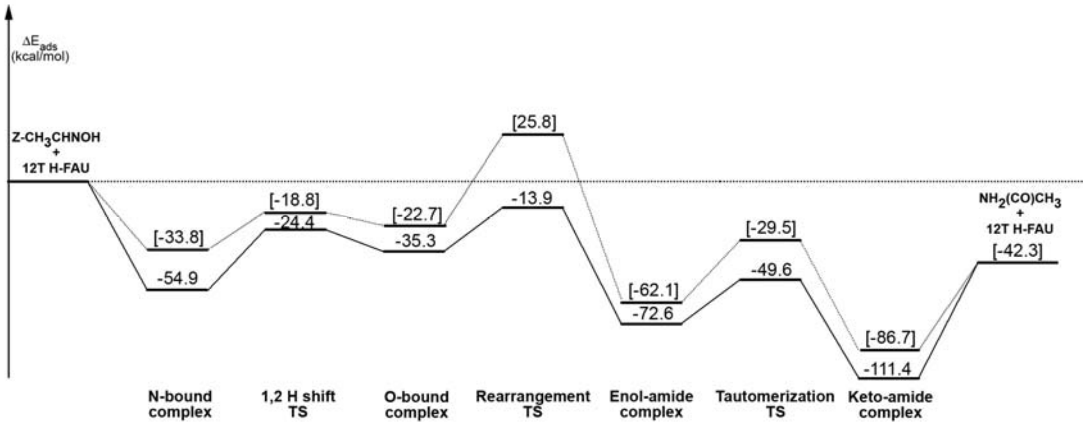

(b)

Figure 24 Energetic profile along the pathway Beckmann rearrangement of four oxime molecules on the 12T H-FAU zeolite at the MP2/6-311G(d,p)//B3LYP level of theory: (a) $H_2C=NOH$, (b) Z-MeHC=NOH systems, respectively. The energetic changes for the embedded cluster (solid line) and the bare cluster (dash line) complexes are in kcal/mol.

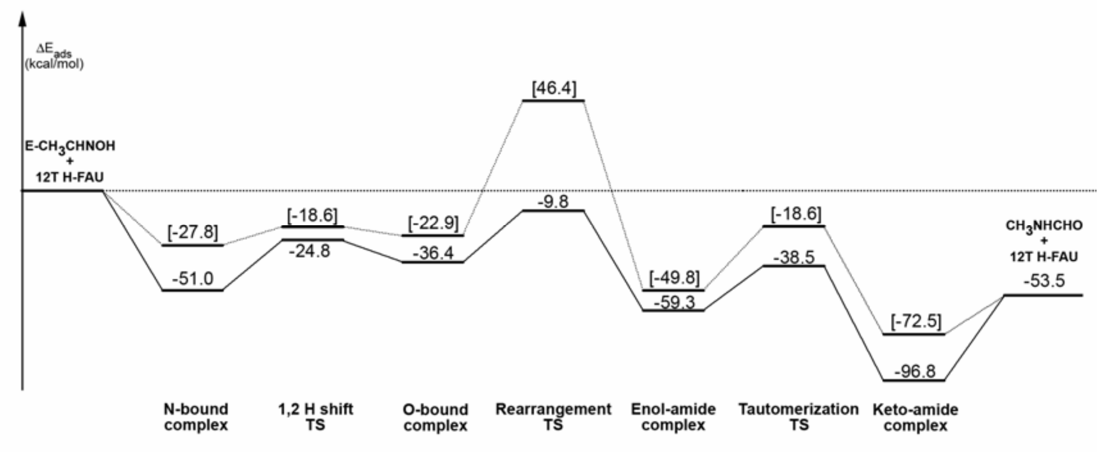

(a)

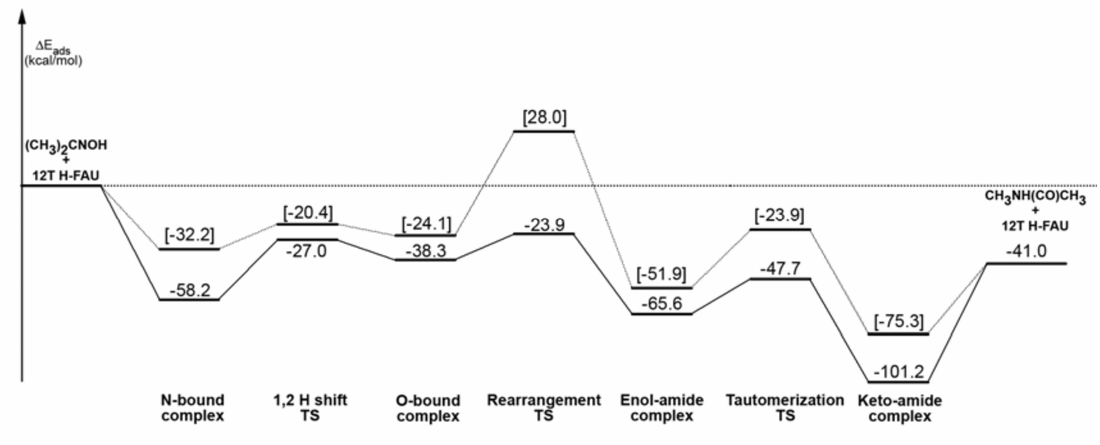

(b)

Figure 25 Energetic profile along the pathway Beckmann rearrangement of four oxime molecules on the 12T H-FAU zeolite at the MP2/6-311G(d,p)//B3LYP level of theory: (a) E-MeHC=NOH, and (b) $Me_2C=NOH$ systems, respectively. The energetic changes for the embedded cluster (solid line) and the bare cluster (dash line) complexes are in kcal/mol. dash line) complexes are in kcal/mol.

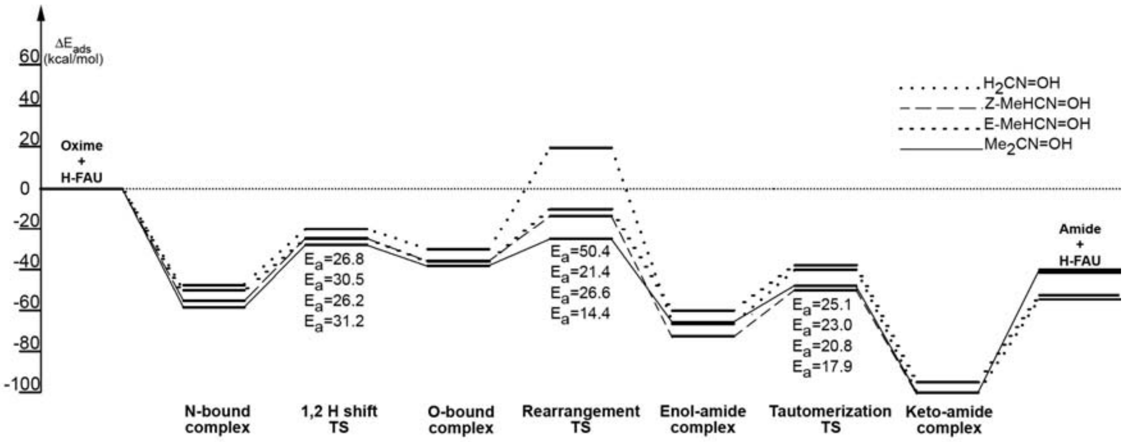

Figure 26 Schematic energy profiles of the Beckmann rearrangement on the 12T embedded cluster model of FAU zeolite showing 1,2 H-shift, rearrangement and tautomerization steps of methylated derivatives. Values at the MP2/6-311G(d,p) //B3LYP level of theory. The energetic changes are in kcal/mol.

4. Discussion

Considering the energy barriers of the three steps (Figures 24-25), the activation energy in each step of the reaction of methylated derivatives which were obtained from the 12T bare cluster model of FAU zeolite is slightly changed by 10 kcal/mol when substituting the H at the carbon center of formaldehyde oxime with mono-methyl and di-methyl substitutions, respectively. However, the rate determining step of the reaction of methylated derivatives, which is the rearrangement, is too large by about 60-70 kcal/mol. But, in the embedded cluster model, it provides different details of the energetic profile. The methyl substitutions at the carbon center taking into account the Madelung potential of the zeolite framework plays a significant role in the changing of the energy barriers, especially the rearrangement step. The rate determining step of the whole reaction of methylated derivatives is not the rearrangement step as obtained from the bare cluster model. In the 1,2 H-shift step, the energy barrier of this step is slightly increased because of the enhancement of the PA gap between N and O of methylated derivatives. The order of ΔPA is $H_2C{=}NOH$

< E-MeHC=NOH < Z-MeHC=NOH < Me_2C=NOH, respectively. This corresponds to the slight increasing of the energy barrier. This step is a rate determining step of the reaction for the Z-acetaldehyde oxime and acetone oxime which has an energy barrier of approximately 30 kcal/mol, whereas in E-MeHC=NOH isomer, either the 1,2 H shift step (26.2 kcal/mol) or the rearrangement step (26.6 kcal/mol) could be the rate limiting step. In the rearrangement step, the reduction of the energy barrier in the case of methylated derivatives is due mainly to the stabilization of the ionic species in the transition state structure which occurs from the extended framework represented by a set of finite point charges in the embedded cluster model. The transition state structure of Z-acetadehyde oxime and acetone oxime occurs via the secondary carbocation, while in the case of formaldehyde oxime and E-acetadehyde oxime, the transition state structure takes place via primary carbocation. The stabilization of the ionic species in this step, which is caused by the added methyl groups and electrostatic field from the zeolite framework, plays a dominant function in the reduction of the energy barrier. In the last step, the added methyl group enhances the basicity at the N and O of the enol-amide molecule. The energy barrier is changed from 25.1 kcal/mol to 17.9 kcal/mol in the case of di-methyl substitution. The decreasing of the energy barrier corresponds to the gap of PA between N and O atoms of corresponding amides of methylated derivatives. The order of ΔPA is H_2C=NOH ≅ Z-MeHC=NOH > E-MeHC=NOH > Me_2C=NOH, respectively as shown in Table 11. After this step, it is the adsorption of the amide molecule on the Brønsted acid site of zeolite. From the embedded cluster model, the adsorption of amides is in the protonated form which has slightly more the adsorption energy than the adsorption energy of the corresponding N-bound complex. These results indicate that the reaction on the Brønsted acid site of FAU zeolite might encounter the problem from a difficulty in the desorption step, which agrees well with the experimental results.

CONCLUSION

In this work, we have examined both the zeolite framework and the substituent effects on the Beckmann rearrangement. All of these systems have been studied by both the bare cluster and the embedded cluster models at the B3LYP/6-31G (d,p) level of theory and the energetic properties have been improved with single point calculations at the MP2/6-311G(d,p) level of theory. In the zeolite system, the most favored path is as follows: protonation of the oxime molecule → N-bound complex → O-bound complex → enol-formed amide complex → amide complex. Using the bare cluster model of the ZSM-5 and the FAU systems, it is indicated that the rate determining step of all selected oximes is the rearrangement step which has an energy barrier of about 60-70 kcal/mol. While the embedded cluster model, including the Madelung potential of the entire infinite zeolite framework, considerably changes the energetic profile of the reaction. The rate determining step of formaldehyde oxime on the H-ZSM-5 zeolite becomes either the rearrangement or the tautomerization step which has an energy barrier of about 30 kcal/mol. While in the FAU system, the rate determining step of reaction is also the rearrangement step, but has the energy barrier higher than that found in the H-ZSM-5 system by about 20 kcal/mol. Comparing the energetic profiles between the H-ZSM-5 and the H-FAU zeolites, it is indicated that the H-ZSM-5 zeolite has a catalytic activity for rearranging the formaldehyde oxime better than the H-FAU zeolite. The inclusion of the substitutent effect in the FAU system strongly influences the reduction of the energy barrier of the Beckmann rearrangement reaction in comparison with that of formaldehyde oxime (50.4 kcal/mol). For the Z-acetaldehyde oxime and acetone oxime, the rate limiting step is the 1,2 H-shift step, which has an energy barrier of 30.5 and 31.2 kcal/mol, respectively, while the rate limiting step of E-acetaldehyde oxime could be either the 1,2 H-shift step (26.2 kcal/mol) or the rearrangement step (26.6 kcal/mol). The results indicate that the bare cluster model can not be used to describe the catalytic activity of zeolite because no contributions from the extended framework are included. The results of both the Beckmann rearrangement of formaldehyde oxime within the different zeolites and the Beckmann rearrangement of methylated derivatives on the FAU zeoltie, which were computed on the embedded cluster model, reveal that when the size of a guest molecule approaches the size of the pores and cavities of the zeolite, the electronic confinement from the zeolite framework plays an important role in increasing the reactivity of zeolite.

LITERATURE CITED

Allavena, M., K. Seitia, E. Kassab, Gy. Ferenczy and J. G. Ángyán. 1990. Quantum-chemical model calculations on the acidic site of zeolites including Madelung-potential effects. **Chem. Phys. Lett.** 168(5): 461-467.

Aucejo, A., M.C. Burguet, A. Corma and V. Fornes. 1986. Beckmann rearrangement of cyclohexanone-oxime on HNaY zeolites: Kinetic and spectroscopic studies. **Appl. Catal.** 22(2): 187-200.

Barbosa, L.A.M.M. and R.A. van Santen. 2000. Study of the hydrolysis of acetonitrile using different Brønsted acid models: Zeolite-type and HCl(H2O)x clusters. **J. Catal.** 191(1): 200-217.

Blatt, A.H. 1933. The Beckmann rearrangement. **Chem. Rev.** 12: 215-260.

Boero, M., C.C. Liew, K. Terakura, M. Parrinello and T. Ikeshoji. 2004. Hydrogen bond driven chemical reactions: Beckmann rearrangement of cyclohexanone oxime into Caprolactam in supercritical water. **J. Am. Chem. Soc.** 126(20): 6280-6286.

Bucko, T., J. Hafner and L. Benco. 2004. Active sites for the vapor phase Beckmann rearrangement over Mordenite: An ab Initio study. **J. Phys. Chem. A** 108(51): 11388-11397.

Camblor, M.A., A. Corma, H. Garcia, V. Semmer-Herledan and S. Valencia. 1998. Active sites for the liquid-phase Beckmann rearrangement of cyclohexanone, acetophenone and cyclododecanone oximes, catalyzed by beta zeolites. **J. Catal.** 177(2): 267-272.

Chang, J.C. and A.N. Ko. 2004. Novel synthesis of caprolactam from cyclohexanone-oxime via Beckmann rearrangement over mesoporous molecular sieves MCM-48. **Catal. Today** 97(4): 241-247.

________________________ 2004. Beckmann rearrangement of cyclohexanone oxime to caprolactam using mesoporous molecular sieves ALSBA-15. **React. Kinet. Catal. Lett.** 83(2): 283-290.

Chaudhari, K., R. Bal, A.J. Chandwadkar and S. Sivasanker. 2002. Beckmann rearrangement of cyclohexanone oxime over mesoporous Si-MCM-41 and Al-MCM-41 molecular sieves. **J. Mol. Catal. A** 177(2): 247-253.

Cho, S.J., C. Cui, J.Y. Lee, J.K. Park, S.B. Suh, J. Park, B.H. Kim and K.S. Kim. 1997. N-protonation vs O-protonation in strained amides: Ab initio study. **J. Org. Chem.** 62(12): 4068-4071.

Chung, Y.M. and H.K. Rhee. 2000. Solvent effects in the liquid phase Beckmann rearrangement of 4-hydroxyacetophenone oxime over H-Beta catalyst. **J. Mol. Catal. A** 159(2): 389-396.

__________________________ 2001. Solvent effects in the liquid-phase Beckmann rearrangement of oxime over H-Beta catalyst II: adsorption and FT-IR studies. **J. Mol. Catal. A** 175(1-2): 249-257.

Corma, A., H. Garcia, J. Primo and E. Sastre. 1991. Beckmann rearrangement of cyclohexanone oxime on zeolites. **Zeolites** 11(6): 593-597.

_________ 2003. State of the art and future challenges of zelite as catalysts. **J. Catal.** 216(1-2): 298-312.

Cox, R.A. 1997. The mechanisms of the hydrolyses of N-nitrobenzenesulfonamides, N-nitrobenzamides and some other N-nitro amides in aqueous sulfuric acid. **J. Chem. Soc., Perkin Trans. 2** 9: 1743-1750.

Curtin, T., J.B. McMonagle and B.K. Hodnett. 1993. Beckmann rearrangement over solid acid catalysts. **Stud. Surf. Sci. Catal.** 75: 2609-2612.

Dahlhoff, G., U. Barsnick and W.F. Holderich. 2001. The use of MCM-22 as catalyst for the Beckmann rearrangement of cyclohexanone oxime to ε-caprolactam. **Appl. Catal. A** 210(1-2): 83-95.

_________, W. Eickelberg and W.F. Holderich. 2001. Recent developments in the catalyst regeneration for the Beckmann rearrangement of cyclohexanone oxime to ε-caprolactam. **Stud. Surf. Sci. Catal.** 139: 335-342.

Dai, L.X., R. Hayasaka, Y. Iwaki, K.A. Koyano and T. Tatsumi. 1996. Vapor phase Beckmann rearrangement of cyclohexanone oxime catalyzed by Hb zeolite. **Chem. Commun.** 9: 1071-1072.

________, K. Koyama and T. Tatsumi. 1998. Catalytic application of mesoporous molecular sieves to vapor-phase Beckmann rearrangement of cyclohexanone oxime. **Catal. Lett.** 53(3-4): 211-214.

Fernandez Ana, B., M. Boronat, T. Blasco and A. Corma. 2005. Establishing a molecular mechanism for the Beckmann rearrangement of oximes over microporous molecular sieves. **Angew. Chem. Int. Ed.** 44(16): 2370-2373.

Flego, C. and L. Dalloro. 2003. Beckmann rearrangement of cyclohexanone oxime over Silicalite-1: an FT-IR spectroscopic study. **Microporous and Mesoporous Mater.** 60(1-3): 263-271.

Fois, G.A., G. Ricchiardi, S. Bordiga, C. Busco, L. Dalloro, G. Spano and A. Zecchina. 2001. The Beckmann rearrangement catalyzed by Silicalite: A spectroscopic and computational study. **Stud. Surf. Sci. Catal.** 135: 2477-2484.

Forni, L., G. Fornasari, G. Giordano, C. Lucarelli, A. Katovic, F. Trifiro, C. Perri and J.B. Nagy. 2004. Effect of exchange procedure and crystal size on high silica MFI zeolite as catalyst for vapor phase Beckmann rearrangement. **Stud. Surf. Sci. Catal.** 154: 2823-2830.

Forni, L., G. Fornasari, C. Lucarelli, F. Trifir๒, G. Giordano, A. Katovic, C. Perri and J.B. Nagy. 2004. Vapor phase Beckmann rearrangement using high silica zeolite catalyst. **Phys. Chem. Chem. Phys.** 6(8): 1842-1847.

Frisch, M. J., G. W. Trucks, H. B. Schlegel, G. E. Scuseria, M. A. Robb, J. R. Cheeseman, V. G. Zakrzewski, J. A. Montgomery, Jr., R. E. Stratmann, J. C. Burant, S. Dapprich, J. M. Millam, A. D. Daniels, K. N. Kudin, M. C. Strain, O. Farkas, J. Tomasi, V. Barone, M. Cossi, R. Cammi, B. Mennucci, C. Pomelli, C. Adamo, S. Clifford, J. Ochterski, G. A. Petersson, P. Y. Ayala, Q. Cui, K. Morokuma, D. K. Malick, A. D. Rabuck, K. Raghavachari, J. B. Foresman, J. Cioslowski, J. V. Ortiz, A. G. Baboul, B. B. Stefanov, G. Liu, A. Liashenko, P. Piskorz, I. Komaromi, R. Gomperts, R. L. Martin, D. J. Fox, T. Keith, M. A. Al-Laham, C. Y. Peng, A. Nanayakkara, C. Gonzalez, M. Challacombe, P. M. W. Gill, B. Johnson, W. Chen, M. W. Wong, J. L. Andres, C. Gonzalez, M. Head-Gordon, E. S. Replogle, and J. A. Pople. 1998. **Gaussian,** Inc., Pittsburgh PA.

Gui, J., Z. Hu, Z. Sun and Y. Deng. 2004. A novel task-specific ionic liquid for Beckmann rearrangement: A simple and effective way for product separation. **Tetrahedron Lett.** 45(12): 2681-2683.

Gutierrez, E., A.J. Aznar and E. Ruiz-Hitzky. 1991. Beckmann rearrangement reactions on acidic solids. **Stud. Surf. Sci. Catal.** 59(2): 539-547.

Kresse, G., J. Hafner. 1993. Ab initio molecular dynamics for open-shell transition metals. **Phys. Rev. B** 48(17): 13115-18.

Heitmann, G.P., G. Dahlhoff and W.F. Holderich. 1999(a). Catalytically active sites for the Beckmann rearrangement of cyclohexanone oxime to caprolactam. **J. Catal.** 186(1): 12-19.

____ 1999(b). Modified Beta zeolites as catalysts for the Beckmann rearrangement of cyclohexanone oxime. **Appl. Catal. A** 185(1): 99-108.

__________________________, J.P.M. Niederer and W.F. Holderich. 2000. Active sites of a [B]-ZSM-5 zeolite catalyst for the Beckmann rearrangement of cyclohexanone oxime to caprolactam. **J. Catal.** 194(1): 122-129.

Hillier, I.H., S.P. Greatbanks and P. Sherwood. 1994. Embedded Cluster Model for the ab Initio study of Brønsted acidity in zeolites. **J. Phys. Chem.** 98: 8134-8139.

Hölderich, W.F., G. Dahlhoff and U. Barsnick. 2001. The use of MCM-22 as catalyst for the Beckmann rearrangement of cyclohexanone oxime to caprolactam. **Appl. Catal.** 210(1-2): 83-95.

Hölderich, W.F., J. Roseler, G. Heitmann and A.T. Liebens. 1997. The use of zeolites in the synthesis of fine and intermediate chemicals. **Catal. Today** 37(4): 353-366.

Ichihashi, H. and M. Kitamura. 2002. Some aspects of the vapor phase Beckmann rearrangement for the production of ε-caprolactam over high silica MFI zeolites. **Catal. Today** 73(1-2): 23-28.

___________ and H. Sato. 2001. The development of new heterogeneous catalytic processes for the production of caprolactam. **Appl. Catal. A** 221(1-2): 359-366.

Ishida, M., A. Shiga, T. Suzuki and H. Ichihashi. 2003. Theoretical study on vapour phase Beckmann rearrangement of cyclohexanone oxime over a high silica MFI zeolite. **Catal. Today** 87(1-4): 187-194.

Jones, B. 1944. Kinetics and mechanism of the Beckmann rearrangement. **Chem. Rev.** 35: 335-350.

Jungsuttiwong, S., J. Limtrakul and T.N. Truong. 2005. Theoretical study of modes of adsorption of water dimer on H-ZSM-5 and H-Faujasite zeolites. **J. Phys. Chem. B** 109(27): 13342-13351.

Kassab, E., M. Allavena, K. Seiti, G. Ferenczy and J. G. Ángyán. 1990. Quantum-chemical model calculations on the acidic site of zeolites including Madelung-potential effects. **Chem. Phys. Lett**. 168: 461-467.

Kath, H., R. Glaser and J. Weitkamp. 2001. Beckmann rearrangement of cyclohexanone oxime on MFI-type zeolites. **Chem. Eng. Technol.** 24(2): 150-153.

Ko, A.N., C.C. Hung, C.W. Chen and K.H. Ouyang. 2001. Mesoporous molecular sieve Al-MCM-41 as a novel catalyst for vapor phase Beckmann rearrangement of cyclohexanone oxime. **Catal. Lett.** 71: 219-224.

Komatsu, T., T. Maeda and T. Yashima. 2000. Kinetic study on the effect of solvent in 'vapor-phase' Beckmann rearrangement of cyclohexanone oxime on Silicalite-1. **Microporous and Mesoporous Mater.** 35-36: 173-180.

Lewis, M. and R. Glaser. 1998. Synergism of catalysis and reaction center rehybridization. An ab initio study of the hydrolysis of the parent carbodiimide. **J. Am. Chem. Soc.** 120(33): 8541-8542.

Li, D., F. Shi, S. Guo and Y. Deng. 2005. Highly efficient Beckmann rearrangement and dehydration of oximes. **Tetrahedron Lett.** 46(4): 671-674.

Limtrakul, J., S. Jungsuttiwong, P. Khongpracha. 2000a. Adsorption of carbon monoxide in H-ZSM-5 zeolites: An Embeded ab initio cluster study. **J. Mol. Catal. A.** 153: 155-163.

____ 2000b. Adsorption of carbon monoxide on H-FAU and Li-FAU zeolites: An Embedded cluster approach. **J. Mol. Struct.** 525: 153-162.

Limtrakul, J., T. Nanok, P. Khongpracha, S. Jungsuttiwong and T.N. Troung. 2001a. Adsorption of unsaturated hydrocarbon on zeolites: The effects of the zeolite framework on adsorption properties of ethylene. **Chem. Phys. Lett.** 39: 161-166.

_________, S. Nokbin, P. Chuichay. 2001b. Effect of high coverage on proton transfer in the zeolite/water system. **J. Mol. Struct.** 560: 169-177.

_________, S. Nokbin, P. Chuichay, P. Khongpracha, S. Jungsuttiwong and T.N. Troung. 2001c. High coverage effect on proton transfer of faujasite/water system: density functional embedded cluster approach. **Stud. Surf. Sci. Catal.** 135: 2469-2476.

Mao, D. and Q. Chen. 2002. Vapor-phase Beckmann rearrangement of cyclohexanone oxime over B2O3 catalysts supported on TiO2-ZrO2 mixed oxide. **React. Kinet. Catal. Lett.** 75(1): 75-80.

Ngamcharussrivichai, C., P. Wu and T. Tatsumi. 2004a. Liquid-phase Beckmann rearrangement of cyclohexanone oxime over mesoporous molecular sieve catalysts. **J. Catal.** 227(2): 448-458.

____ 2004b. Selective production of ε-caprolactam via liquid-phase beckmann rearrangement of cyclohexanone oxime over H-USY catalyst. **Chem. Lett.** 33(10): 1288-1289.

Nguyen, M.T., G. Raspoet and L.G. Vanquickenborne. 1995. Important role of the Beckmann rearrangement in the gas phase chemistry of protonated formaldehyde oximes and their $[CH_4NO]^+$ isomers. **J. Chem. Soc., Perkin Trans. 2** 9: 1791-1795.

____ 1997a. Mechanism of the Beckmann rearrangement in sulfuric acid solution. **J. Chem. Soc., Perkin Trans. 2** 4: 821-825.

____ 1997b. A New Look at the Classical Beckmann Rearrangement: A Strong Case of Active Solvent Effect. **J. Am. Chem. Soc.** 119(10): 2552-2562.

O'Sullivan, P., L. Forni and B.K. Hodnett. 2001. The role of acid site strength in the Beckmann rearrangement. **Ind. Eng. Chem. Res.** 40(6): 1471-1475.

Pabchanda, S., P. Pantu and J. Limtrakul. 2005. Hydrolysis of methoxide species and regeneration of active site in Fe-ZSM-5 catalyst by the ONIOM method. **J. Mol. Catal. A** 239(1-2): 103-110.

Parker Jr., W.O. 1999. Chemical transformations on a weakly acidic catalyst studied by ^{15}N NMR: Butanone oxime on silicalite-1. **Magn. Reson. Chem.** 37(6): 433-436.

Parr, R.G. and W. Yang. 1989. Density functional theory of atoms and molecules. Oxford University Press, New York. 586 p.

Pitarch, J., M.F. Ruiz-Lopez, E. Silla, J.-L. Pascual-Ahuir and I. Tunon. 1998. Neutral and alkaline hydrolyzes of model b-Lactam antibiotics. An ab Initio study of water catalysis. **J. Am. Chem. Soc.** 120(9): 2146-2155.

Pople, J.A. and D.L. Beveridge. 1970. Approximate molecular orbital theory. McGraw-Hill, Inc., New York. 214 p.

Raspoet, G., M.T. Nguyen, M. McGarraghy and A.F. Hegarty. 1998. Experimental and theoretical evidence for a concerted catalysis by water clusters in the hydrolysis of isocyanates. **J. Org. Chem.** 63(20): 6867-6877.

Reddy, J.S., R. Ravishankar, S. Sivasanker and P. Ratnasamy. 1993. Vapor phase Beckmann rearrangement of cyclohexanone oxime over MEL type zeolites. **Catal. Lett.** 17(1-2): 139-140.

Roeseler, J., G. Heitmann and W.F. Hoelderich. 1996. Vapor-phase Beckmann rearrangement using B-MFI zeolites. **Appl. Catal. A** 144(1-2): 319-333.

____________________ 1997. Vapor-phase Beckmann rearrangement using B-MFI zeolites. **Stud. Surf. Sci. Catal.** 105: 1173-1180.

Rungsirisakun, R., B. Jansang, P. Pantu and J. Limtrakul. 2005. The adsorption of benzene on industrially important nanostructured catalysts (H-BEA, H-ZSM-5, and H-FAU): Confinement effects. **J. Mol. Struct.** 733(1-3): 239-246.

Sato, H., K. Hirose and Y. Nakamura. 1993. FT-IR study of the Beckmann rearrangement over pentasil-type zeolite. **Chem. Lett.** 12: 1987-1990.

_______, H. Yoshioka and Y. Izumi. 1999. Homogeneous liquid-phase Beckmann rearrangement of oxime catalyzed by phosphorous pentaoxide and accelerated by fluorine-containing strong acid. **J. Mol. Catal. A** 149(1-2): 25-32.

_______ and H. Ichihashi. 2001. The development of new heterogeneous catalytic processes for the production of ε-caprolactam. **Appl. Catal. A.** 221: 359-366.

Segall, M., D. Lindan, J.D. Philip, M.J. Probert, C.J. Pickard, P.J. Hasnip, S.J. Clark, M.C. Payne. 2002. First-principles simulation: ideas, illustrations and the CASTEP code. **J. Phys.-Condens. Mat**. 14(11): 2717-2744.

Sherwood, P., A.H. De Vries, S.J. Collins, S.P. Greatbanks, N.A. Burton, M.A. Vincent and I.H. Hillier. 1997. Computer simulation of zeolite structure and reactivity using embedded cluster methods. **Faraday Discuss.** 106: 79-92.

Shinohara, Y., S. Mae, D. Shouro and T. Nakajima. 2000. A quantum chemical study of vapor-phase Beckmann rearrangement mechanisms on oxide catalysts. **THEOCHEM** 497: 1-9.

Shouro, D., T. Nakajima and S. Mishima. 1999. Strong basic sites accelerate the deactivation of oxide catalysts supported on FSM-16 for the vapor-phase Beckmann rearrangement of cyclohexanone oxime. **Chem. Lett.** 12: 1319-1320.

Simunic-Meznaric, V., Z. Mihalic and H. Vancik. 2002. Oxime rearrangements: ab initio calculations and reactions in the solid state. **J. Chem. Soc., Perkin Trans. 2** 12: 2154-2158.

Singh, P.S., R. Bandyopadhyay, S.G. Hegde and B.S. Rao. 1996. Vapour phase Beckmann rearrangement of cyclohexanone oxime over SAPO-11 molecular sieve. **Appl. Catal. A** 136(2): 249-263.

Stefanovich, E.V. and T.N. Truong. 1998. A simple method for incorporating Madelung field effects into ab Initio embedded cluster calculations of crystals and macromolecules. **J. Phys. Chem. B** 102(16): 3018-3022.

Stephen P.G., P. Sherwood and I.H. Hillier. 1994. Embedded cluster model for the ab initio study of Brønsted acidity in zeolites. **J. Phys. Chem.**, 98(33): 8134-8139.

Svensson, M., S. Humbel, R. Froese, T. Matsubara, S. Sieber and K. Morokuma. 1996. ONIOM: A multilayered integrated MO+MM method for geometry optimizations and single point energy predictions. A test for Diels-Alder reactions and $Pt(P(t - Bu)_3)_2 + H_2$ oxidative addition. **J. Phys. Chem.**, 100(50): 19357-19363.

Takahashi, T., T. Kai and E. Nakao. 2004. Catalyst deactivation in the Beckmann rearrangement of cyclohexanone oxime over H-ZSM-5 zeolite and silica-alumina catalysts. **Appl. Catal. A** 262(2): 137-142.

Takahashi, T., T. Kai and M.N.A. Nasution. 1995. Catalyst deactivation of high silica metallosilicates in Beckmann rearrangement of cyclohexanone oxime. **Stud. Surf. Sci. Catal.** 97: 431-436.

Takahashi, T., M. Nishi, Y. Tagawa and T. Kai. 1995. Catalyst deactivation of high-silica H-ZSM-5 in the Beckmann rearrangement reaction of cyclohexanone oxime. **Microporous Mater.** 3(4-5): 467-471.

Takahashi, T., K. Ueno and T. Kai. 1993. Vapor phase Beckmann rearrangement of cyclopentanone oxime over high silica H-ZSM-5 zeolites. **Microporous Mater.** 1(5): 323-327.

Tao, W., Y. Hu, D. Mao, J. Xia and Q. Chen. 2005. A novel modification for silicalite-1 with high stability and selectivity in vapor phase Beckmann rearrangement of cyclohexanone oxime. **Chem. Lett.** 34(4): 472-473.

Tatsumi, T. and M. Miyamoto. 1999. Highly selective vapor phase Beckmann rearrangement over H-USY zeolites. **Appl. Catal. A** 189(2): 237-242.

Teunissen, E.H., A.P.J. Jansen and R.A. van Santen. 1995. Ab initio embedded cluster study of the adsorption of NH_3 and NH_4^+ in Chabazite. **J. Phys. Chem.** 99(7): 1873-1879.

Thomas, B., S. Prathapan and S. Sugunan. 2005. Solid acid-catalyzed dehydration/ Beckmann rearrangement of aldoximes: towards high atom efficiency green processes. **Microporous and Mesoporous Mat.** 79(1-3): 21-27.

Treesukol, P., T.N. Truong, K. Srisuk and J. Limtrakul. 2005. Nature of the metal-support interaction in bifunctional catalytic Pt/H-ZSM-5 zeolite. **J. Phys. Chem. B** 109(24): 11940-11945.

Tsai, C.-C., C.-Y. Zhong, I. Wang, S.-B. Liu, W.-H. Chen and T.-C. Tsai. 2004. Vapor phase Beckmann rearrangement of cyclohexanone oxime over MCM-22. **Appl. Catal. A** 267(1-2): 87-94.

Van Santen, R.A., E.H. Teunissen, A.P. Jansen, R. Orlando and R. Dovesi. 1994. Adsorption energies of NH_3 and NH_4^+ in zeolites corrected for the long-range electrostatic potential of the crystal. **J. Chem. Phys.** 101: 5865-5874.

Yamabe, S., N. Tsuchida and S. Yamazaki. 2005. Is the Beckmann rearrangement a concerted or stepwise reaction? A computational study. **J. Org. Chem.** 70(26): 10638-10644.

Yamaguchi, Y., N. Yasutake and M. Nagaoka. 2003. Ab initio study of noncatalytic Beckmann rearrangement and hydrolysis of cyclohexanone-oxime in subcritical and supercritical water using the polarizable continuum model. **THEOCHEM** 639: 137-150.

Yashima, T., N. Oka and T. Komatsu. 1997. Vapor phase Beckmann rearrangement of cyclohexanone oxime on the zeolite catalysts. **Catal. Today** 38(2): 249-253.

Zhang, Y., Y. Wang, Y. Bu, Z. Mi, W. Wu, E. Min, S. Han and S. Fu. 2005. Beckmann rearrangement of cyclohexanone oxime over H-Beta zeolite and H-Beta zeolite-supported boride. **Catal. Commun.** 6(1): 53-56.

APPENDIX

Procedure for creating charges from the SCREEP method
(The Surface Charge Representation of the Electrostatic Embedding Potential)

The SCREEP method proceeds through employed to create charges for representing the zeolite framework. This method does the following steps:

(1) Constructing the SCREEP surface around the unterminated cluster and dividing it into surface elements.

(2) Using cut-off radius, Rcut, determines which part of the Madelung lattice sum will be treated explicitly by direct summation. Prints the list of explicit ions (positions and charges) under the title “Ions in the explicit area not including the cluster”.

(3) Calculating (using the Ewald summation method) electrostatic potential from the rest of the infinite lattice on the SCREEP surface points.

(4) Solving the SCREEP equation, $q = A^{-1}V$ where q is the magnitude of each point in the surface charge, A is the $M \times M$ nonsingular matrix representing the distance between the surface elements and V is the values of the electrostatic potential from the rest of the infinite lattice which equals the difference of electrostatic potentials between the Ewald summation and Explicit point charges, $V = V_{Ewald} - V_{Explicit}$, to determine the SCREEP surface charges. Prints the list of the surface charges (positions and values) under the title “Coord and values of (-) conduc. Surface charges”.

(5) Now, the Madelung potential inside cluster is well represented by the sum of two terms: potential from explicit charges (from step 2) and potential from surface charges (from step 4). List of charges generated at steps 2 and 4 can be copied to the input of Gaussian. The length unit for coordinates is that specified by the parameter.

(6) Calculating both the SCREEP and exact Ewald potentials at user defined set of points inside cluster, finds the RMS difference between these potentials to check the accuracy of the SCREEP potential.

(7) Refitting the electrostatic potential from the first shell of the explicit charges, which are the same positions of the terminated atoms of the terminated cluster model, into the second shell of the explicit charges.

Example of creating charges for 10T cluster model :

Step 1 Constructing Grid Point

Command: *awk –f grid.awk<File Input> File Output*

Grid Point Input

```
20 <NUMBER OF CLUSTER ATOMS>

Si    14.4300     11.1700     12.9700
Si    14.4300     18.6800     12.9700
Si    13.7600     13.4000     10.9700
Si    13.7600     16.4500     10.9700
O     13.9200     12.5200     12.3000
O     13.9200     17.3300     12.3000
O     13.7800     14.9200     11.4300
Si    11.5700     11.0700     17.8800
Si    11.5700     18.7700     17.8800
Si    13.8700     10.5000     15.9200        <COORDINATES
Si    13.8700     19.3500     15.9200         FROM X-ray DATA>
Si    12.4300     13.3900     19.6800
Si    12.4300     16.4500     19.6800
O     12.5600     11.0100     16.6500
O     12.5600     18.8400     16.6500
O     13.8500     11.1200     14.4400
O     13.8500     18.7300     14.4400
O     11.6900     12.4900     18.6000
O     11.6900     17.3600     18.6000
O     12.1800     14.9200     19.2600
r 5.0   <RADIUS FROM CENTER>
step 0.5   <DISTANCE STEP FROM CENTER>
```

Grid Point Output

```
Si      14.43     11.17     12.97
Si      14.43     18.68      12.97
Si      13.76     13.40      10.97
Si      13.76     16.45      10.97
O       13.92     12.52      12.30
O       13.92     17.33      12.30
O       13.78     14.92      11.43
Si      11.57     11.07      17.88
Si      11.57     18.77      17.88
Si      13.87     10.50      15.92
Si      13.87     19.35      15.92
Si      12.43     13.39      19.68
Si      12.43     16.45      19.68
O       12.56     11.01      16.65
O       12.56     18.84     16.65
O       13.85     11.12      14.44
O       13.85     18.73      14.44
O       11.69     12.49      18.60
O       11.69     17.36      18.60
O       12.18     14.92      19.26
 x      13.11     14.92      15.48  <CENTER OF GRID POINT>
 x      13.11     14.92      15.98
 x      13.11     14.92      14.98
 x      13.11     14.92      16.48
 x      13.11     14.92      14.48
    ………
     ………
     ………                               <GRID POINT VALUES>
 x      16.61     15.42      15.48
 x      16.61     14.42      15.48
 x       9.61     15.42      15.48
 x       9.61     14.42      15.48
 x     16.61      15.42      15.98
 x     16.61      14.42      15.98
 x     16.61      14.42      14.48
```

Step 2 Setting Dummies coordinate

Command: *awk –f grid.awk<File Input> File Output*

Input Dummy

```
20   <NUMBER OF ATOMS>

Si         14.4300          11.1700          12.9700
Si         14.4300          18.6800          12.9700
Si         13.7600          13.4000          10.9700
Si         13.7600          16.4500          10.9700
O          13.9200          12.5200          12.3000
O          13.9200          17.3300          12.3000
O          13.7800          14.9200          11.4300
Si         11.5700          11.0700          17.8800
Si         11.5700          18.7700          17.8800
Si         13.8700          10.5000          15.9200
Si         13.8700          19.3500          15.9200
Si         12.4300          13.3900          19.6800
Si         12.4300          16.4500          19.6800
O          12.5600          11.0100          16.6500
O          12.5600          18.8400          16.6500
O          13.8500          11.1200          14.4400
O          13.8500          18.7300          14.4400
O          11.6900          12.4900          18.6000
O          11.6900          17.3600          18.6000
O          12.1800          14.9200          19.2600
r      5.0    <RADIUS  FROM CENTER>
step 5.0    <DISTANCE  STEP FROM CENTER>
```

Output Dummy

```
Si      14.43        11.17        12.97
Si      14.43        18.68        12.97
Si      13.76        13.40        10.97
Si      13.76        16.45        10.97
O       13.92        12.52        12.30
O       13.92        17.33        12.30
O       13.78        14.92        11.43
Si      11.57        11.07        17.88
Si      11.57        18.77        17.88
Si      13.87        10.50        15.92
Si      13.87        19.35        15.92
Si      12.43        13.39        19.68
Si      12.43        16.45        19.68
O        2.56        11.01        16.65
O       12.56        18.84        16.65
O       13.85        11.12        14.44
O       13.85        18.73        14.44
O       11.69        12.49        18.60
O       11.69        17.36        18.60
O       12.18        14.92        19.26
x       13.11        14.92        15.48  <DUMMY COORDINATES>*
```

**Single value due to; radius = step= (5.0)*

(Using to be identify the pore size, i.e., size of the charging surface)

Step 3 Running SCREEP Method

Command: *. / screep<File Input> File Output*

SCREEP Input

```
    3   0   0
    MFI-10T    <REMARK>
    12  12    <NUMBER OF CLUSTER + DUMMY ATOMS>
14.43  11.17  12.97    2.000
13.92  12.52  12.30   -1.000
13.76  13.40  10.97    2.000
13.78  14.92  11.43   -1.000
………
………                                         CLUSTER'S
………                                        COORDINATES
11.69  17.36  18.60   -1.000
12.56  18.84  16.65   -1.000             <X   Y   Z    Charge>
12.43  16.45  19.68    2.000
11.57  18.77  17.88    2.000
13.39  14.96  15.59    0.0       <Dummy's COORDINATE: Step 2>
    WSURF
    3
    FALSE
    Si
    O
    Si
    O
    …              <LIST OF CLUSTER ATOMS CORRESPONDING
    …              TO ABOVE COORDINATES>
    …
    O
    O
    Si
    Si
    X    <DUMMY ATOM>
    3.0   576   -5   30.0   <576: NUMBER OF ATOM IN THE UNIT CELL(S) THAT COVER ALL ATOMS>
      8.46      1.12    8.89    2.000
      1.55     18.77    2.20    2.000
     11.57     11.07    4.50    2.000
     18.47      8.83   11.19    2.000       UNIT CELL(S) 'S COORDINATES
     11.57     18.77    4.50    2.000
     ………                                          <X    Y    Z    Charge>
     ………                                    TO GET EXPLICIT CHARGES
     ………
      6.15      0.55   10.85    2.000
      3.86     19.35    4.16    2.000
     13.87     10.50    2.53    2.000
     16.16      9.40    9.22    2.000
        20.0200          0.0000          0.0000
         0.0000         19.9000          0.0000       TRANSLATION VECTORS
         0.0000          0.0000         26.7700
```

```
1357   11.5    <NUMBER OF GRID POINT AND THE CUT OFF RADIUS>
       13.39    14.96    15.59
       13.39    14.96    16.24
       13.39    14.96    14.94
       13.39    14.96    16.89
       13.39    14.96    14.29
       13.39    14.96    17.54
       13.39    14.96    13.64
       13.39    14.96    18.19
       13.39    14.96    12.99
       13.39    14.96    18.84
       17.29    13.66    16.24
       17.29    16.26    14.94
       17.29    13.66    14.94
       ………
       ………
       ………
        9.49    16.26    16.24
        9.49    13.66    16.24
        9.49    16.26    14.94
        9.49    13.66    14.94
```

Within Rcut: Explicit Charges
Outside Rcut: Surface Charges

GRID POINTS'S COORDINATE

< X Y Z >

FROM STEP 1

SCREEP Output

```
----------------- RESULTS -----------------

 ** Area                =        1017.876   **
 ** Volume              =        3053.628   **
 ** Number of Points =            960       **
Ewald parameter                         ge    =   3.0000000000
Limit of the lattice summation          nb    =   -5
Number of potential values             ntoc  =  960
Number of ions in the unit cell          ik    =  576
Dimensionality                        iza   =    3
 NB,GE = 5  0.127204612
 Ions in the explicit area not including cluster
 RMax =  11.5
13.870000     -0.550000     15.920000      2.000000
14.430000     11.170000     -0.420000      2.000000
17.580000     11.200000     -0.360000      2.000000
16.000000     11.130000     -0.390000     -1.000000
18.060000     12.560000     -1.020000     -1.000000
13.920000     12.520000     -1.090000     -1.000000
………
………
………
4.490000      3.440000       7.110000      2.000000
8.600000      2.590000       4.260000      2.000000
1.550000      3.430000      15.700000      2.000000
17.610000      6.500000     26.370000      2.000000
```

EXPLICIT CHARGES:

< X   Y   Z Charge>

```
# of atoms in the cluster area 645
  Total charge of the cluster 0.
 Total surface charge = -0.26268183
 Coord and values of (-) conduc. surface charges
  14.1820973    14.9600000    24.5550755  -0.0118431
  15.3634644    14.1043979    24.3291868  -0.0118051
  15.3634644    15.8156021    24.3291868  -0.0091026
  14.9780409    14.9600000    24.4487881  -0.0106918
  16.5188320    13.2711145    23.8578943  -0.0116070
  17.5759367    12.5042770    23.1694034  -0.0091305
  17.7347548    14.1248754    23.4274534  -0.0046432
   ………
   ………
   ………
  17.2963287    13.2918547    23.5246008   0.0088916
  16.5188320    16.6488855    23.8578943   0.0031052
  17.7347548    15.7951246    23.4274534   0.0060685
  15.9778580    13.0798110     7.1776355   0.0041229
Ewald parameter                        ge    =   0.1272046120
Limit of the lattice summation         nb    =    5
Number of potential values             ntoc = 1357
Number of ions in the unit cell         ik    =  576
```

Surface Charges

< X   Y   Z   Charge>

```
Dimensionality                  iza  =   3
 Potentials on test points in a.u.
    #    X              Y              Z          GCOSMO           Exact              Error
    1  13.39000  14.96000  15.59000  -0.0756911306  -0.0756887147  -0.0000024159
    2  13.39000  14.96000  16.24000  -0.0684938184  -0.0684934846  -0.0000003338
    3  13.39000  14.96000  14.94000  -0.0820762687  -0.0820714594  -0.0000048093
    4  13.39000  14.96000  16.89000  -0.0593632229  -0.0593648739   0.0000016510
    5  13.39000  14.96000  14.29000  -0.0888357378  -0.0888280705  -0.0000076674
    6  13.39000  14.96000  17.54000  -0.0475239214  -0.0475277202   0.0000037987
    7  13.39000  14.96000  13.64000  -0.0979165726  -0.0979055021  -0.0000110706
    8  13.39000  14.96000  18.19000  -0.0339975828  -0.0340039745   0.0000063916
    9  13.39000  14.96000  12.99000  -0.1174152583  -0.1174002490  -0.0000150093


 Standard deviation =  1.81982125E-05
```

<CAN BE ADJUSTED TO GET THE MINIMUM STANDARD DEVIATION>

Step 4 Fitting the explicit charges

Command: . / Fit charge File Input

Fitting Input

```
Si    13.760000      16.450000      10.970000         0.847611
O    13.780000      14.920000      11.430000        -0.531374
Si    13.760000      13.400000      10.970000         1.041217
………
………                                                                   TERMINATED CLUSTER
………                                                                     <X   Y   Z Charge>
H    15.055649      11.009458      16.623980        -0.142968
H    13.916777      9.031221      15.882578        -0.144498
H    15.899255      11.132568      12.998075        -0.154322
H    13.933889      10.018647      12.202433        -0.153359
13.870000     -0.550000     15.920000     2.000000
14.430000     11.170000     -0.420000     2.000000
17.580000     11.200000     -0.360000     2.000000
16.000000     11.130000     -0.390000     -1.000000
18.060000     12.560000     -1.020000     -1.000000                  EXPLICIT CHARGES
………                                                                  <X   Y   Z Charge>
………
………
11.570000     18.770000      4.500000     2.000000
18.470000      1.120000     11.190000     2.000000
8.460000      8.830000      8.890000      2.000000
13.870000     10.500000      2.530000     2.000000
              14.04    11.71    14.94
              12.74    18.21    16.24
              12.74    11.71    16.24
              ………
              ………                                      GRID POINTS
              ………                                      <X     Y     Z>
              12.74    18.21    14.94
              12.74    11.71    14.94
              14.04    18.21    16.89
              14.04    11.71    16.89
              14.04    18.21    14.29
```

Fitting Output

```
  Si   13.760000      16.450000      10.970000        0.847611
  O    13.780000      14.920000      11.430000       -0.531374
  Si   13.760000      13.400000      10.970000        1.041217
  .........
  .........
  .........
  H    15.055649      11.009458      16.623980       -0.142968
  H    13.916777       9.031221      15.882578       -0.144498
  H    15.899255      11.132568      12.998075       -0.154322
  H    13.933889      10.018647      12.202433       -0.153359
         17.5800  11.2000  13.0300       1.3470
         17.5800  18.6500  13.0300       1.3470
         13.7400   8.7800  11.0800       1.3470
         16.1700  17.3100   9.1700       1.3470
         11.4200  17.3000   9.1300       1.3470
         17.5000  13.0600   9.8700      -0.2451
         16.1900  13.0400   7.6700      -0.2451
         11.8300  13.1600   7.7300      -0.2451         MODIFIED EXPLICIT
         .........                                          CHARGES
         .........
         .........                                     <X   Y   Z  Charge>
         20.1000  22.9400  16.1600      -1.0000
         21.6400  24.8700  15.3400      -1.0000
          1.4300   0.5400  10.9000       2.0000
          4.4900   3.4400   7.1100       2.0000
          8.6000   2.5900   4.2600       2.0000
          1.5500   3.4300  15.7000       2.0000
         17.6100   6.5000  26.3700       2.0000
Total explicit points      622
Total explicit charge      -0.000636
RootMeanSquare Poten.  1.522686
```

Appendix B

Pople style basis set

1. Minimal basis sets (STO-*n*G basis sets)

A common naming convention for minimal basis sets is STO-nG, where n is an integer and indicates how many primitive Gaussian type orbital basis sets (PGTOs) are used for representing a Slater type orbital basis set (STOs). Here is a list of commonly used minimal basis sets: STO-2G, STO-3G, STO-6G etc, the STO-3G basis is a widely used minimum basis set. This type of basis set has been determined for many elements of the periodic table. The designation of the carbon/hydrogen STO-3G basis is (6s3p/3s)/[2s1p/1s].

2. Split-valence basis sets (*k-nlm*G basis sets)

The *k* in front of the dash indicates how many PGTOs are used for representing the core orbitals. The *nlm* after the dash indicates both how many functions the valence orbitals are split into, and how many PGTOs are split for representing the valence orbitals. Two values (e.g. *nl*) indicates a split valence, while three values (e.g. *nlm*) indicate a triple split valence. The most common addition to basis sets in the Pople style is the addition of polarization functions, denoted by an asterisk, *. Two asterisks, **, indicate that polarization functions are also added to light atoms (hydrogen and helium). These are auxiliary functions with one additional node. For example, a minimal basis of a hydrogen atom would be a function approximating the 1s atomic orbital. When polarization is added to this basis set, a set of p-function is also added to the basis set. This adds some additional needed flexibility within the basis set, effectively allowing molecular orbitals involving the hydrogen atoms to be more asymmetric about the hydrogen nucleus. This is an important result when considering accurate representations of bonding between atoms, because the very presence of the bonded atom changes makes the energetic environment of the electrons spherically asymmetric. Similarly, a set of d-type functions are polarization functions for second row elements. Another common addition to basis sets is the addition of diffuse functions, denoted by a plus sign, +. Two plus signs, ++, indicate that diffuse functions are also added to light atoms (hydrogen and helium). These are very shallow Gaussian basis functions, which more accurately represent the "tail" portion of the atomic orbitals, which are distant from the atomic nuclei. These additional basis functions can be important when considering anions. Here is a list of commonly used split-valence basis sets: 3-21G, 6-31G, 6-31G(d), 6-31G(d,p), 6-31+G(d), 6-311G, 6-311G(d), 6-311+G(d) etc.

3-21G

This is a split valence basis, where the core orbitals are a contraction of three PGTOs, the inner part of the valence orbitals is a contraction of two PGTOs and the outer part of the valence is represented by one PGTO. The designation of the carbon/hydrogen 3-21G basis set is (6s3p/3s)/[3s2p/2s].

6-31G

This is also a split valence basis, where the core orbitals are a contraction of six PGTOs, the inner part of the valence orbitals is a contraction of three PGTOs and the outer part of the valence is represented by one PGTO. The designation of the carbon/hydrogen 6-31G basis set is (10s4p/4s)/[3s2p/2s]. In the terms of contraction basis functions, it contains the same number as 3-21G but the representation of each functions is better since more PGTOs are used.

6-311G

This is a triple split valence basis, where the core orbitals are a contraction of six PGTOs and the valence orbitals are split into three functions which are represented by three, one, and one PGTOs, respectively.

6-31G(d,p)

It is sometime donated 6-31G**. This is a split valence basis with an additional one set of d polarization functions for heavy atoms and one set of p polarization functions for hydrogen.

Appendix C

Appendix Table 1 Optimized geometries of N-bound, 1,2 H-shift and O-bound complexes of Z-acetaldehyde oxime on the 12T bare cluster and embedded cluster at the B3LYP level of theory. The values in square parentheses are taken from the bare cluster model. (Distances are in pm. and angles in degrees.)

Parameters	Models					
	N-bound complex		1,2 H-shift TS		O-bound complex	
O1-H1	[146.6]	171.1	[98.5]	101.2	[103.4]	152.1
N-H1	[109.3]	104.3	[197.8]	183.6	-	-
N-O1	[255.0]	273.3	[292.1]	281.1	-	-
N-O5	[135.2]	136.0	[141.7]	145.1	[144.0]	154.1
N-C1	[128.3]	128.7	[128.1]	128.1	[127.7]	127.5
O5-H1	-	-	[202.6]	185.7	[125.7]	103.7
O5-H2	[101.6]	99.4	[98.2]	97.6	[99.0]	100.4
O5-O1	-	-	[289.0]	278.8	[252.5]	250.1
O5-O2	[264.7]	284.0	[284.4]	308.4	[268.7]	265.5
O2-H2	[163.9]	185.3	[194.4]	233.3	[181.0]	179.1
C1-C2	[148.8]	148.3	[149.5]	149.0	[149.5]	148.7
C1-H3	[108.7]	108.9	[108.9]	109.0	[109.0]	109.4
O1-H1-N	[170.6]	165.2	[159.6]	160.7	-	-
O1-H1-O5	-	-	[145.2]	151.4	[160.2]	160.0
O2-H2-O5	[170.8]	171.2	[151.2]	133.2	[145.8]	141.9
C1-N-O5	[120.7]	121.2	[113.0]	112.4	[111.6]	109.5
O1-O2-O5-N	[6.6]	8.2	[68.4]	66.1	[104.0]	103.9

Appendix Table 2 Optimized geometries of rearrangement transition state and enol-amide complexes of Z-acetaldehyde oxime on the 12T bare cluster and embedded cluster at the B3LYP level of theory. The values in square parentheses are taken from the bare cluster model. (Distances are in pm. and angles in degrees.)

Parameters	Models			
	Rearrangement TS		Enol-Amide complex	
O1-H1	[176.4]	207.8	[101.4]	150.0
N-O5	[222.6]	220.3	-	-
N-C1	[120.1]	121.0	[126.5]	124.4
N-H3	[123.4]	135.0	[102.0]	102.0
O5-H1	[99.0]	97.8	[159.0]	104.4
O5-H2	[97.8]	97.4	[98.6]	100.0
O5-O1	[273.8]	300.9	[255.5]	249.2
O5-O2	[276.1]	307.3	-	-
O2-H2	[204.2]	237.4	[200.0]	186.5
C1-O5	-	-	[137.9]	147.6
C1-C2	[144.8]	146.4	[150.4]	149.2
C1-H3	[132.8]	123.0	-	-
O1-H1-O5	[167.2]	158.3	[157.5]	156.5
O2-H2-O5	[128.7]	128.2	[131.0]	133.4
C1-N-O5	[97.9]	109.5	-	-
N-C1-O5	-	-	[118.2]	112.5
O5-H2-N	-	-	-	-
O1-O2-O5-N	[83.5]	109.2	-	-

Appendix Table 3 Optimized geometries of tautomerization transition state and keto-amide complexes of Z-acetaldehyde oxime on the 12T bare cluster and embedded cluster at the B3LYP level of theory. The values in square parentheses are taken from the bare cluster model. (Distances are in pm. and angles in degrees.)

Parameters	Models			
	Tautomerization TS		Keto-Amide complex	
O1-H1	[103.1]	148.6	[143.2]	171.0
N-C1	[129.3]	127.2	[130.9]	130.8
N-O2	-	-	[270.2]	289.2
N-H2	[135.5]	140.2	[104.5]	102.8
N-H3	[101.4]	101.7	[101.0]	101.4
O5-H1	[149.6]	104.7	[106.5]	100.2
O5-H2	[129.5]	122.0	-	-
O5-O1	[250.5]	251.1	[249.4]	270.0
O2-H2	-	-	[166.1]	186.9
C1-O5	[132.7]	140.5	[128.4]	129.8
C1-C2	[149.0]	148.2	[149.8]	149.0
O1-H1-O5	[164.6]	164.6	[174.1]	168.7
O2-H2-N	-	-	[173.6]	172.7
N-C1-O5	[105.1]	101.0	[122.9]	122.2
O5-H2-N	[103.5]	103.9	-	-
O5-H2-N-C1	[0.3]	3.6	-	-
O1-O5-N-O2	-	-	[14.3]	11.5

Appendix Table 4 Optimized geometries of N-bound, 1,2 H-shift and O-bound complexes of E-acetaldehyde oxime on the 12T bare cluster and embedded cluster at the B3LYP level of theory. The values in square parentheses are taken from the bare cluster model. (Distances are in pm. and angles in degrees.)

Parameters	Models					
	N-bound complex		1,2 H-shift TS		O-bound complex	
O1-H1	[162.1]	205.4	[98.6]	101.4	[103.5]	154.6
N-H1	[107.2]	103.2	[204.6]	185.6	-	-
N-O1	[264.8]	295.0	[300.6]	283.8	-	-
N-O5	[135.3]	135.9	[142.0]	145.9	[143.0]	154.6
N-C1	[128.1]	128.6	[127.7]	127.7	[127.6]	127.7
O5-H1	-	-	[203.7]	183.1	[150.0]	103.4
O5-H2	[102.8]	100.5	[98.3]	97.8	[98.4]	100.3
O5-O1	-	-	[289.2]	274.3	[250.5]	253.6
O5-O2	[254.8]	266.7	[277.1]	289.0	[275.7]	266.6
O2-H2	[152.7]	166.4	[186.6]	210.1	[196.6]	181.8
C1-H3	[108.8]	108.9	[109.4]	109.2	[109.2]	109.1
C1-C2	[148.2]	147.9	[149.3]	148.9	[149.5]	149.2
O1-H1-N	[158.6]	143.6	[163.9]	162.1	-	-
O1-H1-O5	-	-	[143.9]	174.7	[162.0]	158.2
O2-H2-O5	[171.4]	175.9	[151.8]	136.5	[135.8]	140.0
C1-N-O5	[119.2]	119.7	[111.2]	110.6	[111.2]	106.9
O1-O2-O5-N	[34.0]	32.1	[17.5]	24.2	[118.5]	106.6

Appendix Table 5 Optimized geometries of rearrangement transition state and enol-amide complexes of E-acetaldehyde oxime on the 12T bare cluster and embedded cluster at the B3LYP level of theory. The values in square parentheses are taken from the bare cluster model. (Distances are in pm. and angles in degrees.)

Parameters	Models			
	Rearrangement TS		Enol-Amide complex	
O1-H1	[168.0]	191.1	[101.5]	131.2
N-O5	[203.1]	249.1	-	-
N-C1	[121.4]	118.6	[125.5]	123.8
N-C2	[186.1]	187.0	[145.6]	146.2
O5-H1	[100.3]	97.4	[154.1]	111.8
O5-H2	[98.7]	96.8	[97.6]	97.9
O5-O1	[263.6]	287.1	[255.1]	242.6
O5-O2	[270.8]	325.0	-	-
O2-H2	[186.7]	269.6	[268.0]	263.6
C1-O5	-	-	[137.6]	144.6
C1-H3	[108.4]	108.6	[109.4]	108.9
C1-C2	[181.4]	181.3	-	-
O1-H1-O5	[157.9]	167.0	[172.5]	173.9
O2-H2-O5	[141.3]	116.9	[107.1]	106.8
C1-N-O5	[106.9]	99.8	-	-
N-C1-O5	-	-	[121.2]	116.8
O1-O2-O5-N	[120.7]	127.1	-	-

Appendix Table 6 Optimized geometries of tautomerization transition state and keto-amide complexes of E-acetaldehyde oxime on the 12T bare cluster and embedded cluster at the B3LYP level of theory. The values in square parentheses are taken from the bare cluster model. (Distances are in pm. and angles in degrees.)

Parameters	Models			
	Tautomerization TS		Keto-Amide complex	
O1-H1	[103.7]	149.4	[129.2]	161.1
N-C1	[128.1]	126.4	[130.9]	130.1
N-O2	-	-	[284.4]	308.5
N-H2	[137.4]	143.8	[103.8]	102.8
N-C2	[144.9]	145.9	[146.1]	147.4
O5-H1	[147.6]	104.9	[113.0]	101.2
O5-H2	[129.2]	121.5	-	-
O5-O1	[250.0]	253.8	[241.6]	206.2
O2-H2	-	-	[180.9]	207.1
C1-O5	[132.7]	139.7	[126.8]	128.7
C1-H3	[108.8]	108.9	[109.3]	108.9
O1-H1-O5	[168.0]	172.2	[171.6]	165.4
O2-H2-N	-	-	[174.0]	168.8
N-C1-O5	[107.2]	103.3	[126.8]	127.2
O5-H2-N	[103.9]	103.5	-	-
O5-H2-N-C1	[2.3]	3.1	-	
O1-O5-N-O2	-	-	[13.3]	1.0

Appendix Table 7 Optimized geometries of N-bound, 1,2 H-shift and O-bound complexes of acetone oxime on the 12T bare cluster and embedded cluster at the B3LYP level of theory. The values in square parentheses are taken from the bare cluster model. (Distances are in pm. and angles in degrees.)

Parameters	Models					
	N-bound complex		1,2 H-shift TS		O-bound complex	
O1-H1	[166.6]	217.6	[98.9]	102.0	[104.3]	153.6
N-H1	[106.1]	102.7	[202.6]	183.8	-	-
N-O1	[267.6]	302.8	[296.6]	281.7	-	-
N-O5	[135.7]	136.5	[142.8]	146.6	[144.6]	156.0
N-C1	[128.9]	129.7	[128.4]	128.6	[128.2]	128.2
O5-H1	-	-	[197.5]	180.0	149.2]	103.2
O5-H2	[102.4]	100.0	[98.4]	97.7	[98.6]	99.3
O5-O1	-	-	[285.2]	272.1	[250.4]	253.6
O5-O2	[256.2]	270.6	[277.7]	289.3	[272.7]	272.9
O2-H2	[154.5]	170.9	[185.8]	210.9	[189.1]	193.8
C1-C2	[149.4]	149.1	[150.4]	149.9	[150.4]	149.7
C1-C3	[149.2]	149.2	[150.2]	150.2	[150.3]	150.7
O1-H1-N	[157.3]	139.1	[158.0]	159.9	-	-
O1-H1-O5	-	-	[146.5]	149.0	[161.9]	161.6
O2-H2-O5	[171.2]	173.7	[154.2]	136.0	[140.7]	134.7
C1-N-O5	[120.0]	120.6	[112.0]	113.0	[111.6]	109.3
O1-O2-O5-N	[36.6]	38.4	[70.7]	69.0	[108.6]	106.8

Appendix Table 8 Optimized geometries of rearrangement transition state and enol-amide complexes of acetone oxime on the 12T bare cluster and embedded cluster at the B3LYP level of theory. The values in square parentheses are taken from the bare cluster model. (Distances are in pm. and angles in degrees.)

Parameters	Models			
	Rearrangement TS		Enol-Amide complex	
O1-H1	[160.5]	200.5	[102.1]	160.3
N-O5	[246.7]	247.0	-	-
N-C1	[119.3]	119.5	[126.0]	123.6
N-C2	[187.8]	192.6	[144.9]	145.6
O5-H1	[98.7]	97.3	[155.8]	102.0
O5-H2	[97.6]	96.9	[98.6]	99.8
O5-O1	[256.3]	293.8	[253.8]	255.7
O5-O2	[268.8]	306.5	[271.4]	267.5
O2-H2	[189.5]	244.4	[196.1]	186.8
C1-O5	-	-	[138.9]	150.8
C1-C2	[183.5]	177.5	-	-
C1-C3	[145.7]	146.6	[150.4]	149.1
O1-H1-O5	[162.2]	159.9	[159.3]	153.6
O2-H2-O5	[136.4]	121.6	[134.1]	135.8
C1-N-O5	[76.0]	98.1	-	-
N-C1-O5	-	-	[116.8]	111.4
O1-O2-O5-N	[79.3]	141.2	-	-

Appendix Table 9 Optimized geometries of tautomerization transition state and keto-amide complexes of acetone oxime on the 12T bare cluster and embedded cluster at the B3LYP level of theory. The values in square parentheses are taken from the bare cluster model. (Distances are in pm. and angles in degrees.)

Parameters	Models			
	Tautomerization TS		Keto-Amide complex	
O1-H1	[105.3]	157.6	[140.3]	167.2
N-C1	[128.8]	126.9	[131.3]	131.3
N-O2	-	-	[278.7]	330.9
N-H2	[136.4]	142.8	[104.1]	102.4
N-C2	[144.7]	145.5	[146.3]	147.4
O5-H1	[142.8]	102.7	[107.1]	100.3
O5-H2	[126.3]	120.9	-	-
O5-O1	[248.0]	258.4	[246.8]	263.5
O5-O2	[330.2]	296.8	-	-
O2-H2	-	-	[174.8]	229.7
C1-O5	[134.2]	142.5	[128.6]	129.9
C1-C3	[148.7]	148.0	[150.1]	149.6
O1-H1-O5	[176.8]	165.7	[171.7]	159.6
O2-H2-N	-	-	[175.6]	169.5
N-C1-O5	[104.9]	101.3	[122.3]	122.7
O5-H2-N	[105.0]	104.2	-	-
O5-H2-N-C1	[2.4]	3.2	-	-
O1-O5-N-O2	-	-	[24.9]	5.1